Spontaneous Imbibition in Sand

Viscosity Effects on Oil Recovery and Flow Using Polymer and Glycerol

Master thesis in reservoir physics

Håkon Kyte Haugland

Department of Physics and Technology

University of Bergen

June 2016

“Do or do not, there is no try.”

-Yoda

Abstract

Spontaneous imbibition experiments have historically been performed using all faces open (AFO) boundary condition. Due to complex flow patterns consisting of both counter- and co-current flow, modelling flow using established differential equations has been difficult. Recently, however, an alternative boundary condition termed *two ends open free* spontaneous imbibition (TEOFSI) was studied in detail, and supporting theory was established. In this thesis, co-current spontaneous imbibition was performed using the TEOFSI boundary condition, with one end in contact with wetting phase and the other end in contact with non-wetting phase. Columns of unconsolidated sand were packed in glass imbibition tubes and completely saturated with non-wetting phase. Brine, polymer and glycerol were used as the wetting phase, whereas air and mineral oils with varying viscosity were used as the non-wetting phase. During experiments, front position was recorded and non-wetting phase production was measured separately at each end of the imbibition tube.

The viscosity of the non-wetting phase (μ_{nw}) was varied over 4 orders of magnitude to study its effect on oil recovery and front behaviour. Recovery decreased from 98% of the pore volume at μ_{nw}/μ_w = 0.016 to 77% of the pore volume at μ_{nw}/μ_w = 63.7. Brine displaced the oil in a piston-like manner for all 4 experiments, except initially for higher viscosity ratios when a sharp front developed some distance from the inlet due to early fingering of the wetting phase and entrapment of the non-wetting phase. Measurements of the front position were matched with theoretical calculations using a method based on the assumption of piston-like displacement during co-current imbibition by Haugen et al. (2014). Due to successfully matching the experimental data, capillary pressure at the front and relative permeability to brine behind the front was calculated. The estimated relative permeability decreased, whereas the capillary pressure increased, with increasing viscosity of the non-wetting phase.

The viscosity of the wetting phase (μ_w) was varied using HPAM polymer and glycerol to study low viscosity ratios in the range of 0.033 to 0.034. Spontaneous imbibition results show that glycerol yielded a 5% higher recovery compared with polymer, using matching aqueous phase viscosity. The lower recovery for polymer may have been caused by polymer retention or wettability alteration. Further studies are required to quantify and understand the mechanisms behind the experimentally observed differences, but it is likely to be influenced by polymer retention during spontaneous imbibition with polymer as the wetting phase.

Acknowledgements

First of all I would like to thank my main supervisor Associate Professor Martin Fernø and co-supervisor Dr. Bergit Brattekås at the Department of Physics and Technology at the University of Bergen for valuable guidance and support writing this thesis. In addition, I would like to thank co-supervisor Professor Arne Graue for accepting me into the Reservoir Physics group, and running the group at the Department of Physics and Technology.

I would like to thank Leif Egil Sandnes and Roald Langøen at the mechanical workshop at Department of Physics and Technology for their expertise in manufacturing valuable parts of my experimental setup. I would also like to thank Sverre S. Aksnes at Department of Earth Science UIB for lending me equipment and granting access to their lab.

Five years of studying at the University of Bergen has passed and several people have contributed to making this a good time. I would like to thank all members of "*Svigjengen*" for participating in this journey, and wish you all good luck on the road ahead. Several useful and not so useful discussions have contributed to the overall experience in writing this thesis. Special thanks to Trond Vabø, Tore Føyen and Silje Lande for participating, helping and sharing the tasks during long sessions in the lab.

Finally I would like to thank family and friends for engaging me in activities not related to the thesis, ensuring my sanity throughout the semester.

Bergen, June 2016

Håkon Kyte Haugland

Table of contents

Introduction

The study of spontaneous imbibition is of widespread interest and research on the topic is in a growth phase. Several research groups are actively studying various aspects of spontaneous imbibition including; pressures acting during spontaneous imbibition (Li et al., 2006), capillary back pressure and relative permeability behind the imbibition front (Haugen et al., 2014), imaging of front development (Fernø et al., 2013), and entrapment of the non-wetting phase during spontaneous imbibition (Meng et al., 2015).

Recovery of oil by spontaneous imbibition is driven by surface energy, through the action of capillary pressure (Morrow and Mason, 2001). Current understanding of spontaneous imbibition is derived from experimental studies, where different boundary conditions have been applied. Historically, the most used boundary condition has been all faces open (AFO), mainly due to the simplicity of the experiments, as well as reproducibility of results (Mason et al., 2009). However, as flow during these experiments occur both co- and counter-currently, it is difficult to model the flow with established differential equations. An alternative boundary condition termed two ends open free spontaneous imbibition (TEOFSI) by Dong et al. (1998), has recently been studied in detail, and supporting theory was established (Haugen et al., 2014).

The use of polymers is the most widely applied technology to increase the viscosity of the drive fluid during flooding of a hydrocarbon reservoir (Sydansk and Romero-Zeron, 2010). In spontaneous imbibition, glycerol has been used to increase the viscosity of the aqueous phase to alter the viscosity ratio (Kyte and Rapoport, 1958, Fischer and Morrow, 2006). By increasing the viscosity of the wetting phase during spontaneous imbibition, the viscosity ratio favours piston-like displacement. Comparing the use of polymer and glycerol to increase aqueous phase viscosity is one of the goals of this thesis.

By introducing advanced visualisation techniques such as MRI imaging and PET (Fernø et al., 2013, Fernø et al., 2015), or more simple visualisation techniques such as observing the imbibition front using glass tubes (Meng et al., 2015), the nature of the imbibition front has been studied. Building on the experience gained in collaboration with Vabø (2016), an experimental setup utilizing imbibition glass tubes, fitted with an end piece holding a paper filter, was developed. In this thesis spontaneous imbibition tests were conducted in unconsolidated sand, using the TOEFSI boundary condition, where both wetting- and non-wetting phase viscosities were varied. Polymer and glycerol were used to alter the viscosity of the wetting phase, whereas oils with different viscosity were used as the non-wetting phase. The main focus of the thesis, in addition to investigating the effects of polymer and glycerol on aqueous phase viscosity, was to investigate how the viscosity ratio affects recovery and front behaviour during spontaneous imbibition.

This thesis contains five parts, divided into sections. The first part includes three sections that set the theoretical stage for the experimental work. In the second part, the experimental method is covered in detail, describing fluids, materials and experimental setups used for spontaneous imbibition. In the third part the experimental results are reported and discussed, whereas part four concludes the work, as well as give suggestions for future possibilities. The fifth and final part contains additional information in form of an appendix and references.

1 Theory

1.1 Fundamentals

1.1.1 Porosity in unconsolidated porous media

Unconsolidated porous media consist of sediments that have accumulated over time, similar to sedimentary rocks. The difference between sedimentary rocks and unconsolidated porous media are the pressures and temperatures the sediments have been exposed to.

Sediments are rock fragments or minerals broken off bedrock, mineral crystals that precipitate out of water, and shells or shell fragments (Marshak, 2011). They are formed by weathering of pre-existing rock, and depending on the depositional environment, the size, sorting and shape of the sediments may vary. All of these factors will influence the porosity, an essential rock property when it comes to storage of fluids within the sediments.

Porosity, φ, is defined as the ratio of void volume of a porous medium to the total or bulk volume of the medium (Jenkins, 1966). By increasing the porosity, the volume available for hydrocarbon storage increases. As mentioned above several factors influence the porosity. First, the clasts that comprise the sediments are classified by size, from boulders to mud (see Table 1) (Marshak, 2011), and depending on the size and sorting of the clasts, the porosity may vary. The sorting of the media refers to the degrees of which the sediments are all the same size. The sorting ranges from "well sorted" sediments, which consists of sediments of the same size, to "poorly sorted", where the sediments are mixed in size (Marshak, 2011). Generally, well sorted sands have more porosity than poorly sorted sands. This is due to smaller grains filling the voids between the larger grains (Rogers and Head, 1961).

Table 1: Classification of clast size.

Boulders	More than 256 millimeters (mm)
Cobbles	Between 64 mm and 256 mm
Pebbles	Between 2 mm and 64 mm
Sand	Between 1/16 mm and 2 mm
Silt	Between 1/256 mm and 1/16 mm
Mud	Less than 1/256 mm

Second, the clasts may have different shapes. The angularity of the clasts describes whether they have smooth or angular corners and edges, whereas the sphericity refers to the degree of roundness or the degree to which the clast resemble a sphere.

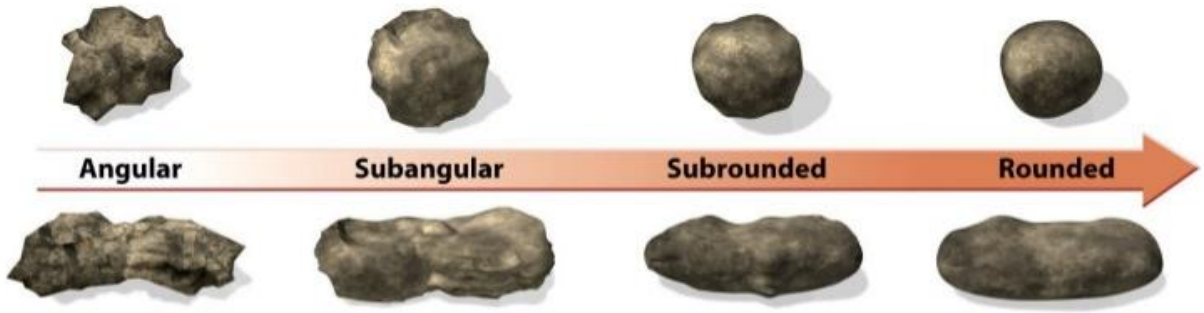

Figure 1: Figures showing clasts with different shapes (Marshak, 2011).

Unconsolidated media, often referred to as a pack of sediments, can be assembled in many different ways. Graton and Fraser (1935) described cases of the different packings (see Figure 2). The simplest form of packing is a "cubic packing". This is a homogeneous layered system consisting of rows with perfectly round spheres. The rows are parallel to each other, both horizontally and vertically. This leads to a high portion of void space between the spheres, and as a result this increases the porosity. The next case is an "orthorhombic packing". This is the same network as above, except here the spheres lie 60° to one another. The third case is a "rhombohedral packing". Here, the spheres are packed in an octahedron, making the space between the spheres smaller. This tighter packing leads to a lower porosity. The porosities of the different cases are unaffected by the size of each individual sphere, as long as they are all equal.

Table 2: Porosity values of the different packing arrangements, where *r* is the sphere radius (Graton and Fraser, 1935).

	Case 1	Case 2	Case 3
Bulk volume	8.00 r^3	6.93 r^3	5.66 r^3
Void volume	3.81 r^3	2.74 r^3	1.47 r^3
Porosity	47.64 %	39.54 %	25.95 %

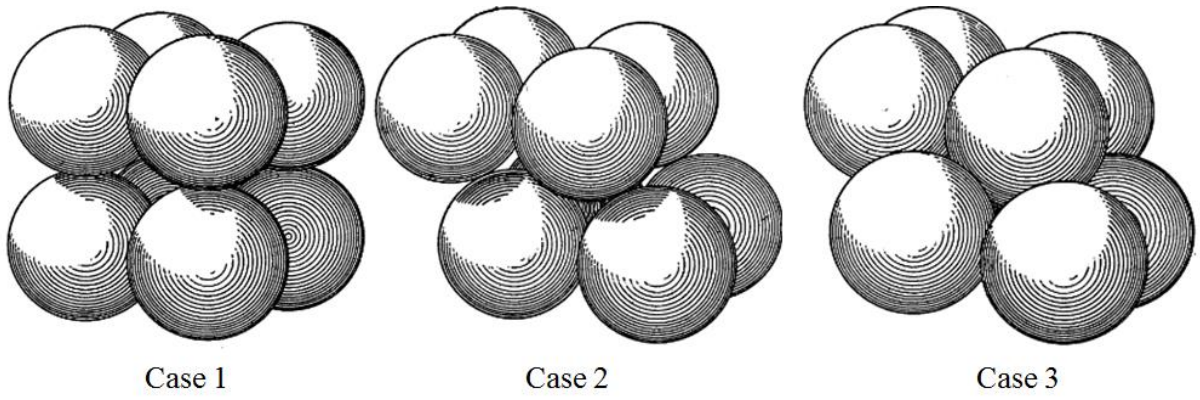

Figure 2: Three different types of packing. Case 1 is a cubic packing, Case 2 is an orthorhombic packing and Case 3 is a rhombohedral packing (Graton and Fraser, 1935).

1.1.2 Capillary pressure

In porous media, capillary pressure relates the pressure in each fluid phase when two or more immiscible fluids are in contact with each other. For a curved interface between oil and water there will be an increase in the pressure along the interface to balance the interfacial tension forces. This capillary pressure is described by Laplace's equation

$$P_c = p_o - p_w = \sigma\left(\frac{1}{r_1} + \frac{1}{r_2}\right) \tag{1}$$

where p_o is the pressure in the oil phase and p_w is the pressure in the water phase, σ is the interfacial tension, r_1 and r_2 is the radii of curvature of the interface, measured perpendicular to each other (Dullien, 2012). For fluids other than oil and water, the capillary pressure is defined as:

$$P_c = p_{nw} - p_w \tag{2}$$

where p_{nw} is the pressure in the non-wetting phase and p_w is the pressure in the wetting phase (Anderson, 1987a).

For a small capillary tube, a simple relationship between contact angle and capillary pressure can be derived. Figure 3 shows an interface between oil and water, with a contact angle of θ through the water. Assuming the capillary tube is small enough, the interface can be part of a sphere with radius r_s. Due to the sphere, both radii of curvature will be equal to r_s, and as Figure 3 shows r_s is larger than the radius of the tube, r_t. The relationship between the two radii is given by:

$$\frac{r_t}{r_s} = \cos\theta \tag{3}$$

Rearranged, Equation (3) becomes

$$\frac{1}{r_s} = \frac{\cos\theta}{r_t} \tag{4}$$

Substituting Equation (4) into Laplace's equation (1) gives:

$$P_c = \frac{2\sigma\cos\theta}{r_t} \tag{5}$$

The interfacial tension between oil and water creates a force upwards. This is balanced by an increase in the oil pressure, greater than the pressure in the water. These forces are responsible for the rise (or depression) of the curved interface relative to the height of a flat interface (Anderson, 1987a).

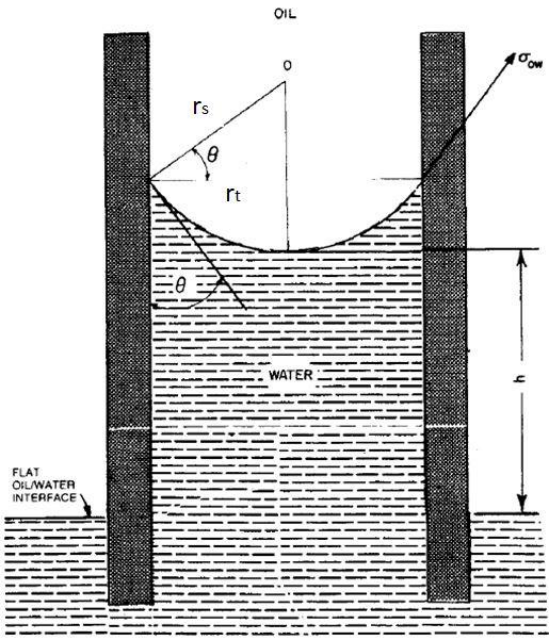

Figure 3: Interface between oil and water in a small capillary tube (Anderson, 1987a).

1.1.3 Wettability

Wettability is defined as "the tendency of one fluid to spread on or adhere to a solid surface in presence of other immiscible fluids" (Craig, 1971). For a rock/oil/brine system, wettability is a measure of the rocks preference for either oil or brine. If a rock is water-wet, the water has a tendency to occupy the smaller pores and occupy most of the rock surface. Likewise, if a system is oil-wet, oil will have a tendency to occupy the smaller pores and oil will preferentially be in contact with the rock surface (Anderson, 1986a).

Consider a cleaned sandpack saturated with oil. Despite the fact that the oil is coating the grain surface, the sandpack is still preferentially water-wet. A way to test the wetting preference is to allow water to imbibe into the sandpack. If the sandpack is water-wet, the water will displace the oil from the surface, which indicates that the sand grains would rather be in contact with water than to be in contact with the oil. There are several degrees of wetting and depending on the interactions between rock, oil and brine, the wettability may range from strongly water-wet to strongly oil-wet. If the rock has no preference to either oil or water, the system is said to be of neutral or intermediate wettability (Anderson, 1986a). Also, Brown and Fatt (1956) reported a third wettability condition, called fractional wettability. This is a wetting condition where different areas of the porous media have different wetting preferences.

Amott (1959) presented a method that measures the average wettability of a core by combining spontaneous and forced displacement. Using the ratio of spontaneous imbibition to forced imbibition reduces the influence of other factors such as initial fluid saturation, relative permeability and viscosity. The Amott method consists of four displacement processes, following a centrifuging under brine until residual oil saturation is reached. The four steps are: 1) measure the volume of water displaced by spontaneous imbibition after the core has been immersed in oil, 2) measure total volume of water displaced by oil after forced displacement,

3) measure volume of oil displaced by spontaneous imbibition after the core has been immersed in water, and 4) total volume of oil displaced by water after forced displacement. The results from the test are shown by "displacement-by-oil" and "displacement-by-water" ratios. The "displacement-by-oil ratio" (δ_o) is the ratio between water volume spontaneously displaced (V_{wsp}) to total water volume displaced (V_{wt}) (see equation 6). Likewise, the "displacement-by-water ratio" (δ_w) is the ratio between oil volume spontaneously displaced (V_{osp}) to total oil volume displaced (V_{ot}) (see equation 7).

$$\delta_o = \frac{V_{wsp}}{V_{wt}} \tag{6}$$

$$\delta_w = \frac{V_{osp}}{V_{ot}} \tag{7}$$

The forced displacement may be conducted using centrifuge or by injecting fluids into the core using a pump. This is of particular interest for this thesis as unconsolidated samples may not be centrifuged (Anderson, 1986b).

1.1.4 Flow equations

Flow resulting from pressure gradients in a tube is often referred to as Poiseuille flow. The Hagen-Poiseuille equation is specific for pressure-driven flow in a tube of circular cross section (Kirby, 2010). The Hagen-Poiseuille equation is given as:

$$Q = -\frac{\pi r^4}{8\mu}\frac{\partial p}{\partial \mathrm{z}} \tag{8}$$

Where Q is the volumetric flow rate, r is the radius of the tube, μ is the viscosity of the fluid and $\frac{\partial p}{\partial \mathrm{z}}$ is the pressure gradient in the z-direction. This equation is valid for a Newtonian fluid during steady flow through a tube with circular cross section and all the flow is in the z-direction. However, this requires the channel to be perfectly straight and infinitely long. If the entrance effects are neglected and the infinite-tube result is used for a finite tube, the equation can be rewritten and used in further derivation of the Washburn equation in section 1.3.1. As long as $r/L \ll 1$ and $r/L \ll 1 / Re$, this approximation is good. Here, r/L is the radius of the tube, divided by the total length of the tube. *Re*, or Reynolds number, is a dimensionless quantity used to predict flow patterns. It is given as:

$$Re = \frac{2\rho|\overline{u_z}|r}{\mu} \tag{9}$$

where ρ is the density of the fluid, $|\overline{u_z}|$ is the mean velocity of the fluid in the z-direction, μ is the viscosity of the fluid and r is the radius of the tube. If $Re < 2300$ the flow is laminar. By

using this approximation, the pressure gradient is assumed to be uniform across the length of the tube. The term $-\frac{\partial p}{\partial z}$ can be replaced with $\frac{\Delta P}{L}$ and the equation 8 becomes:

$$Q = \frac{\pi}{8} r^4 \frac{1}{\mu} \frac{\Delta P}{L} \tag{10}$$

where Q is the positive volumetric flow rate from inlet to outlet, r is the radius of the tube, μ is the viscosity of the fluid, ΔP is the pressure differential across the tube and L is the length of the tube (Kirby, 2010).

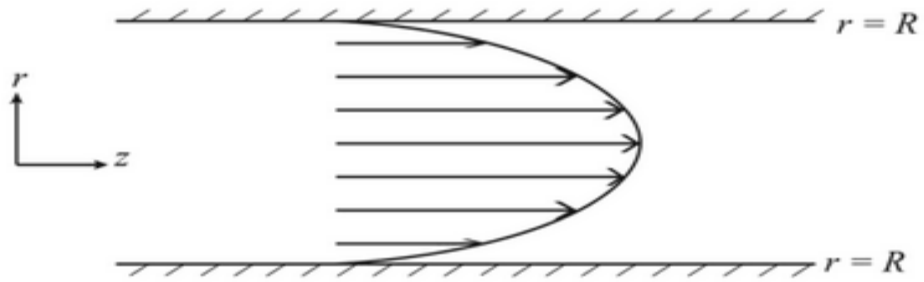

Figure 4: Poiseuille flow in a circular tube (Kirby, 2010).

Hagen-Poiseuilles equation for flow in capillary tubes is essential for understanding flow during spontaneous imbibition. This will be further discussed in section 1.3.1.

1.2 Enhanced oil recovery in unconsolidated media

Before discussing enhanced oil recovery (EOR), primary, secondary and tertiary recovery should be defined. Primary oil recovery consists of all oil production derived from the natural energy of the reservoir. This involves compaction due to overburden weight, expansion of dissolved gas, gas cap expansion, natural water drive from an underlying aquifer and gravity drainage. It is important to note that primary recovery only occurs when there are only production wells in the reservoir. Secondary oil recovery is the next step, in which energy is added to reservoir in order to produce oil. Waterflooding and natural gas injection are the most common fluids injected to add pressure in the reservoir. Tertiary oil recovery is any additional oil recovery beyond that of primary and secondary oil recovery. This involves ways of augmenting the flow or the recovery by injecting agents such as: Surfactants, alkaline agents, thermal energy or miscible gases (Sydansk and Romero-Zeron, 2010).

EOR is a term defined in several ways over the years. A common definition of EOR is oil produced due to injection of materials not normally present in the oil reservoir (Lake, 1989). However, this covers a broad range of materials that can be used in order to increase the oil production, as well as being applied to all phases of recovery. Latil (1980) on the other hand describes enhanced oil recovery as all recovery methods other than natural production. For this thesis, however, the first, broader definition will be used.

Due to its natural abundancy and low cost water is a fluid commonly injected in hydrocarbon reservoirs to provide pressure support after depleting the pressure in the reservoir, as well as targeting a larger volume of the hydrocarbon reservoir. However, water has a relatively low viscosity compared with oil, and may not be the most suitable fluid to inject in regards to achieving the optimal mobility conditions for high oil production. Unfavourable mobility conditions will lead to early breakthrough of the injected fluid and thus a lower recovery. Aronofsky (1952) defined the mobility ratio as:

$$M = \frac{\left(K_r/\mu\right)_w}{\left(K_r/\mu\right)_o} \tag{11}$$

Where K_{rw} and K_{ro} is the relative permeability to water and oil, and μ_w and μ_o is the viscosity of water and oil. A favourable displacement will only occur if the mobility ratio $M \leq 1$. This form of displacement is often referred to as "piston-like-displacement", as the front moves like a piston through the reservoir. If this is the case, oil moves at velocity greater than, or equal to, that of the water. This creates a sharp front that displaces much of the oil and there is no tendency for oil to be bypassed, except for residual oil capillary trapped in the middle of the large pores. In the case of a mobility ratio greater than 1 ($M > 1$) however, water may be moving faster than the oil, and thus some of the oil is bypassed and left behind. Water then fingers through the reservoir causing an early breakthrough and poor volumetric sweep. The term volumetric sweep efficiency (E_V) is defined as

$$E_V = E_A E_I \tag{12}$$

Where E_A is the volumetric sweep efficiency and E_I is the vertical sweep efficiency. The areal sweep efficiency is influenced by the mobility ratio, flooding pattern type, and both throughput and reservoir heterogeneity. Vertical sweep efficiency is affected by the variation in reservoir layer permeability and the mobility ratio (Satter et al., 2008)

Injecting water may be a good way to keep the pressure up in a hydrocarbon reservoir. However, it is well known that waterflooding behaves differently depending on the wettability of the reservoir rock. As the reservoir rock becomes more oil-wet, the relative permeability to water increases and the relative permeability to oil decreases. This enables the water to flow more easily compared to the oil and thus causing less efficient recovery and earlier breakthrough (Anderson, 1987b). By neglecting capillary effects and assume a horizontal system, the effects of relative permeability and viscosity ratio can be described by the fractional flow equation. A simplified version is given as (Anderson, 1987b):

$$f_w(S_w) = \frac{1}{1 + \frac{\mu_w}{\mu_o}\frac{K_{ro}}{K_{rw}}} \tag{13}$$

Where f_w is the fractional flow of water, S_w is the water saturation, μ_w and μ_o are the water and oil viscosities and K_{ro} and K_{rw} are the oil and water relative permeabilities, respectively.

1.2.1 Polymers

The use of polymers is the most widely applied technology in regards to increasing the viscosity of the drive fluid during flooding of a hydrocarbon reservoir (Sydansk and Romero-Zeron, 2010). Polymers are long chains of repeating units (monomers) linked by covalent bonds (Baviere, 1991). By adding polymers to the water, the viscosity of the water will increase and the relative permeability of the displacing phase (water) will decrease due to retention/adsorption in the porous media (Sydansk, 2006). When increasing the viscosity of the water, the mobility ratio becomes more favourable and as a consequence the volumetric sweep efficiency increases (Broseta et al., 1995).

There are mainly two types of polymers used for EOR, synthetic polymers and biopolymers, each with its pros and cons. The synthetic polymers are often polyacrylamides (PAM), and the performance varies depending on the molecular weight and the degree of hydrolysis. If the polyacrylamide is hydrolysed, a part of the acrylamide is replaced by acrylic acid, and the polymer is referred to as hydrolysed polyacrylamide (HPAM) (Needham and Doe, 1987). PAM and HPAM are sensitive to salt. As a result of this, fresh water is preferred when preparing the polymer solutions. In addition, these polymers are exposed to mechanical degradation by shear stress (Chang, 1978).

Biopolymers is a biologically produced polymer known as xanthan gum (Jeanes et al., 1961). In contrast to synthetic polymers, biopolymers are more resistant to salinity and mechanical shearing effects, which make them easier to handle in an oil field setting with injection pumps and other in situ equipment. However, biopolymers are known to plug both the formation and the well it is injected in. In addition, they are vulnerable to bacterial attacks. A way to

decrease the bacterial degradation is to add bactericides, something which increases the cost of the process (Chang, 1978, Zolotukhin and Ursin, 2000).

Polymer retention is a term used to describe mechanisms which causes a reduction in the mean velocity of polymer molecules as they propagate through the porous media (Zolotukhin and Ursin, 2000). Retention may be caused by: 1) adsorption on the surface of the pores, 2) mechanical entrapping in pores, and 3) hydrodynamic retention (Sorbie, 2013).

Adsorption causes the polymers to be bound to the surface of the pores. The larger the surface area, higher levels of adsorption is observed (Sorbie, 2013). Thus, a porous media with a higher porosity will experience a higher retention due to adsorption of polymers. Mechanical entrapping of the polymer molecules simply refers to molecules being trapped due to narrow pore throats. Gogarty (1967) measured the size of partially hydrolysed polyacrylamide units and found that the units where larger than some of the pore throats, effectively stopping the flow in these pore throats. Precipitation of polymers, or hydrodynamic retention of polymers, is a retention mechanism which is not as well defined and understood. It refers to the polymer trapped in stagnant flow zones. The idea originated after a polymer retention experiment in which the retention changed when the fluid flow rate was adjusted to a new value (Desremaux et al., 1971, Maerker, 1973, Chauveteau and Kohler, 1974). The hydrodynamic retention increases with the flow rate (Chauveteau and Kohler, 1974). Figure 5 shows the different retention mechanisms.

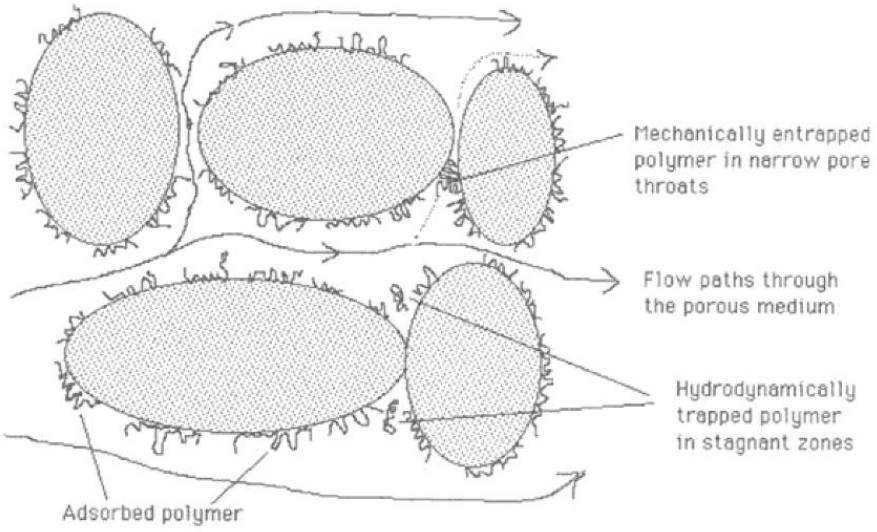

Figure 5: Illustration showing the different retention mechanisms (Sorbie, 2013).

Retention of polymers may lead to a decrease in the concentration of polymers available for flow and a decrease in the velocity of the polymer front. This is a negative effect which makes the mobility control effect in the remote areas of the reservoir a challenging task. However, retention may also cause a reduction in the rock permeability. This will in turn reduce the mobility of both the polymer and the chase water, which often is the aim of the polymer injection in the first place (Zolotukhin and Ursin, 2000).

As mentioned above, polymers are exposed to mechanical degradation by shear stress. Due to their high molecular weight, both polyacrylamides and xanthan gums give non-Newtonian flow characteristics. Both polymers are shear-tinning, which means that the relative viscosity decreases as the shear rate increases (Donaldson et al., 1989). In the work of Romero-Zeron et al. (2010), HPAM was used during polymer flooding of unconsolidated porous media. Viscosities of three polymer solutions with different concentration of HPAM were measured at four different speeds, see Figure 6. It shows that the viscosity of the polymer solutions decreases as the shear stress increases. This effect was more apparent as the concentration of polymer was increased.

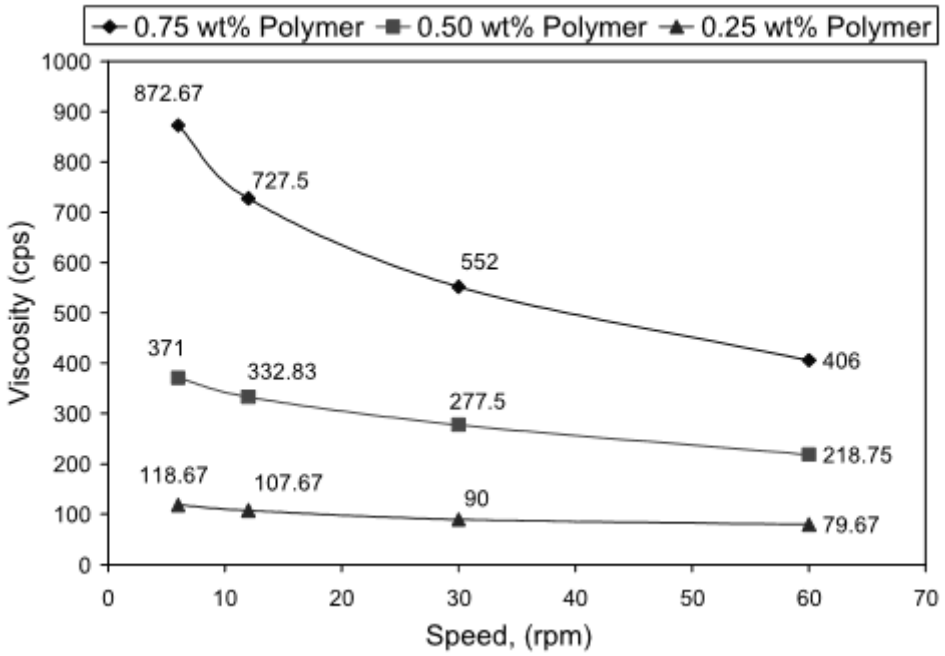

Figure 6: Viscosities of three polymer solutions with different concentrations, measured at four different speeds (6, 12, 30 and 60 rpm). Figure taken from (Romero-Zeron et al., 2010).

1.3 Spontaneous imbibition

Spontaneous imbibition, also referred to as dynamic spontaneous imbibition, is defined as a process where a wetting fluid is drawn into a porous medium by capillary action (Morrow and Mason, 2001). In common day activities this includes the use of cloth or paper to wipe surfaces for spilt liquid, or the adsorption of water into a sponge. Spontaneous imbibition is driven by surface energy and viscous forces resist the process. The interactions between them determine the rate of imbibition (Mason and Morrow, 2013). Two main forms of spontaneous displacement are recognized: co-current spontaneous imbibition and counter-current spontaneous imbibition. Co-current displacement occurs when both the wetting phase and the non-wetting phase flow in the same direction, whereas counter-current imbibition indicates that the wetting phase and the non-wetting phase are flowing in the opposite direction (Li et al., 2003). In addition to spontaneous imbibition, the literature distinguishes between two additional types of imbibition; 1) pseudo-quasistatic imbibition, in which the wetting phase is increased by an incremental decrease in the capillary pressure, and 2) dynamic forced imbibition, where the non-wetting phase is displacement by the means of an external pressure or gravity (Li et al., 2003, Morrow and Mason, 2001).

1.3.1 Imbibition into idealized porous media – Washburn equation

As imbibition depends on capillary action, considering flow into a single capillary tube is a good place to start. Washburn (1921) provided a detailed analysis of imbibition into a single capillary tube using mercury, water and air, as well as other fluids in his experiments. He derived an equation known as the Washburn equation, which describes flow of liquids under capillary pressure. The equation was derived from Poiseuilles equation for flow in capillary tubes. However, it should be mentioned that Bell and Cameron (1906) had previously related distance advanced to square root of time for tubes. Mason and Morrow (2013) presented the derivation of flow equations for spontaneous imbibition:

Consider a capillary tube with radius r and total length L_{tube}, saturated with a perfectly wetting fluid. The capillary pressure developed at a meniscus at length L along the tube is equal to:

$$P_c = \frac{2\sigma}{r} \tag{14}$$

For a partially wetted fluid the term would be similar to equation (5) in section 1.1.2. The flow through the capillary tube can be calculated by the Poiseuille equation:

$$q = \frac{\pi}{8} r^4 \frac{1}{\mu} \frac{\Delta P}{L} \tag{15}$$

For a single capillary tube initially saturated with a non-wetting phase, immersed with one end in the wetting phase and one in the non-wetting phase, the capillary pressure will pull wetting phase in and push the non-wetting phase out. The viscosity ratio between the two phases will determine the rate of the imbibition. In addition, there may be an extra pressure drop $\Delta P_{applied}$ across the tube. Summing equation (14) and (15) yields

$$\frac{2\sigma}{r} + \Delta P_{applied} = q\left(\frac{8\mu_{nw}}{\pi r^4}(L_{tube} - L) + \frac{8\mu_w}{\pi r^4}L\right) \quad (16)$$

Substituting for velocity, which depends on the flow q and the cross sectional area of the tube yields

$$(\mu_{nw}(L_{tube} - L) + \mu_w L)dL = \frac{1}{8}\left(\frac{2\sigma}{r} + \Delta P_{applied}\right)r^2 dt \quad (17)$$

Integrating from L = 0, t = 0 to L and t gives

$$\mu_{nw}L_{tube}L - \frac{1}{2}(\mu_{nw} - \mu_w)L^2 = \frac{1}{8}\left(\frac{2\sigma}{r} + \Delta P_{applied}\right)r^2 t \quad (18)$$

This equation shows the relation between tube radius and velocity of the interface. The larger the tube radius, the faster the interface moves. Resistance to flow is dominated by square of the tube radius, compared to the increase in capillary pressure (which depends on the reciprocal of the tube radius).

To be able to compare the shape of the production curves the equation is normalized with respect to when the interface reaches the end of the tube, t_{end}. This gives

$$\frac{1}{2}(\mu_{nw} + \mu_w)L_{tube}^2 = \frac{1}{8}\left(\frac{2\sigma}{r} + \Delta P_{applied}\right)r^2 t_{end} \quad (19)$$

Dividing equation (18) with (19) yields

$$\frac{t}{t_{end}} = \frac{1}{(\mu_{nw} + \mu_w)}\left(2\mu_{nw}\frac{L}{L_{tube}} - (\mu_{nw} - \mu_w)\frac{L^2}{L_{tube}^2}\right) \quad (20)$$

If μ_{nw} is reduced to zero, equation (20) above is reduced to the Washburn equation, and distance advanced in the tube is proportional to square root of time. As the equation shows the extra applied pressure $\Delta P_{applied}$ falls away and becomes negligible. Also, it is required that the pressure applied is constant, not negative, and exceeds the capillary pressure generated by the meniscus into the tube. A negative pressure will result in no imbibition by the wetting fluid. Figure 7 shows the different production curves of this function for different viscosity ratios. If the viscosities of the two fluids are similar, the distance advanced will be linear with time. For all other viscosity ratios the relationship between distance advanced and time will be quadratic.

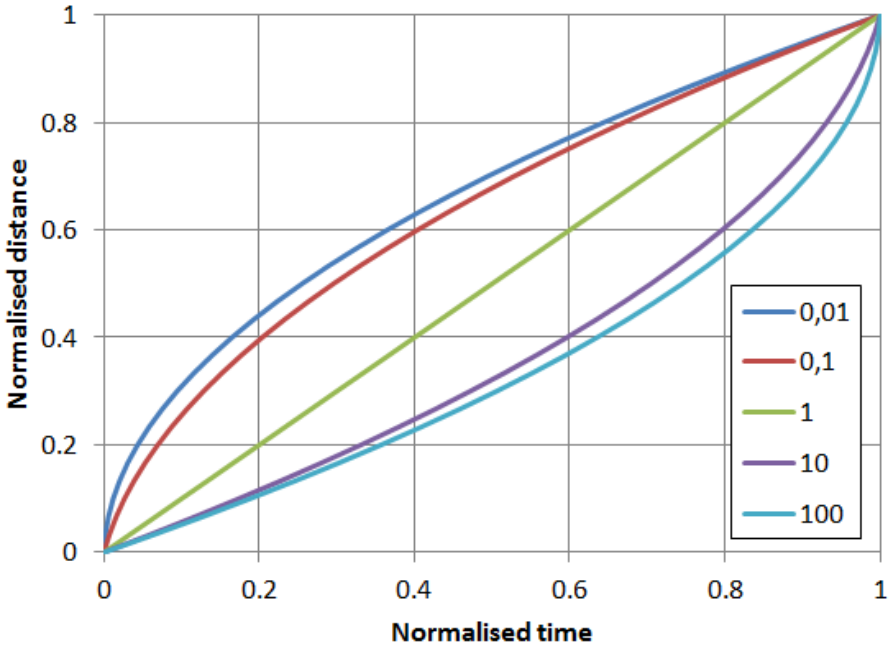

Figure 7: Normalized distance advanced as a function of normalized time in a single capillary tube with co-current displacement for various viscosity ratios. The graph was made by using equation 20 and varying the viscosity ratio from 0.01 to 100.

1.3.2 Scaling

Spontaneous imbibition is a complex process which depends on several factors. Interfacial tension, fluid viscosities (μ_w and μ_{nw}), sample shape, size, porosity, permeability and boundary conditions all have different effects, which need to be accounted for. In order to compare the results of different experiments with each other, several different scaling groups of dimensionless time have been proposed.

Mattax and Kyte (1962) performed scaled imbibition test on small reservoir core samples in order to predict performance of a reservoir made up of many matrix unit blocks. A scaling group was proposed under the following conditions:

1. The shape and boundary conditions of the laboratory model must be identical.
2. The reservoir oil/water viscosity ratio must be duplicated in laboratory tests.
3. Gravity effects can be neglected
4. Initial fluid distributions must be duplicated.
5. The relative permeability functions must be the same for the matrix blocks and the laboratory tests.
6. Capillary pressure functions must be proportional to each other.

Their proposed equation was given as:

$$t_{D,MK} = Ct\sqrt{\frac{k}{\varphi}\frac{\sigma}{\mu_w}\frac{1}{L^2}} \tag{21}$$

Where $t_{D,MK}$ is a dimensionless time. C is a units conversion factor which is 0.018849 if the imbibition time t is in minutes, k the permeability is in milllidarcy (mD), φ the porosity, σ the interfacial tension is in dyn/cm, μ_w the water viscosity is in cP and L a characteristic length in cm (Mattax and Kyte, 1962).

A more generalized version of the scaling group by Mattax and Kyte (1962) was developed by Ma et al. (1997) for counter-current spontaneous imbibition. After revising the definition of characteristic length and including the effects of viscosity ratio, the presented equation was:

$$t_{D,MMZ} = t\sqrt{\frac{k}{\varphi}}\frac{\sigma}{\sqrt{\mu_o\mu_w}}\frac{1}{L_C^2} \tag{22}$$

Here, the characteristic length, L_c, is given as:

$$L_C = \sqrt{\frac{V_b}{\sum_{i=1}^{n} A_i / l_{A_i}}} \tag{23}$$

where l_{Ai} is the distance that the imbibition front travels from the imbibition face to the no-flow boundary, V_b is the bulk volume of the matrix, A_i the area open to imbibition with respect to the ith direction, and n is the total number for surfaces open to imbibition.

The equation was applied to data sets from Mattax and Kyte (1962), Hamon and Vidal (1986) and (Zhang et al., 1996), and a good correlation was shown. The comparison is shown in Figure 8.

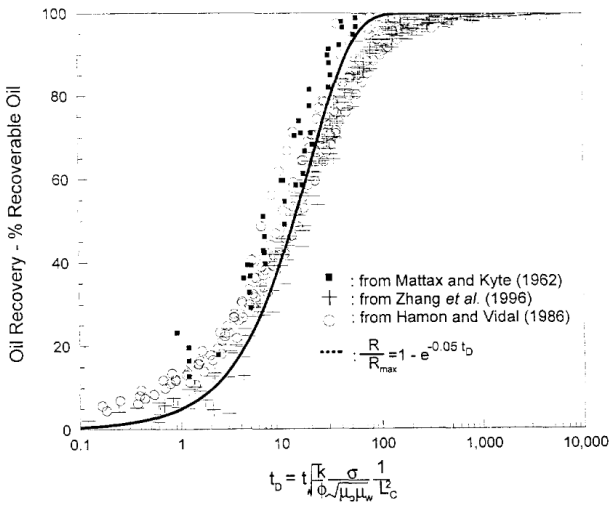

Figure 8: A generalized correlation of data from Mattax and Kyte (1962), Hamon and Vidal (1986) and Zhang et al. (1996) and a single parameter model to fit to all data (Ma et al., 1997).

1.3.3 Effects of boundary conditions

In the study of spontaneous imbibition, several different boundary conditions have been investigated. The choice of which boundary conditions to apply determines the solution to the continuum equations that describe the process, and because they are one of the things experimentalist can control, they are very important to understand (Mason and Morrow, 2013). There are mainly four possible boundary conditions, see Figure 9.

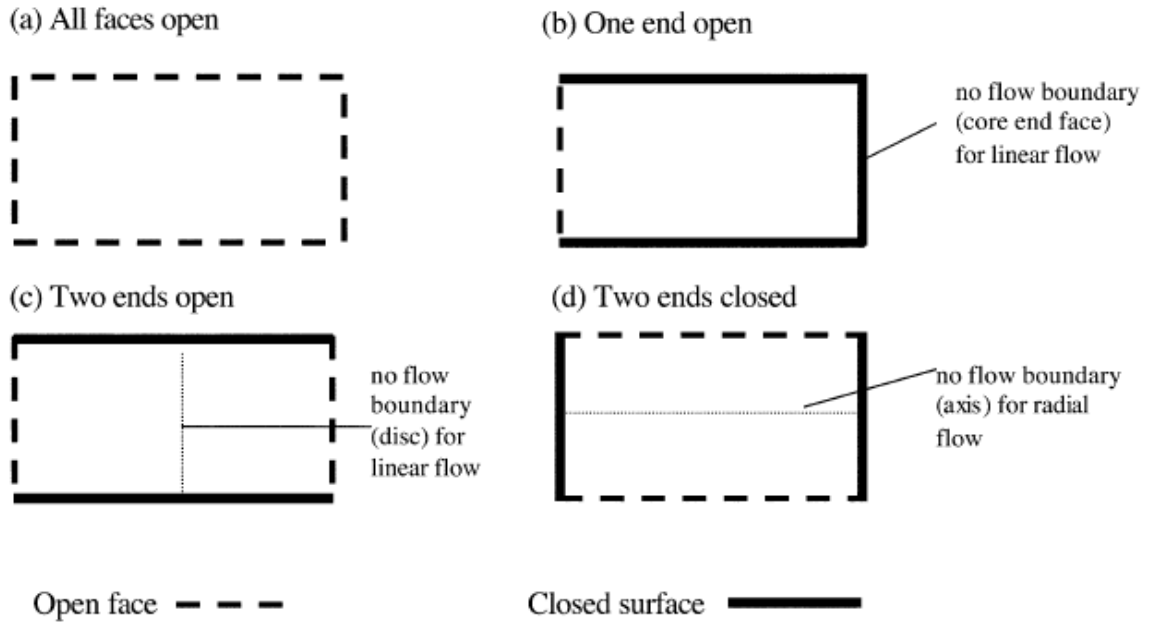

Figure 9: Boundary conditions used for core samples during spontaneous imbibition. a) All faces open (AFO), b) One end open (OEO), c) Two ends open (TEO), and d) Two ends closed (TEC). From (Morrow and Mason, 2001).

Traditionally, all faces open (AFO) has been the most used boundary condition as it easy to perform and appears to give the most reproducible results. Although it is easy to perform it consist of both counter- and co-current flow, and thus it is hard to describe the process with the current established differential equations (Meng et al., 2015).

This thesis will focus on spontaneous imbibition with the two ends open (TEO) boundary condition. This condition was initially believed to have a no flow boundary at the middle of the core sample (see Figure 9c), and that the non-wetting phase would produce purely counter-currently at each open end. However, Mason et al. (2010) and Wickramathilaka et al. (2011) showed that production of the non-wetting phase (oil) was asymmetrical at each face even though invasion of the wetting phase (water) was symmetric. This means that some of the oil had to cross the no-flow boundary at the middle of the core. Mason et al. (2010) attributed the asymmetrical production of oil to small differences in the capillary back pressure, caused by non-uniformities in the core properties. Experiments on TEO spontaneous imbibition in cores set vertically performed by Wickramathilaka et al. (2011) supported this theory. They showed that the front was established at the same end face of the core regardless of the core orientation.

A special form of TEO spontaneous imbibition, termed two ends open free spontaneous imbibition (TEOFSI) by Dong et al. (1998), was studied by Haugen et al. (2014). Here, spontaneous imbibition was conducted with one end of the core in contact with the wetting phase (brine), and the other in contact with the non-wetting phase (oil). The production of oil was measured at each end. Oil production always started at both ends, but counter-current production at the end face open to brine ceased after some time. Afterwards, brine continued to enter at one end, and oil produced at the other. The reason for this behaviour was that oil production at the end face in contact with brine was opposed by the capillary back pressure in the brine, while the end face in contact with oil had zero capillary back pressure. Following the end of counter-current production, a purely co-current flow regime was established, and thus piston-like displacement could be assumed.

1.3.4 Pressures acting during spontaneous imbibition

Haugen et al. (2014) described theory of pressures acting during spontaneous imbibition with OEO and TEO boundary conditions. Figure 10 a) shows the pressures acting during spontaneous imbibition of brine into a core saturated with oil, where one end is open to flow, and the other is closed. Here, P_w is the brine pressure, x_f is the front position, $P_{nw,f}$ is the pressure in the non-wetting phase at the front, $P_{w,f}$ is the pressure in the wetting phase at the front, $P_{c,f}$ is the effective capillary pressure at the front and $P_{c,o}$ is the capillary back pressure at the open face. Ahead of the front a positive oil pressure forms. This pressure is equal to the sum of the capillary back pressure at the open face and the pressure required of the oil to flow counter-currently. However, if the closed end is opened, the oil will flow co-currently and a pressure gradient will form in the oil ahead of the front, as shown in Figure 10 b). Counter-current production is dependent on the capillary back pressure. The closer the front is to the brine open face, and the more viscous the oil is, the more likely it is for counter-current production to continue (Haugen et al., 2014). Figure 10 b) shows the pressures acting during two ends open free spontaneous imbibition. Brine enters at one end only, but oil can be produced at both ends. For the oil to be produced counter-currently at the face open to brine, the oil pressure must exceed the capillary back pressure. How much of the total oil produced counter-currently is affected by several factors, but if the oil has a lower viscosity compared with the brine, little oil is produced counter-currently (Haugen et al., 2014).

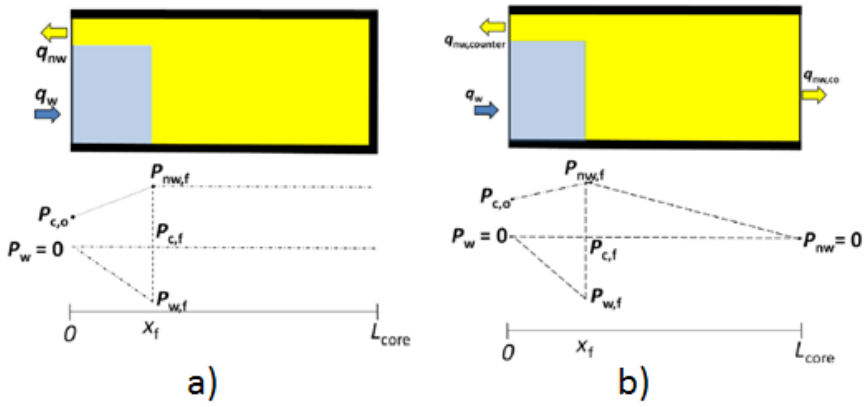

Figure 10: Schematic of pressures acting with a) one-end-open spontaneous imbibition, and b) two ends open free spontaneous imbibition (TEOFSI). Figure taken from Haugen et al. (2014).

1.3.5 Piston-like co-current displacement

Building on the established differential equations described in chapter 1.3.1, Haugen et al. (2014) described co-current imbibition in porous media with TEOFSI boundary condition:

If piston-like displacement is assumed, with constant saturation behind the front, Darcy's law describes the flow of the wetting and the non-wetting phases:

$$q_w = -\frac{K k_w A}{\mu_w}\frac{\left(P_{w,f} - 0\right)}{\left(x_f - 0\right)} \tag{24}$$

$$q_{nw} = -\frac{K k_{rnw} A}{\mu_{nw}}\frac{\left(0 - P_{nw,f}\right)}{\left(L_{core} - x_f\right)} \tag{25}$$

Where K is the absolute permeability, k_w and k_{rnw} are the relative permeabilities, A is the area, L_{core} is the length of the core and x_f is distance advanced by the front.

The capillary pressure at the imbibition front ($P_{c,f}$) is the difference between the pressure in the non-wetting phase ($P_{nw,f}$) at the front and the pressure in the wetting phase ($P_{w,f}$) at the front:

$$P_{c,f} = P_{nw,f} - P_{w,f} \tag{26}$$

For co-current displacement the rate of the non-wetting phase (q_{nw}) must be equal and opposite to the rate of the wetting phase (q_w):

$$q_w = -q_{nw} \tag{27}$$

The conservation of volume requirement for the advance of the front gives

$$\frac{dx_f}{dt} = \frac{q_w}{\varphi A\left(S_{wf} - S_{wi}\right)} \tag{28}$$

Where φ is the porosity, S_{wf} is the saturation of the non-wetting phase behind the front and S_{wi} is the saturation ahead of the front. The solution of these equations is similar to the equations for a single capillary tube in chapter 1.3.1. Integrating from $x_f = 0$, $t = 0$ to x_f at time t gives

$$\frac{x_f^2}{L_{core}^2} + 2\frac{{\mu_{nw}}/{k_{nw}}}{\left(\left({\mu_w}/{k_w}\right) - \left({\mu_{nw}}/{k_{nw}}\right)\right)}\frac{x_f}{L_{core}} = \frac{2KP_{c,f}}{\varphi L_{core}^2\left(S_{wf} - S_{wi}\right)}\frac{1}{\left(\left({\mu_w}/{k_w}\right) - \left({\mu_{nw}}/{k_{nw}}\right)\right)}t \tag{29}$$

The pressure in the non-wetting phase ahead of the front is given by

$$\frac{P_{nw,f}}{P_{c,f}} = \frac{1}{1 + (\mu_w/k_w)(k_{nw}/\mu_w)\left(1/\left(\left(L_{core}/x_f\right) - 1\right)\right)} \tag{30}$$

$$\text{Let } \left(\frac{1}{((\mu_w/k_w)(k_{nw}/\mu_w)-1)}\right) = D \tag{31}$$

For a core saturated with non-wetting phase, the relative permeability ahead of the front (k_{nw}) is 1. In addition, μ_w and μ_{nw} can be measured separately. This leads to if D can be determined, k_w can be calculated.

Substituting and adding D^2 to each side of equation 29 gives

$$\frac{x_f^2}{L_{core}^2} + 2D\frac{x_f}{L_{core}} + D^2 = D^2 + \frac{2KP_{c,f}}{\varphi L_{core}^2(S_{wf}-S_{wi})}\frac{1}{\left(\left({\mu_w}/{k_w}\right)-\left({\mu_{nw}}/{k_{nw}}\right)\right)}t \tag{32}$$

Which can be simplified to give

$$\left(\frac{x_f}{L_{core}} + D\right)^2 = D^2 + \frac{2KP_{c,f}}{\varphi L_{core}^2(S_{wf}-S_{wi})}\frac{1}{\left(\left({\mu_w}/{k_w}\right)-\left({\mu_{nw}}/{k_{nw}}\right)\right)}t \tag{33}$$

Now let

$$\frac{2KP_{c,f}}{\varphi L_{core}^2(S_{wf}-S_{wi})}\frac{1}{\left(\left({\mu_w}/{k_w}\right)-\left({\mu_{nw}}/{k_{nw}}\right)\right)} = E \tag{34}$$

This gives

$$\left(\frac{x_f}{L_{core}} + D\right)^2 = D^2 + Et \tag{35}$$

For a single displacement with constant fluid and core properties, D and E will be constants, and thus equation 35 can be solved to give

$$\frac{x_f}{L_{core}} = \sqrt{D^2 + Et} - D \tag{36}$$

Equation 36 now gives the expected position of the front at a given time *t*. If plotted against the experimentally measured position of the front, a value for *D* which makes a plot with a straight line can be found. After D has been found, a value of E can be determined that gives a gradient of unity. Due to the relative permeability being 1 ahead of the front (assuming a fully saturated sample), and that the fluid viscosities can be measured, the fitted value D and equation 31 can be used to find the relative permeability to brine behind the front, k_w. If the remaining values (φ, L_{core}, S_{wf}, S_{wi}, K, μ_w and μ_{nw}) can be measured, the fitted value of E along with equation 37 can be used to find the capillary pressure at the front, $P_{c,f}$.

$$P_{c,f} = E\frac{\varphi L_{core}^2(S_{wf}-S_{wi})}{2K}\left(\frac{\mu_w}{k_w} - \frac{\mu_{nw}}{k_{nw}}\right) \tag{37}$$

1.3.6 Entrapment of non-wetting phase during spontaneous imbibition

Meng et al. (2015) conducted spontaneous imbibition experiments using TOEFSI boundary conditions. Glass tubes were filled with either quartz sand or glass beads. The geometry of the glass beads was regular with a narrow size distribution and the quartz sand was irregular with a wide size distribution. By adding a 1 mm thick slice of low-permeability sandstone at the inlet, the capillary back pressure was raised to avoid counter-current production of oil. In addition, a wire mesh was placed at the inlet in order to hold the sand or glass beads in the tube at the inlet side. In order to ensure that the entire cross-section was in contact with brine, and to hold the wire mesh and sandstone, an end piece mounted on the inlet. In order for air to be removed from the end piece, a vent was punched at the top of the end piece. The outlet end of the glass tube was sealed with a rubber stopper. Figure 11 shows a schematic of the glass tube containing glass beads or sands.

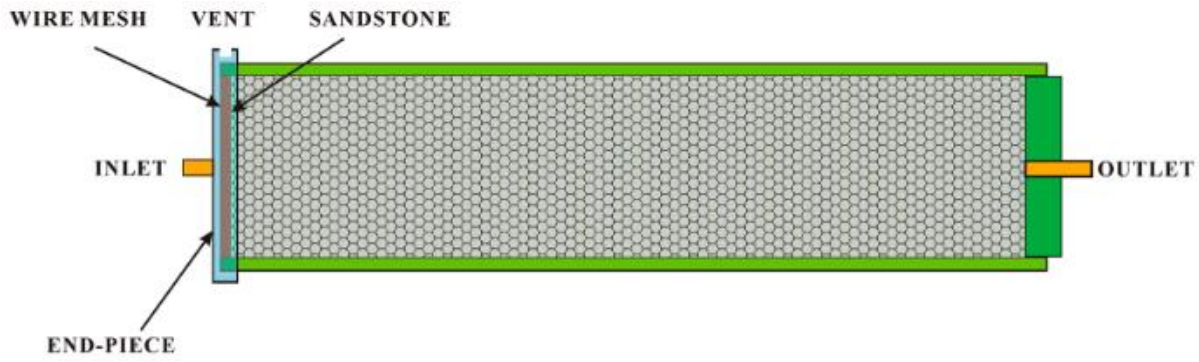

Figure 11: Schematic taken from Meng et al. (2015) showing the glass column containing either glass beads or quartz sand.

The tubes were filled with the same amount of either glass beads or quartz sand, around 49.5±0.2g and 53.0±0.2g for a 40cm column, respectively. This way the porosities were the same for all the packed columns. Measurements showed that the porosity was 36.2% for the glass-bead-packed columns and 34.2% for the quartz-sand-packed columns. Permeability was measured using nitrogen and it was shown that the glass-bead-packed columns had a permeability of 3450 x 10^{-3} μm^2 (±3%) and the quartz-sand-packed columns had a permeability of 2450 x 10^{-3} μm^2 (±3%). The packed columns were either saturated 100% with oil under vacuum after purging the air with CO_2, or experiments were run with air as the non-wetting phase. The wetting phase in all the experiments was synthetic brine (1 cP). The oils used were kerosene (2.8 cP), white oil-15 (25.6 cP) and white oil-32 (103.4 cP). Before being used in the experiments they were filtered through a column of alumina and silica gel in order to remove polar components that may affect the wetting properties of the oil. The outlet tube was filled with air for air-brine experiments and oil for oil-brine experiments. After the imbibition started, time, production and position of the front was recorded. Figure 12 shows the full apparatus for both a) air-brine experiments and b) oil-brine experiments. The main difference between the setups is how the production is measured.

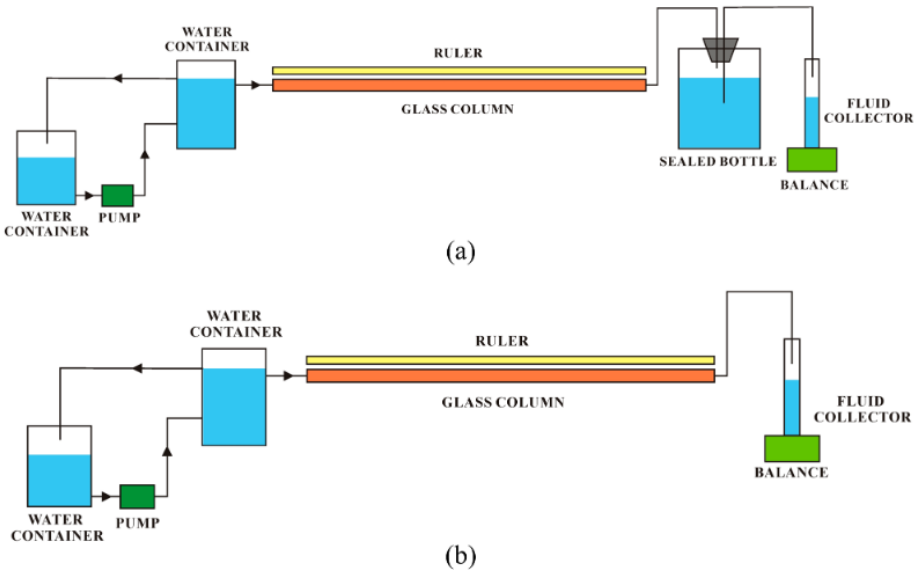

Figure 12: Schematic from Meng et al. (2015) showing the full apparatus used in the experiments. a) Shows the apparatus for air-brine experiments and b) shows the apparatus for oil-brine experiments.

Meng et al. (2015) measured fractional oil and gas recovery and plotted it versus during time, see Figure 13. The results showed that pore size distribution has a significant impact on the entrapment of oil during spontaneous co-current imbibition. In the experiments with glass beads, which had a narrow size distribution, the magnitude of entrapment had no significant correlation with viscosity of the non-wetting phase. However, for the experiments with quartz sand, which had a wider size distribution, the magnitude of entrapment increased rapidly with increase in the viscosity of the non-wetting phase. For flow in multiple capillary tubes, the meniscus in the smaller pores will move faster than the meniscus in the larger pores, if the porous media has a non-uniform pore size distribution (Dong et al., 1998, Unsal et al., 2007). As the meniscus advances in the small pore and reach a pore throat, the pore throat will, due to its large curvature, quickly be filled with the wetting phase. This will in turn lead to snap-off in the large pore and the non-wetting phase may be trapped (Meng et al., 2015). As the viscosity of the non-wetting phase is increasing, the difference in rate of advance between the smaller pores and the larger pores increases (Dong et al., 2006), and thus a larger portion of the non-wetting phase is trapped. On the contrary, if a porous media has a narrow pore size distribution, the rate of advance will not differ as much between the larger pores and the smaller pores. This will lead to a smaller portion of the non-wetting phase being trapped, and therefore the effect of viscosity on entrapment of the non-wetting phase will be less apparent (Meng et al., 2015).

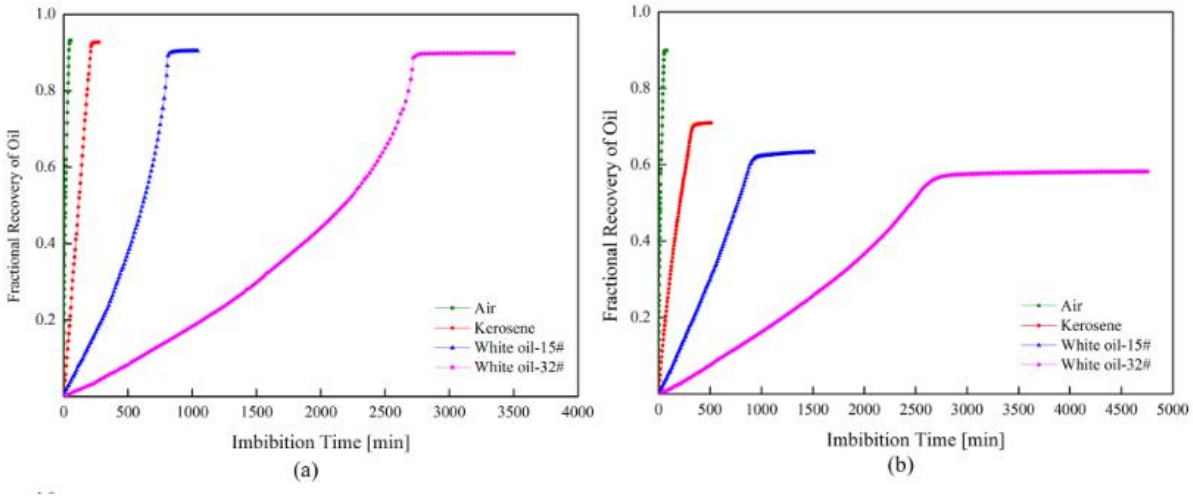

Figure 13: Experimental results from Meng et al. (2015) showing fractional recovery of oil during spontaneous imbibition in a) glass bead packs and b) quartz sand packs. The wetting phase was brine in all experiments, and the non-wetting phase was either air or different oils.

In addition to measuring the effects of viscosity on entrapment, Meng et al. (2015) applied the theory provided by Haugen et al. (2014) (described in chapter 1.3.5), in order to calculate the capillary pressure ($P_{c,f}$) at the imbibition front, as well as the relative permeability (k_w) behind the imbibition front. An assumption was made that the average water saturation was always equal to the value when the imbibition front reached the end of the pack, as this made the calculation easier. By plotting measured x_f versus the calculated x_f, a straight line with a gradient of unity could be obtained by adjusting the values of D and E, see equation 36. During the process, E was kept constant and D was adjusted until the total calculated imbibition time was equal to the total measured imbibition time. After D was found, the value of E that gave the curve a straight line was found. Lastly, the relative permeability to brine behind the front could be calculated. The results showed that the relative permeability to brine behind the front had no significant variation with the increase in non-wetting phase viscosity for glass-bead-packed columns. However, the relative permeability decreased with increasing viscosity for the quartz-sand-packed columns. It was believed that the reason for this was the difference in magnitude of entrapment between the glass-bead- and the quartz-sand-packed columns (Meng et al., 2015). The relative permeability to brine behind the imbibition front for the different experiments is plotted in Figure 14.

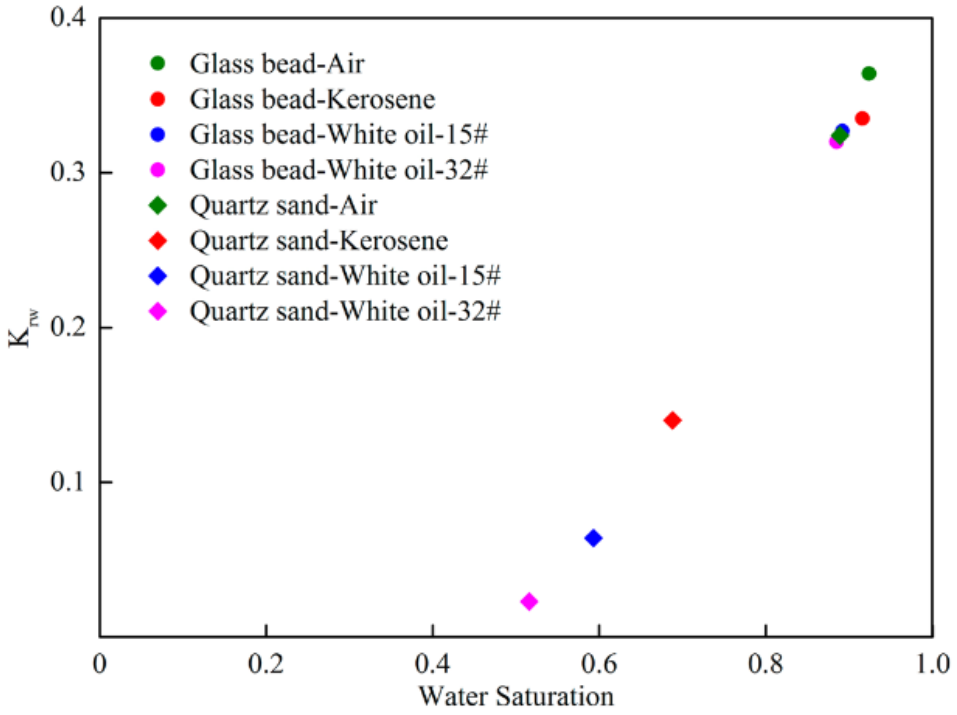

Figure 14: Calculated relative permeability to brine behind the front plotted against average water saturation when the imbibition front reached the end for both glass-bead- and quartz-sand-packed columns. From (Meng et al., 2015).

2 Methods and experimental setups

2.1 Fluids and sample materials

2.1.1 Oils

For the experimental work in this thesis, three different mineral oils were used: Decane 95%, Marcol 82 and DTE FM 32. The mineral oils were filtered in order to remove surface active components that may alter the wettability of the samples, similar to the filtration technique used by Fernø et al. (2013). The column consisted of glass wool, aluminium oxide and silica gel, see Figure 15. Silica gel and aluminium oxide adsorbed the polar components and the glass wool kept the adsorbing components from exiting the glass funnel. Densities of the filtered oils were measured after removal of air by filling 500±0.25 ml volumetric flasks and recording the weight. The oil viscosity was measured using a rotational viscometer (Brookfield DV-II+ Pro). The properties of the mineral oil are given in table 3.

Table 3: Mineral oil properties.

Oil	Weight of 500ml (g)	Density, ρ (g/cm^3)	Viscosity, μ (cP)
Decane 95%	363.16±0.01	0.726±0.001	0.96±0.01
Marcol 82	422.13±0.01	0.844±0.001	32.6±0.20
DTE FM 32	425.66±0.01	0.851±0.001	73.2±0.70

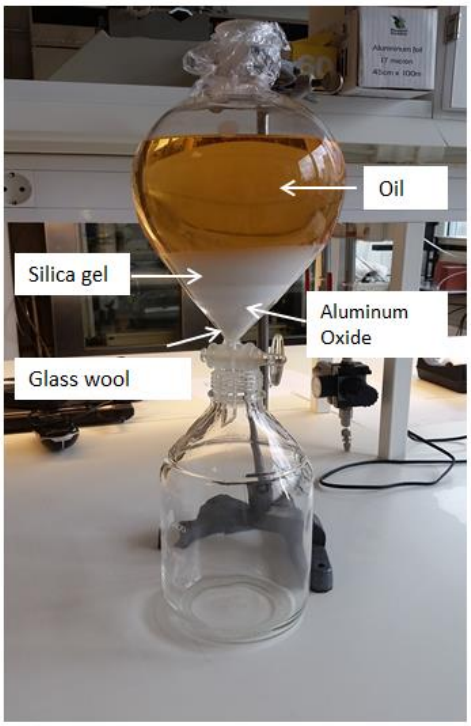

Figure 15: Filtration of oil with a sepatory funnel filled with silica gel, aluminium oxide. The glass wool prevents the adsorbing components to flow with the oil into the beaker below.

2.1.2 Brine and polymer preparation

Brine has been used as the wetting phase in all spontaneous imbibition tests in this thesis. Basis brine was prepared by adding 50g NaCl per litre (equivalent to 0.856M) of distilled water. 0.5ml NaN_3 was added after 10 litres of brine had been prepared to prevent bacterial growth.

To study the effects of viscosity ratio on spontaneous imbibition, polymer and glycerol was added to the brine. Glycerol has been previously used to viscosify the wetting phase to adjust the oil/water viscosity ratio (Kyte and Rapoport, 1958, Rapoport and Leas, 1953, Fischer and Morrow, 2006). Glycerol is an odor- and colourless fluid which is soluble in water in all proportions and insoluble in hydrocarbons. The viscosity for glycerol mixed with water varies non-linearly from 1 cP for pure water, to 1650 cP for pure glycerol at 20º C (Fischer and Morrow, 2006). Table 4 shows the physical properties of the mixtures used in this thesis. Basis brine had a viscosity of 1.15±0.02 cP, while the brine/glycerol mixture had a viscosity of 28.3±0.7 cP.

Table 4: Physical properties of the brine and brine/glycerol mixture used as the wetting phase during spontaneous imbibition.

Brine	Density, ρ (g/cm^3)	Viscosity, μ (cP)
0 wt% glycerol	1.034±0.001	1.15±0.02
70 wt% glycerol	1.203±0.001	28.3±0.70

The polymer used was a hydrolysed polyacrylamide (HPAM) called Alcoflood 935, which is a water-soluble polymer in powder form. The following procedure was followed to dissolve the powder in brine at 5000ppm (0.5 wt%) concentration to increase aqueous phase viscosity:

1. Water was weighed in a beaker using a scale.
2. A vortex was created in the beaker using a magnetic stirrer, and the polymer powder was added gradually in order to prevent lumping of the polymer molecules (see Figure 16).
3. After all of the polymer was added, the solution was stirred overnight.

As more polymer powder was added to the solution, the viscosity of the solution increased. This was observed through the size of the vortex created in the beaker. As the viscosity of the polymer solution increased, the vortex would become gradually smaller, as shown in Figure 16. In order to keep the vortex in the beaker, the intensity of the magnetic stirrer was increased gradually.

The viscosity of the polymer solution was measured using a rotational viscometer (Brookfield DV-II+ Pro). A total of three samples were taken from the tank used to contain the wetting phase during the two spontaneous imbibition tests where polymer was used as the wetting phase. Sample 1 was collected from the tank before the first spontaneous imbibition test, sample 2 was collected between the two tests, and sample 3 was collected after the last test was finished, see Figure 17. The viscosity was measured on several different speeds (2, 4, 10, and 12 rpm). Due to the shear thinning behaviour of the polymer, the viscosity decreased with increased rpm. In addition, the viscosity decreased with time. This is believed to be due to evaporation of the solution, although plastic foil covered the tank to prevent it.

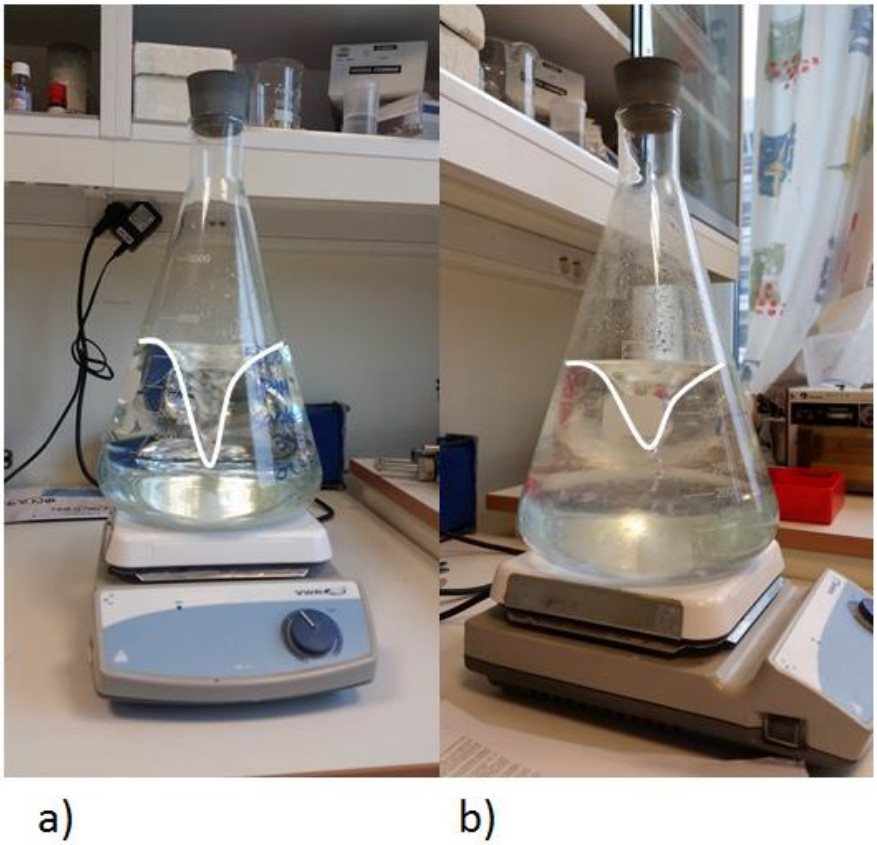

Figure 16: Polymer preparation. a) After about 2 grams of polymer powder added b) After approximately 15 grams of polymer powder added. As more polymer powder was added, the size of the vortex would decrease. At the left picture the magnetic stirrer is at 2/6 strength. At the right picture the magnetic stirrer is at full strength.

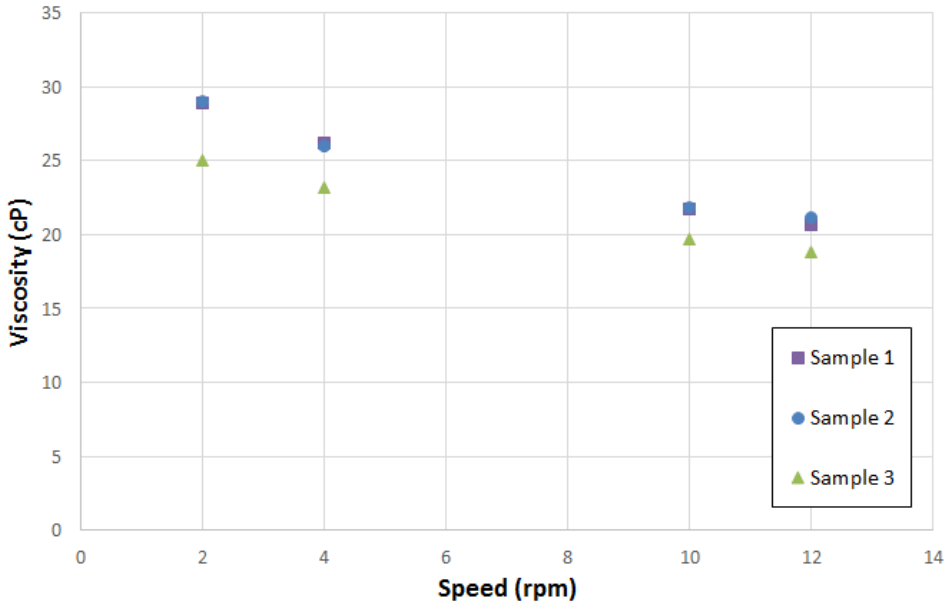

Figure 17: Measured polymer viscosity at different rotation speeds. A total of three samples were collected from the tank containing the wetting phase during the two spontaneous imbibition tests. Sample 1 was collected before the first experiment, sample 2 was collected between the two tests, and sample 3 was collected after the last test was finished.

2.1.3 Sand and glass bead preparation

In order to get a homogeneous packing of sand, geological sieves were used to control the grain size of the sand, see Figure 18. A batch of quartz sand with grainsize <5000µm was sifted out to a grain size of 212-250µm. Further, the sand was fired in a furnace to ensure that the grains were strongly water-wet. The procedure followed these steps:

1. Two sieves with a mesh size of 212 and 250µm were stacked on a sample collector. 2-3 dl of sand was added in the top sieve and the stack was shaken. After some time the top sieve (250µm) was removed and the remaining 212µm sieve was shook for a sufficient amount of time. Only the sand remaining in the 212µm sieve was collected. After a while the sieves started to get plugged with sand grains. In order to remove the trapped sand, compressed air was blown though the sieves. This process was repeated until enough sand was collected.
2. In order to improve the sieving the sand was sifted using water. Again, two sieves with mesh size 212 and 250µm was stacked on a closed sample collector. After adding 1-2 dl sand in the top sieve, water was sprinkled with a shower head. This was done in order to remove the silt and clay which was stuck on the sand grains.
3. The sand was dried at 80 °C for 5 days in a heating cabinet.
4. Lastly, the dry sand was fired at 200 °C for five hours in a furnace.

Figure 18: Geological sieves used during sieving of sand. One sieve had a mesh size of 250 µm, whereas the other had a mesh size of 212 µm.

In order to study the effect of pore size distribution, glass beads were used as the porous media during spontaneous imbibition. In contrast to the sand used, the glass beads had a high degree of sphericity, with well rounded edges, and a size distribution from 150-212µm. Before use, the glass beads were washed with hydrochloric acid, as instructed by the supplier. After being washed with hydrochloric acid, the glass beads were placed in a glass funnel containing a paper filter, and washed with distilled water until the effluent had a neutral pH. Lastly, the glass beads were dried in a heating cabinet at 60 ºC for 4 days.

Initially, it was planned to conduct spontaneous imbibition experiments similar to the experiments conducted with quartz sand, using oils with different viscosity. Unfortunately, only 1 experiment was conducted, using brine as the wetting phase, whereas decane was used as the wetting phase.

2.2 Experimental setups

2.2.1 The imbibition tube

In order to study the front during co-current spontaneous imbibition, glass tubes filled with sand were used, similar to Meng et al. (2015). Initial studies conducted in collaboration with Vabø (2016), described in detail below, showed that imbibition tubes with a glass filter embedded at the inlet added an additional resistance to flow. As a result, imbibition tubes without the embedded filter were used instead. The imbibition tubes were 50 cm long with an inner diameter of 20.4mm. At each end there was an area with glass threads (GL25) on the outer circumference, which enabled the use of an end piece at the inlet end. The end piece held in place a paper filter, which was in capillary contact with the sand in the tube. An end piece made of polyoxymethylene (POM) used at the inlet, shown in Figure 20, was machined with internal threads (GL25). Note that the pore size of the filter was not measured. Further, grooves were machined into the end piece in order to hold a rubber O-ring, which sealed around the paper filter. The rubber O-ring had a diameter of 46 mm and they were 3 mm thick. A metal grid was added to support the fragile paper filter during experiments and sample preparation. A POM spacer with an internal diameter of 22 mm was held in place with three screws to keep the parts together. Thread sealing tape was used in order to get the end piece firmly in place on the tube. The end piece was placed so that the end of the imbibition tube was aligned with the end piece.

Figure 19: Imbibition tube made of glass used in experiments. 50 cm long with an internal diameter of 20.4 mm, and with glass threads (GL 25) at each end.

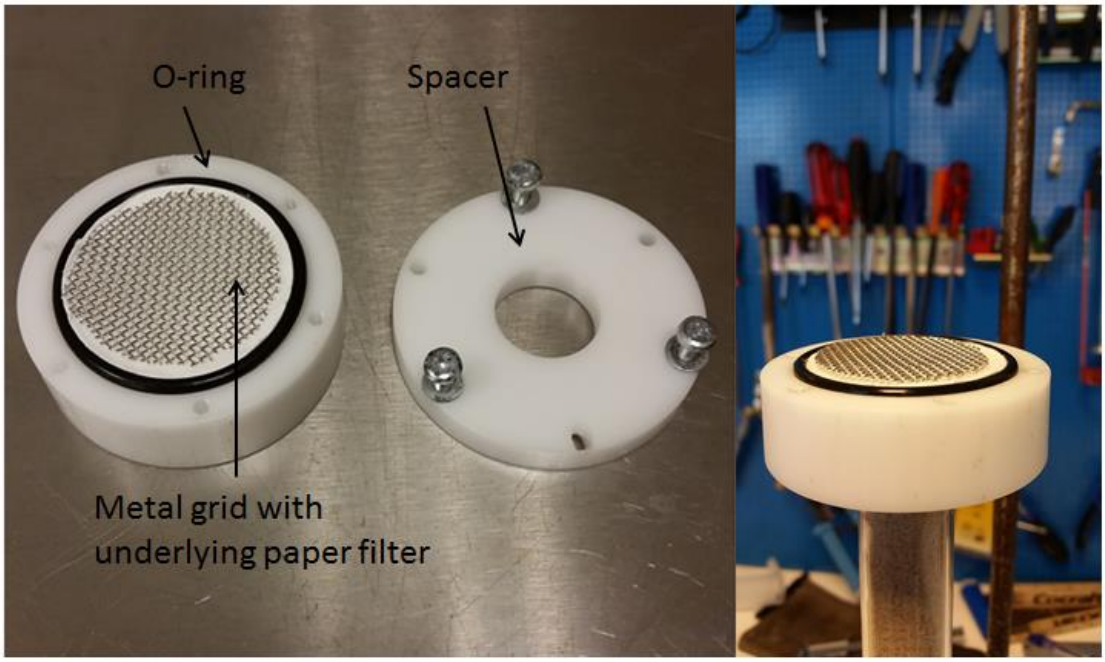

Figure 20: Left: End piece with each of the components; the O-ring, metal grid and spacer. Right: End piece mounted on an imbibition tube.

After mounting the end piece at the inlet end, the imbibition tubes were filled with sand to create the porous media. The imbibition tube was placed vertically with the inlet end at the bottom and about 2-4 cm of sand was poured into the tube from the outlet side. In order to consolidate the sand to a small degree, and to get a homogenous packing, the imbibition tube was tapped gently. This was repeated until the imbibition tube was filled with sand approximately 2 cm from the outlet end. Further, a thin (1-2mm) layer of glass wool was added in order to keep the sand from flowing out of the tube with the fluids. Lastly, an end piece was mounted at the outlet. During the initial experiments (GB1, SP1, SP2 and SP3), conical rubber plugs were pierced with a 1/8 inch stainless tube. In later experiments, the diameter was increased from 1/8 inch to ¼ inch. When air was used as the non-wetting phase, a 90° end piece was used (see Figure 21). When oil was used as the non-wetting phase, a straight end piece with a Swagelok fitting was used. This will be described further below.

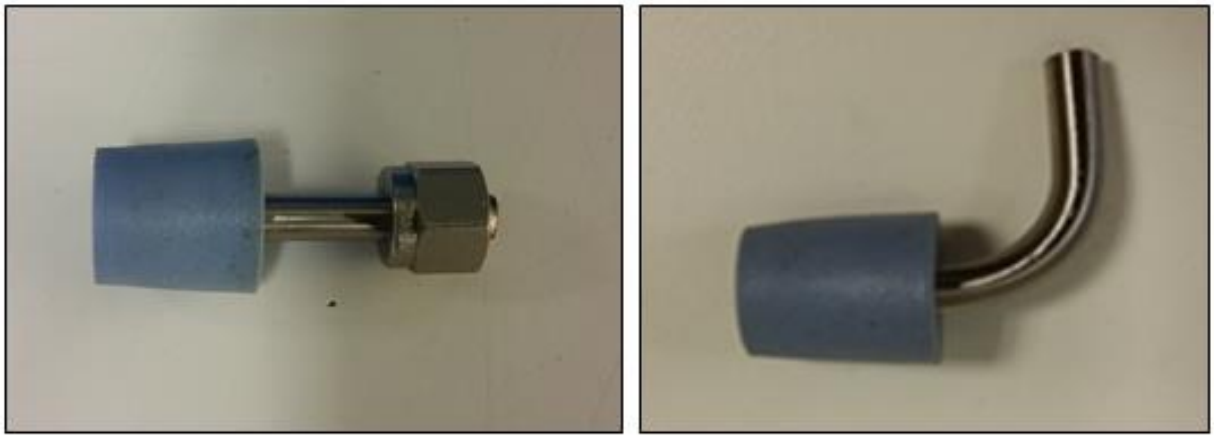

Figure 21: Conical rubber end pieces pierced with 1/4 inch stainless steel tubing. Left: straight end piece with Swagelok fitting. Right: 90° end piece.

During the experiments where air was the non-wetting phase, the imbibition tubes were packed with sand and weighed before the experiment was started. In addition, the weight after imbibition was recorded. For the experiments where oil was the non-wetting phase, the imbibition tubes were packed with sand, and flushed with CO_2, before air was removed under vacuum and saturated with oil. The weight was recorded before and after the sand pack was saturated with oil. To calculate the porosity, the following equation was used;

$$\varphi = \frac{\frac{m_{after} - m_{before}}{\rho_{oil}}}{\pi * (r_{tube})^2 * L_{packing}} \tag{38}$$

Where φ is the porosity of the sand pack, ρ_{oil} is the density of the oil, m_{after} and m_{before} are the weight of the imbibition tube before and after saturating with oil, r_{tube} is the inner radius of the tube and $L_{packing}$ is the length of the sand column inside the tube.

In order to achieve vacuum in the sample a second end piece made of POM was machined (see Figure 22). This was designed with the intention of being used only when saturating the sand packs with oil, and that it could easily be removed before the start of the experiments. A groove was machined into the end piece to support a sealing O-ring, which was placed between the POM spacer and the second end piece. Threads were machined internally in the second end piece in order to support a transition to Swagelok tubing.

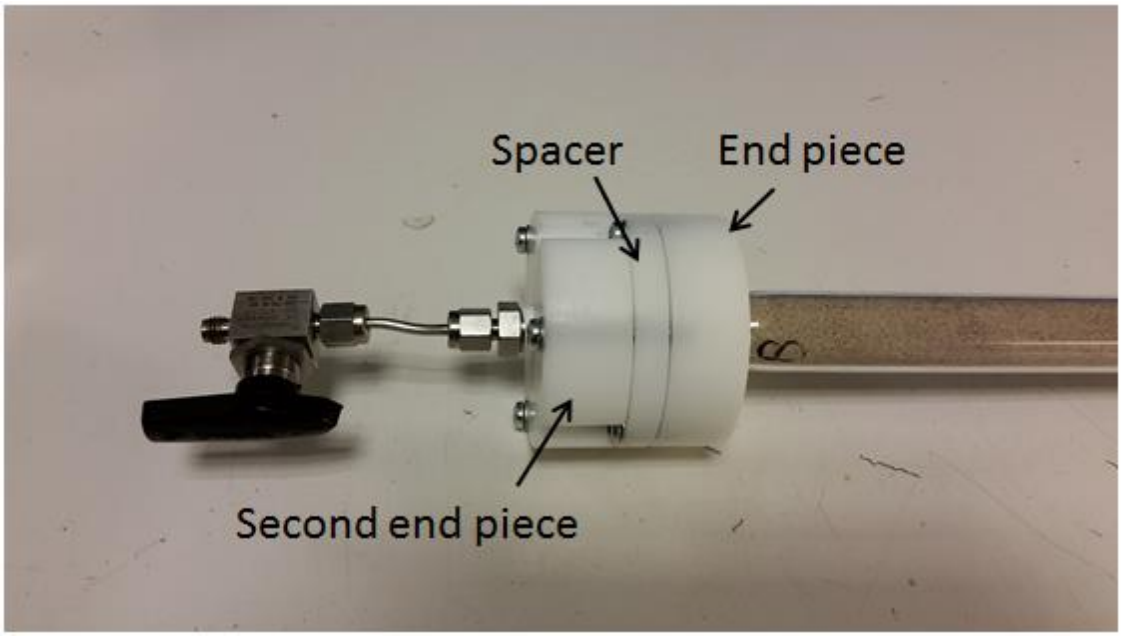

Figure 22: End piece used when saturating the imbibition tube with oil, fastened with three screws. This end piece was designed in such a way that it was easy to remove before starting the experiments.

2.2.2 Experimental setups A, B and C

In collaboration with Vabø (2016), three different setups were used for spontaneous imbibition in unconsolidated porous media. He showed that it was possible to conduct experiments with co-current spontaneous imbibition using glass tubes similar to the ones described in the chapter above. The main difference between the imbibition tubes in the work of Vabø (2016) and the work in this thesis was the removal of a 3 mm thick glass filter embedded at the inlet of the imbibition tube. This filter served as a membrane that prevented counter-current flow during the experiments, see Figure 23. However, as the filter added an additional resistance to flow, it was decided to use a different approach for this thesis. The pore size within the glass filters varied between 40-100 μm and 16-40 μm, but always remained less than the pore size of the sandpacks.

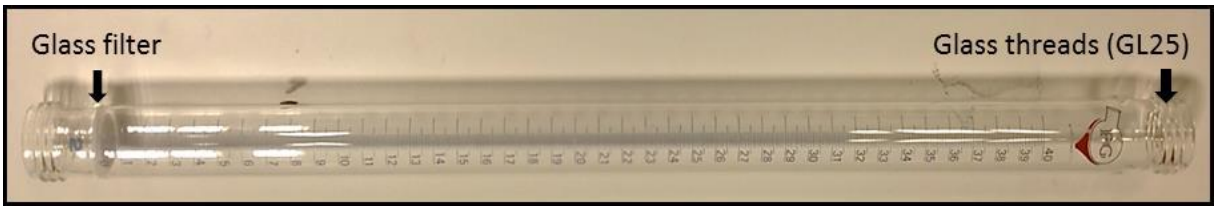

Figure 23: Imbibition tube used by Vabø (2016). Here, a 3 mm thick glass filter was embedded in the tube at the inlet side in order to serve as a semipermeable membrane that prevented counter-current flow.

Initially, experiments were conducted where air or oil was displaced by brine with different viscosities. An experimental setup was made where the non-wetting phase (oil or air) produced from the sandpack during spontaneous imbibition flowed into bulk wetting phase (water) at the outlet, see Figure 24. After successfully achieving piston-like displacement with air as the non-wetting phase, experiments using the oil as the non-wetting phase showed signs of non-piston-like displacement, which in turn led to an analysis regarding the outlet end effects in the experimental setup.

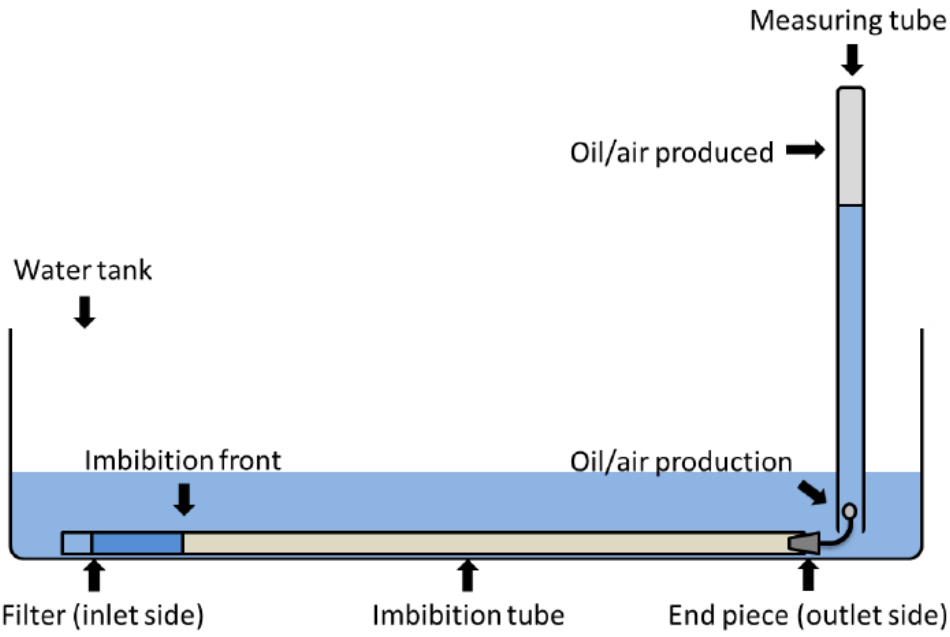

Figure 24: An illustration from Vabø (2016), showing his experimental setup A and B for spontaneous co-current imbibition. Here, the non-wetting phase (oil and air) produced through the wetting phase (water) into a measuring tube.

For the outlet end effects, Vabø (2016) suspected that an additional pressure was required for the oil to produce through the exit tube and into the brine. To test this, an imbibition tube was filled with decane, and placed vertically into a beaker filled with water, see Figure 25. Oil would start to produce at the bottom of the imbibition tube and into the water. After production seized, the height of both the oil column A and the water column B was measured. Further, the tube would be lifted and oil would again start to produce, and the height of the columns was measured once they reached equilibrium. Several tests were conducted and the average additional pressure was calculated to 101 Pa.

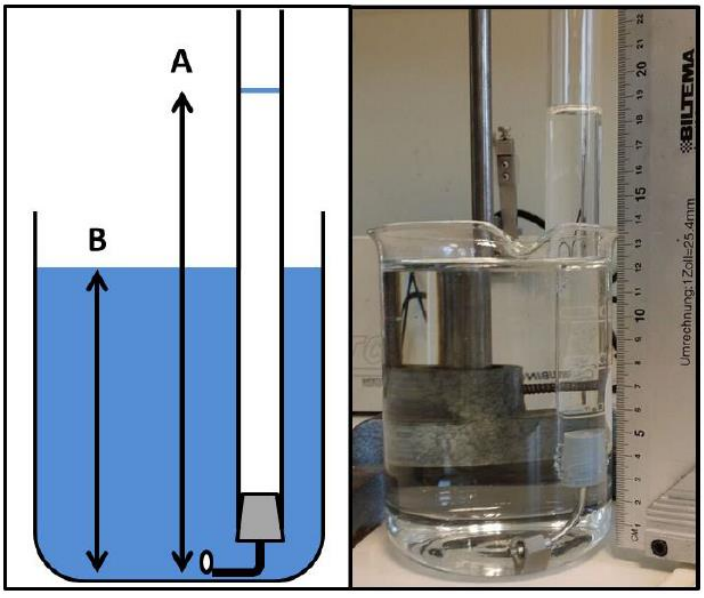

Figure 25: Schematic and picture from Vabø (2016) of setup used to test whether an additional pressure in the oil phase was needed to produce oil through the tubing and into the brine. The height of the oil column (A) and the height of the water column (B) were measured after the system reached equilibrium.

Following the discovery of an additional pressure at the outlet, a new experimental setup (setup C) was made. In the new setup, the inlet side was connected to an external water tank, and the production of the non-wetting phase, i.e. oil, was produced into air at atmospheric pressure, see Figure 26. A POM end piece with internal threads (GL25) connected the imbibition tube to the external water tank.

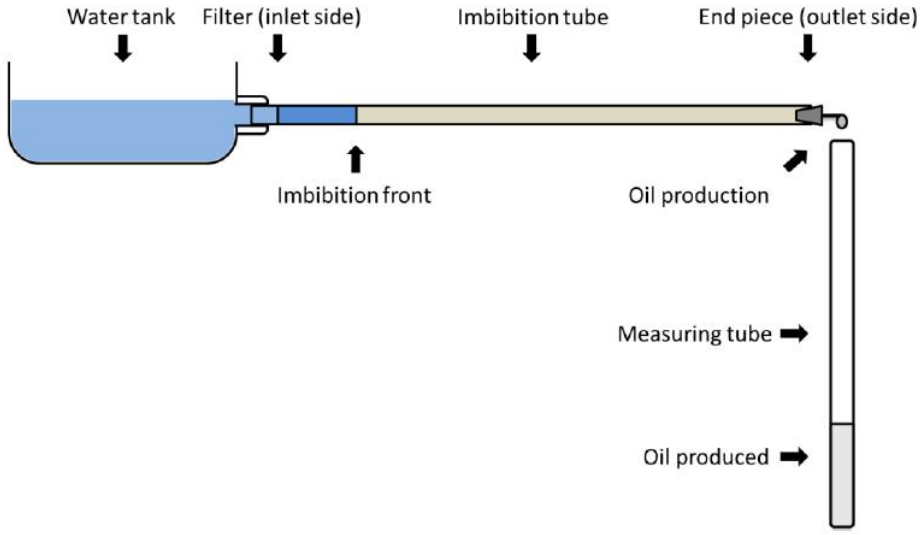

Figure 26: A schematic from Vabø (2016) that shows the experimental setup C, after analysis of the different end effects. Here, water imbibes through the POM end piece into the imbibition tube, and oil is produced into air at the outlet.

2.2.3 Experimental setup D

After running experiments using setup C described above without getting piston-like displacement, it was decided to alter the experimental setup. Instead of having an internal water tank, a new water tank was made from acrylic glass, in which the imbibition tube was lowered. A 16 mm hole was drilled and a stainless steel ¼ inch bulkhead union Swagelok fitting was placed in the hole, see Figure 27. To measure the counter-current production, a measuring tube saturated with the wetting phase (brine, brine/glycerol mixture or HPAM polymer), was placed above the inlet side. During some of the experiments, oil droplets would aggregate on the top of the inlet end piece and float into the measuring tube. The position of the imbibition front was measured using a measuring tape, glued to the inside wall of the tank. The experiments were initiated with the tank dry. First the imbibition tube was connected to the male-male Swagelok connection at the outlet. Afterwards, the second end piece used during saturation of the imbibition tube (shown in Figure 22), was removed. Third, and lastly, the tank was filled with the invading phase, i.e. water or HPAM polymer. To record production at both ends of the imbibition tube, as well as the position of the front, webcams were used.

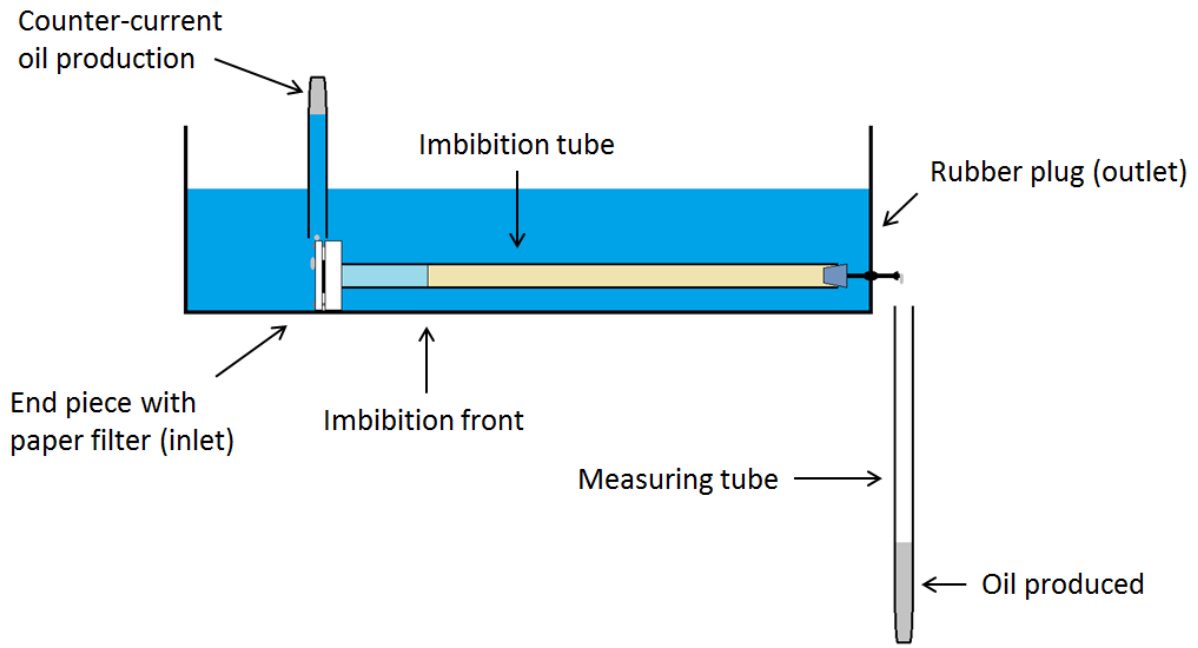

Figure 27: Schematic of experimental setup D for spontaneous imbibition. Water imbibed at the inlet end through the paper filter, and oil produced both counter-currently and co-currently. The imbibition front position and oil production were monitored using webcams.

For experiments where air was displaced by brine, an experimental setup similar to experimental setup A and B in the work of Vabø (2016) was used, see Figure 28. The main difference from his work was the new end piece at the inlet end, which had a lower resistance to flow. The air production was gathered in a measuring tube filled with brine, placed vertically upside down above the outlet rubber plug.

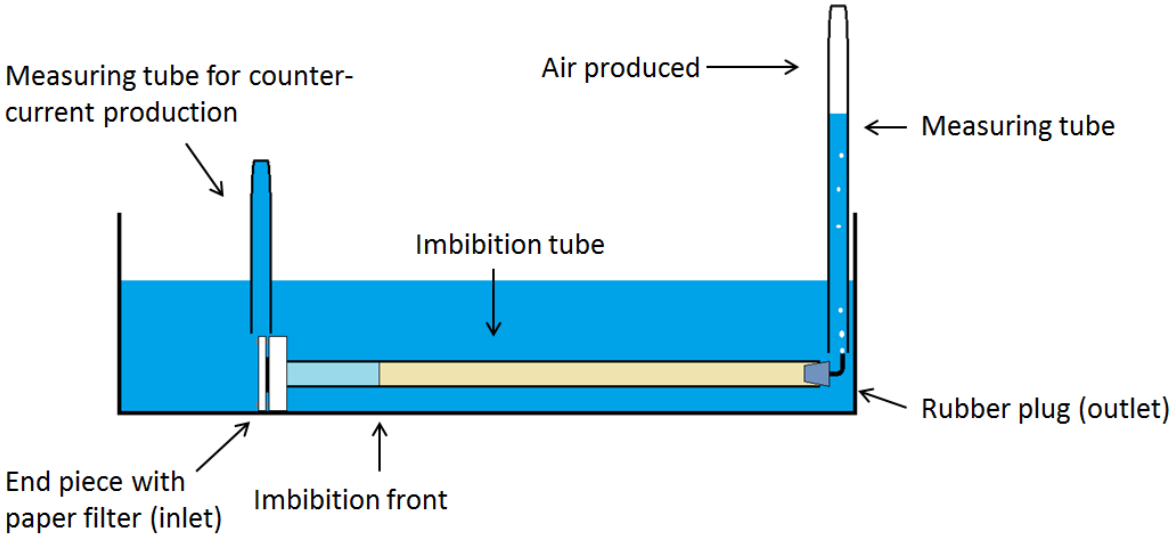

Figure 28: Schematic of experimental setup D used when air was the non-wetting phase. Note the 90° stainless tubing used at the outlet in order to get the production of air into the measuring tube.

3 Results and discussion

3.1 Brine displacing oil in glass beads

3.1.1 Overview and production curves

Following the work of Vabø (2016), one experiment was conducted where spontaneous imbibition was performed in a glass bead pack, using experimental setup C, see Figure 26. Table 5 shows the properties of the imbibition tube used in the experiment. Here, the wetting phase was brine, whereas decane was used as the non-wetting phase.

Table 5: Properties of imbibition tube used during spontaneous imbibition using experimental setup C.

Name	Weight glass beads (g)	Total weight before saturation with oil (g)	Total weight after saturation with oil (g)	Length of the pack (cm)	Porosity (frac)	OOIP (ml)	Cumulative oil production (frac PV)
GB 1	224.9	522.03	564.56	44.4	0.403	58.6	0.487

Figure 29 shows the oil production as a fraction of pore volume plotted versus time, and Figure 30 shows the production rate versus time. Before the imbibition tube was connected to the water tank, brine was poured on the filter in order to saturate it with brine, and to produce oil counter-currently. Less than 0.2ml of oil was produced and only a small area of the filter was saturated with brine. After the experiment was initiated, the rate of oil production was initially high, but decreased as the imbibition continued. However, after about 500 minutes of production, the rate increased again. This increase in rate coincides with fingering of brine through the oil, shown in Figure 32 (note that the pictures in this figure were taken after the experiment was finished). The finger was not visible to the web camera monitoring the front. As a result of the large pocket of oil being bypassed, the total production after 879 minutes was 48.7% of the pore volume. The ultimate recovery was lower than expected, when compared with previous experiments conducted in collaboration with Vabø (2016). Spontaneous imbibition conducted in a sandpack using experimental setup C, with decane as the non-wetting phase, had a recovery of 0.871 (Vabø, 2016). The reason for the low recovery in system GB1 was the unstable front, caused by the fingering of brine.

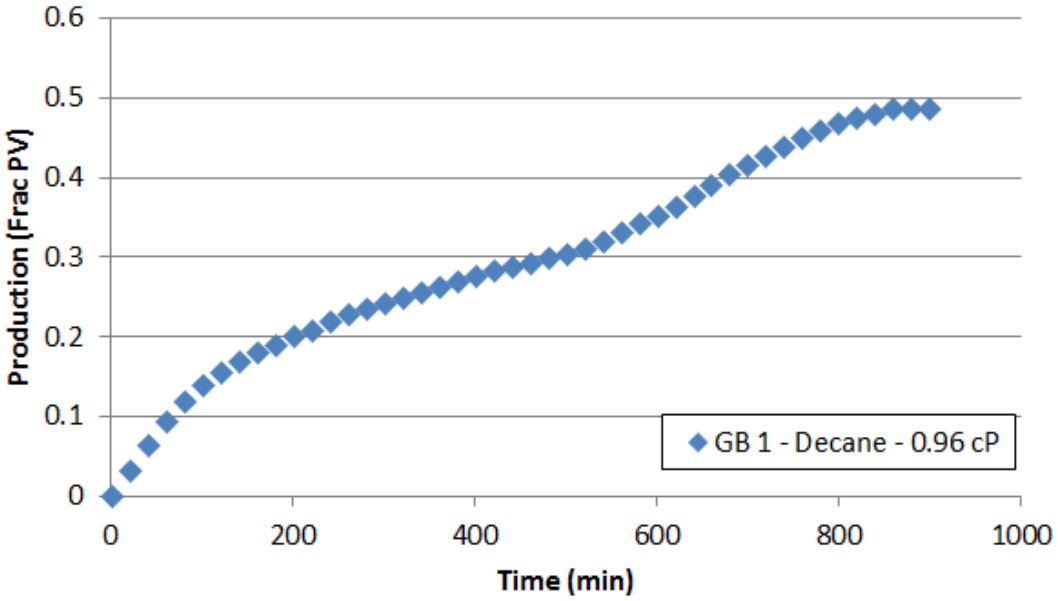

Figure 29: Co-current spontaneous imbibition in glass bead pack with brine (1.15 cP) as the wetting phase and decane (0.96 cP) as the non-wetting phase. This curve shows the production (frac PV) plotted versus time (min) for sample GB1.

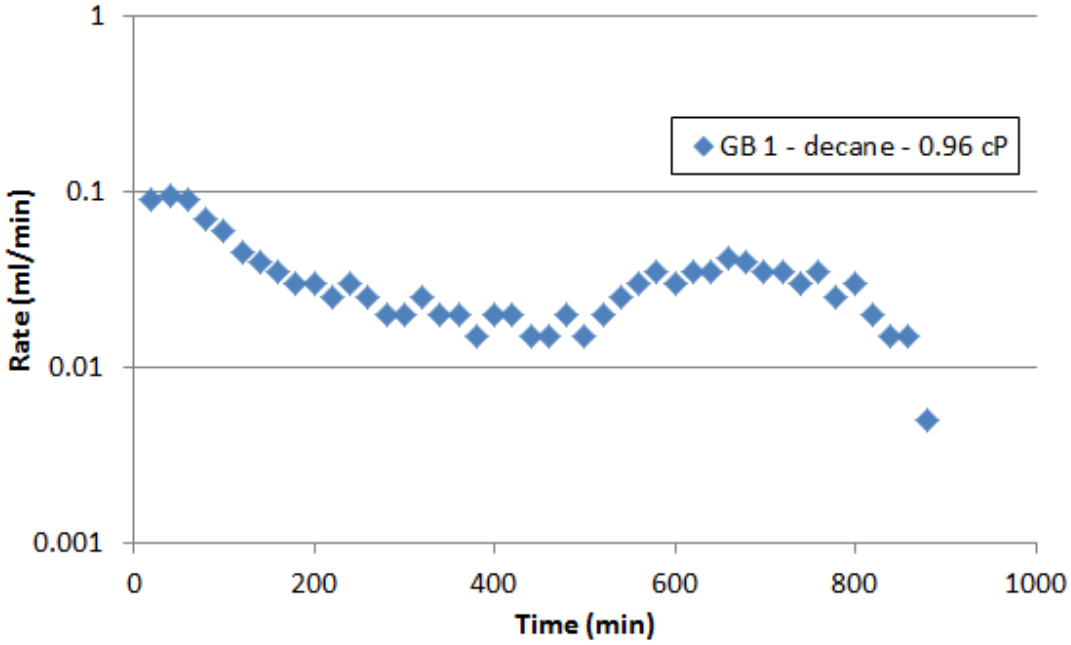

Figure 30: Co-current spontaneous in glass bead pack with brine as the wetting phase and decane as the non-wetting phase. Here, the production rate (ml/min) is plotted versus time (min).

3.1.2 Front behaviour during spontaneous imbibition in glass beads

In the start of the experiment, brine imbibed into the imbibition tube in the lower part of the tube (see Figure 31). After about 30 minutes, a stable front was formed. However, a small pocket of oil was left in front of the filter, reducing further imbibition of brine into the imbibition tube across that whole cross-sectional area. After producing for approximately 500 minutes, fingering of brine was observed, see Figure 32. Brine imbibed through a small channel, bypassing a large pocket of oil. Standnes (2004) showed that the rate of spontaneous imbibition, both counter-current and co-current, is sensitive to the area open to the wetting phase, whereas the area open to the non-wetting phase has less of an impact. This may be a possible explanation to the decrease in rate at the start of the experiment. However, the increase in rate after producing for approximately 500 minutes is harder to explain. As it coincides with fingering of brine, the rate may have been increased due to an acceleration of the front. Since the front had to displace a smaller cross-section, it moved faster, and hence the rate increased as a result.

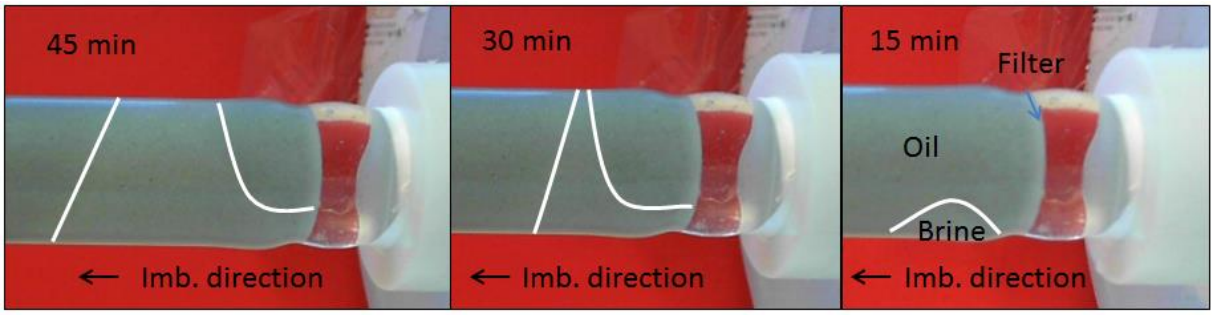

Figure 31: Pictures of initial front behaviour during spontaneous imbibition in glass beads. After 15 minutes a small area of brine was observed in the lower part of the tube. After 30 minutes a stable front was formed, but a small pocket of oil was still left in contact with the filter. This provided a restriction for further imbibition of brine into that area of the tube.

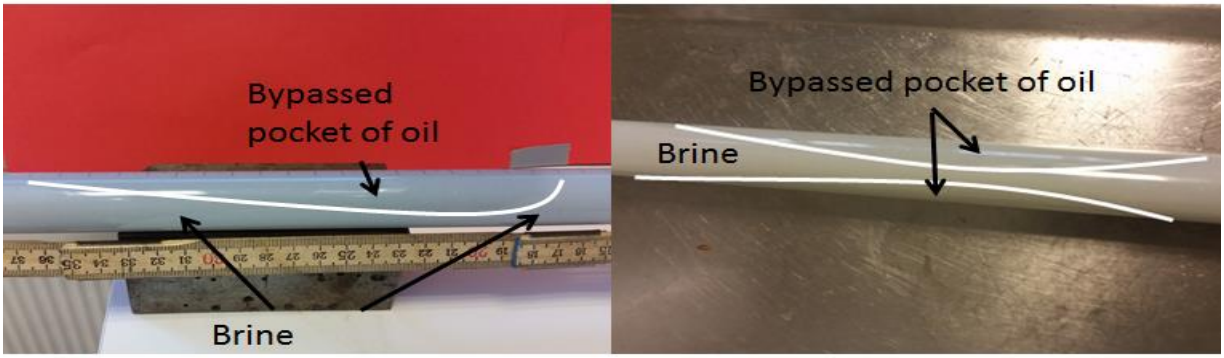

Figure 32: Pictures of the bypassed pocket of oil, taken after the experiment was finished. Left: taken directly after the experiments was finished. Right: Taken from a different angle after the imbibition tube had been removed from the water tank.

3.2 Brine displacing air in a sand pack

3.2.1 Overview and production curves

Following the failure to produce piston-like displacement during co-current imbibition, it was decided that the experimental setup had to be altered to increase the control of boundary conditions. A test experiment was conducted to see if experimental setup D (see Figure 28), using a different imbibition tube with a paper filter, was capable of achieving piston-like displacement during co-current imbibition. Here, the wetting phase was brine, and air was used as the non-wetting phase. The experiment was conducted in cooperation with Tore Føyen. Table 6 shows the properties of the imbibition tube used during spontaneous imbibition into a sandpack saturated with air. Note that the porosity was calculated as an average of porosities from later experiments, where the sandpacks were saturated with oil and the porosity was calculated.

Table 6: Properties for imbibition tube used during spontaneous imbibition into sand packs saturated with air. Note that the porosity was not measured, but calculated from following experiments, where the imbibition tubes were saturated with oil and the porosity calculated.

Name	Weight before imb. (g)	Weight after imb. (g)	Weight sand (g)	Length of the pack (cm)	Calculated porosity (frac)	Cumulative air production (ml)	Cumulative air production (frac PV)
SP1	530.71	591.58	235.39	48.3	0.394	59.8	0.96

Figure 33 shows the production curve for system SP1, where spontaneous co-current imbibition was performed in a sandpack. SP1 had a total production of 59.8 ml after 37 minutes of production, which is 96 % of the total pore volume. When plotted against square root of time, see Figure 34, the production curve shows a linear trend. This indicates that much of the resistance to flow is in the brine and that the resistance in the non-wetting air is almost negligible.

One important observation was that no air was produced counter-currently. At the inlet end, the capillary back pressure was elevated due to the paper filter in the end piece. At the outlet end, the air produced through the outlet plug, into the measuring tube (which was filled with brine). This means that the paper filter elevated the capillary back pressure enough that counter-current production of air was avoided.

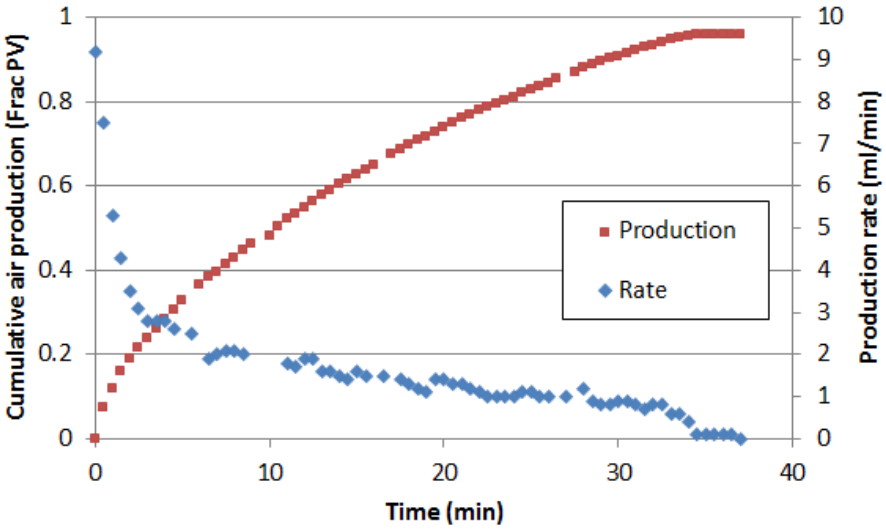

Figure 33: Co-current spontaneous imbibition with experimental setup D. Here, brine was the wetting phase whereas air was used as the non-wetting phase. This plot shows cumulative air production (Frac PV) versus time (min) on the primary axis, whereas production rate is plotted versus time on the secondary axis.

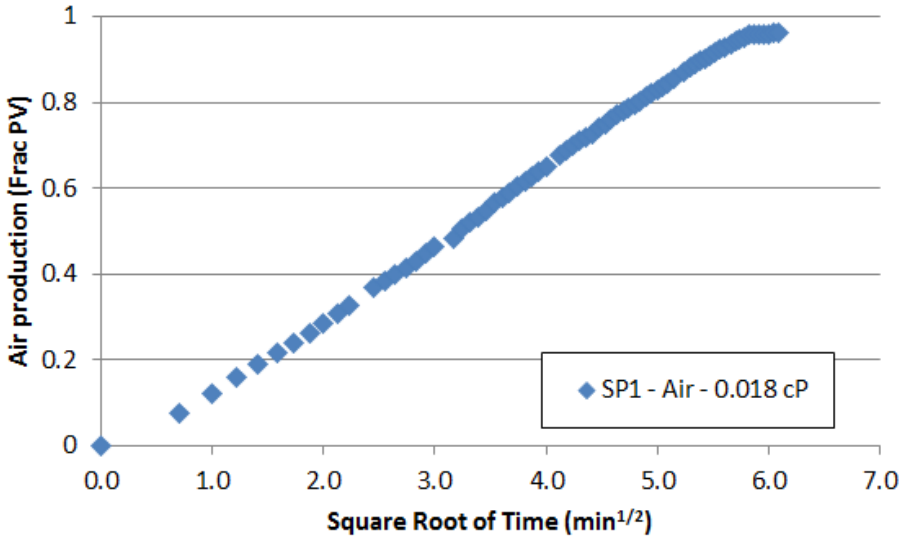

Figure 34: Co-current spontaneous imbibition with experimental setup D. Here, brine was used as the wetting phase, whereas air was used as the non-wetting phase. This plot shows cumulative air production (ml) versus square root of time ($min^{1/2}$).

3.2.2 Front behaviour during spontaneous imbibition

In order to observe front behaviour during spontaneous co-current imbibition, a web camera was used to monitor the front. Pictures were taken every 30 seconds to ensure that the movement of the front was captured. As shown in Figure 35, the front was stable after 1 minute of production. After 10 minutes of production, a segregated front was observed. The bottom part of the front was approximately 2cm ahead of the front at the top. This observation indicates that gravitational forces must be taken into account when discussing front stability in experiments where air is the non-wetting phase. The segregation of the front was most severe during the middle of the experiment (after 10-15 minutes), and towards the end of the experiment (shown in Figure 36). However, the front alternated between having a piston-like and segregated behaviour through the experiment. This may be explained by local areas of

high permeability, as well as gravitational forces affecting the front. After breakthrough, brine filled the remaining space and produced the remaining air, shown in Figure 37. Although most of the air was produced, some small pockets of air was left behind and trapped in the imbibition tube.

The viscosity of the air is assumed to be 0.018 cP (Beal, 1946), whereas the viscosity of brine is 1.15 cP. This makes the viscosity ratio μ_{nw}/μ_w = 0.016. At this viscosity ratio, piston-like displacement is expected. Increasing the viscosity of the brine would most likely promote a more disperse front behaviour, as seen in the work of Vabø (2016). However, this has not been tested with experimental setup D.

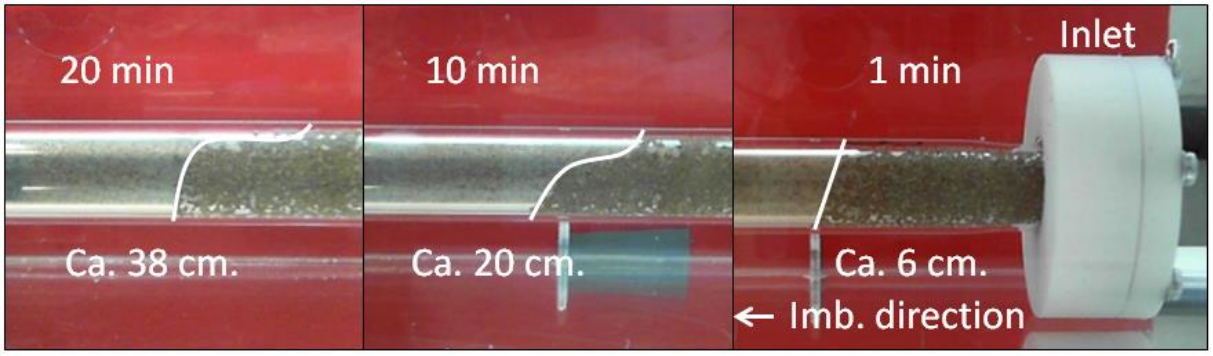

Figure 35: Initial front behaviour during spontaneous co-current imbibition, where brine was the wetting phase and air was used as the non-wetting phase. Here, the front is shown at 1, 10 and 20 minutes after production start.

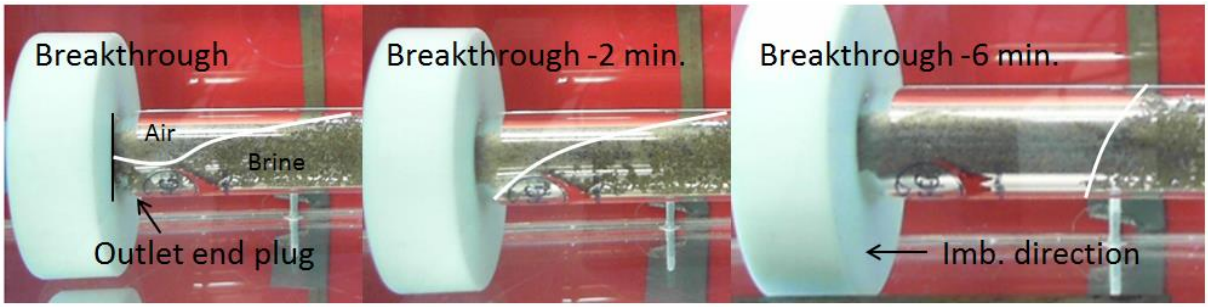

Figure 36: Late front behaviour during spontaneous imbibition, where brine was the wetting phase and air was the non-wetting phase. Here, the front is shown at breakthrough (left), 2 minutes before breakthrough (middle), and 6 minutes before breakthrough (right).

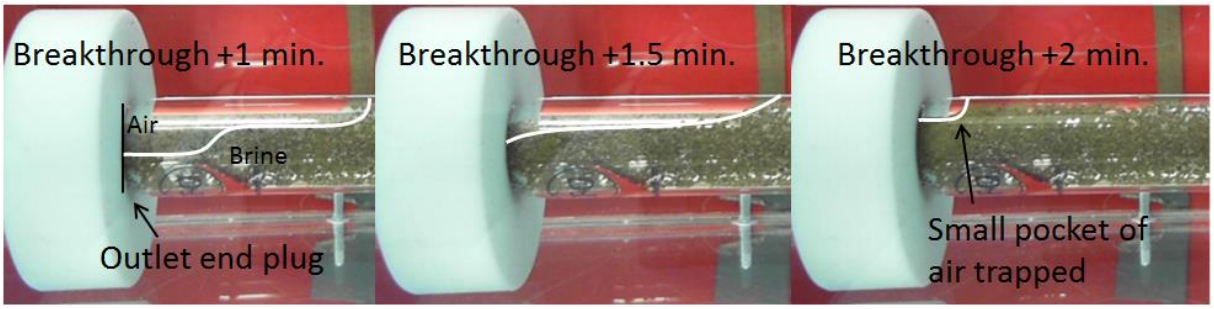

Figure 37: Front behaviour after breakthrough during spontaneous imbibition with brine as the wetting phase and air as the non-wetting phase. Here, the front is shown in the minutes after breakthrough.

3.2.3 Comparison of normalised production curves

As limited data was obtained for experiments with air as the non-wetting phase, comparison with data from Vabø (2016) was appropriate. Figure 38 shows the normalised production curves for SP1, as well as three normalised production curves from Vabø (2016). The production was normalised to total production at breakthrough, and time was normalised to the breakthrough time. This gives a better visualisation, and easier comparison of the experimental data. For SP1 (blue diamonds), brine with a viscosity of 1.15 cP was used as the wetting phase, for SPA1 (orange squares), brine with a viscosity of 1.07 cP was used as the wetting phase, SPA2 (grey triangles) used glycerol/brine mixture with a viscosity of 30.1 cP as the wetting phase, and SP4 (purple dots) used a glycerol/brine mixture with a viscosity of 9.62 cP as the wetting phase. All the experiments used air as the non-wetting phase. The viscosity ratios for the different tests are shown in the legend in Figure 38 below.

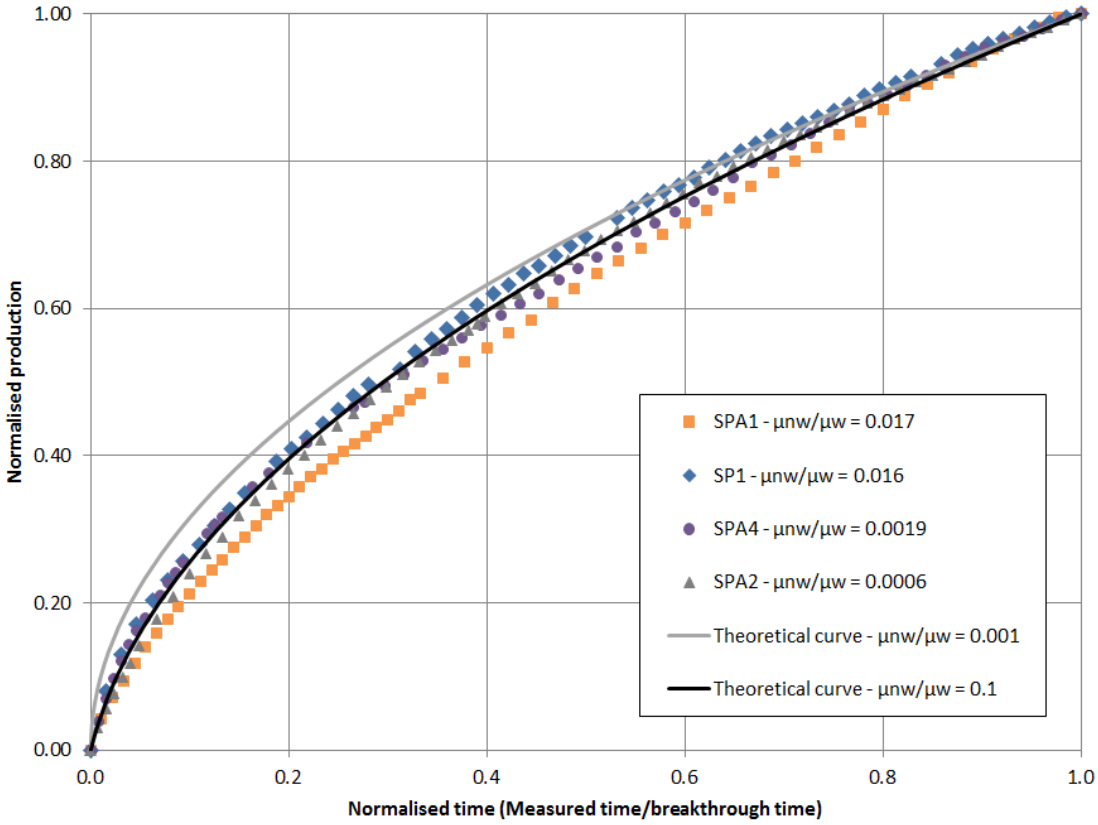

Figure 38: Co-current spontaneous imbibition. Brine or brine mixed with glycerol was the wetting phase, while air was used as the non-wetting phase. The figure shows normalised cumulative production versus normalised time. Time and production was normalised to breakthrough time and total cumulative production at breakthrough. Viscosity ratio is shown in the legend. Results SPA1, SPA2 and SPA4 where conducted by Vabø (2016), using experimental setup A. Theoretical curves are calculated using equation 20.

According to the theory in chapter 1.3.1, the production profiles should vary with viscosity ratio during spontaneous imbibition (see Figure 7). For low viscosity ratios ($\mu_{nw}/\mu_w < 1$) the production rate should be high at the start of the experiment and decrease as the experiment progresses. Note that this assumes a single capillary tube, constant saturation of the wetting phase behind the front, uncompressible fluids and piston-like displacement. For all viscosity ratios lower than 0.001, the shapes of the theoretical curves are similar to the one shown in Figure 38.

As Figure 38 shows, the production profiles are close to theory for the given data sets. In addition, it shows that increasing the viscosity of the wetting phase, while keeping the viscosity of the non-wetting phase constant, has minor impact on the normalised production curves. However, the production profile of SP1 ($\mu_{nw}/\mu_w = 0.016$) lies above the other curves for t > 0.2, although both SPA2 ($\mu_{nw}/\mu_w = 0.0006$) and SPA4 ($\mu_{nw}/\mu_w = 0.0019$) have a lower viscosity ratio. This contradicts the theory, as it was expected that SPA2 and SPA4 would be above SP1, closer to the theoretical production curve with a viscosity ratio of 0.001. This behaviour may be explained by the extra restriction to flow provided by the filter embedded in the imbibition tubes used by Vabø (2016). When comparing tests conducted using experimental setup A with each other, it is worth noting that SPA2 lies below SPA4 before t = 0.4. SPA4 should be position between SPA1 and SPA2, but lies above SPA2 for t < 0.4. This means that the production rate was higher at the start of the experiment for SPA4 than for SPA2, although the viscosity ratio was lower than SPA2 than SPA4. As SPA1 had the highest viscosity ratio, it was expected to have a lower production rate at the start of the experiment, and lie below the other curves, which it did.

3.3 Brine displacing oil in sandpacks

3.3.1 Overview and production curves

A total of three experiments were performed where oil was used as the non-wetting phase. All of the experiments in this chapter were completed in cooperation with Tore Føyen. Following the successful test of spontaneous imbibition using experimental setup D, a series of experiments where oil was used as the non-wetting phase was initiated to test the setup even further. Table 7 shows an overview of the properties of the imbibition tubes used in these experiments. Note that the porosity for system SP2 was calculated as an average of all other sandpacks with this setup, due to the weight not being recorded before and after saturating the system with oil.

Table 7: Properties of the imbibition tubes used for spontaneous imbibition where oil was used as the non-wetting phase. *Note that the porosity of SP2 could not be calculated directly, but calculated as an average of the porosity of all other sandpacks with experimental setup D.

Name	Weight sand (g)	Weight before saturating with oil (g)	Weight after saturating with oil (g)	Length of the pack (cm)	Porosity (frac)	Pore volume (ml)	R_f at break-through (frac PV)	Total R_f (frac PV)
SP2	254.2	-	-	48.4	0.394*	62.33*	0.85	0.88
SP3	251.21	807.23	857.44	48.3	0.377	59.49	0.83	0.84
SP4	260.17	922.04	975.60	48.3	0.399	62.94	0.72	0.77

Figure 39 shows the production curves for systems SP2, SP3 and SP4. In all experiments, brine with a viscosity of 1.15 cP was used as the wetting phase. System SP2 (blue diamonds) used decane (0.96 cP), system SP3 (orange squares) used Marcol 82 (32.6 cP), and system SP4 (grey triangles) used DTE FM 32 (73.2 cP) as the non-wetting phase.

System SP2 had a total cumulative oil production of 88.0% of the pore volume after 900 minutes of production. Of the total 88.0%, 10.2% of the pore volume was produced counter-currently and the remaining 77.8% was produced co-currently. System SP3 had a total cumulative oil production of 83.9% of the pore volume after 2160 minutes of production. In this experiment all of the oil was produced co-currently. SP4 had a total cumulative oil production of 77.1% of the pore volume after 4128 minutes of production. Of the total 77.1%, 3.1% of the pore volume was produced counter-currently, while 74% was produced co-currently. A noteworthy observation is that no counter-current was observed for SP3. The reason for this is not clear, and will be discussed below.

As the production curves show, the rates of recovery, as well as the ultimate recovery decrease with increase in the non-wetting phase viscosity. Meng et al. (2015) had similar observations for spontaneous imbibition in quartz-sand-packed columns, although the effect seemed stronger. The decrease in ultimate recovery was attributed to non-uniform pore size distribution, due to angular shape and a wide size distribution of the sand grains. The size distribution of the sand Meng et al. (2015) used was from about 50-600μm. In this thesis, the sand was sifted to have a grain size from 212-250μm. However, the angular and irregular shape of the sand might be enough to cause a non-uniform pore distribution, and thus cause a lower recovery as the viscosity of the non-wetting phase was increased.

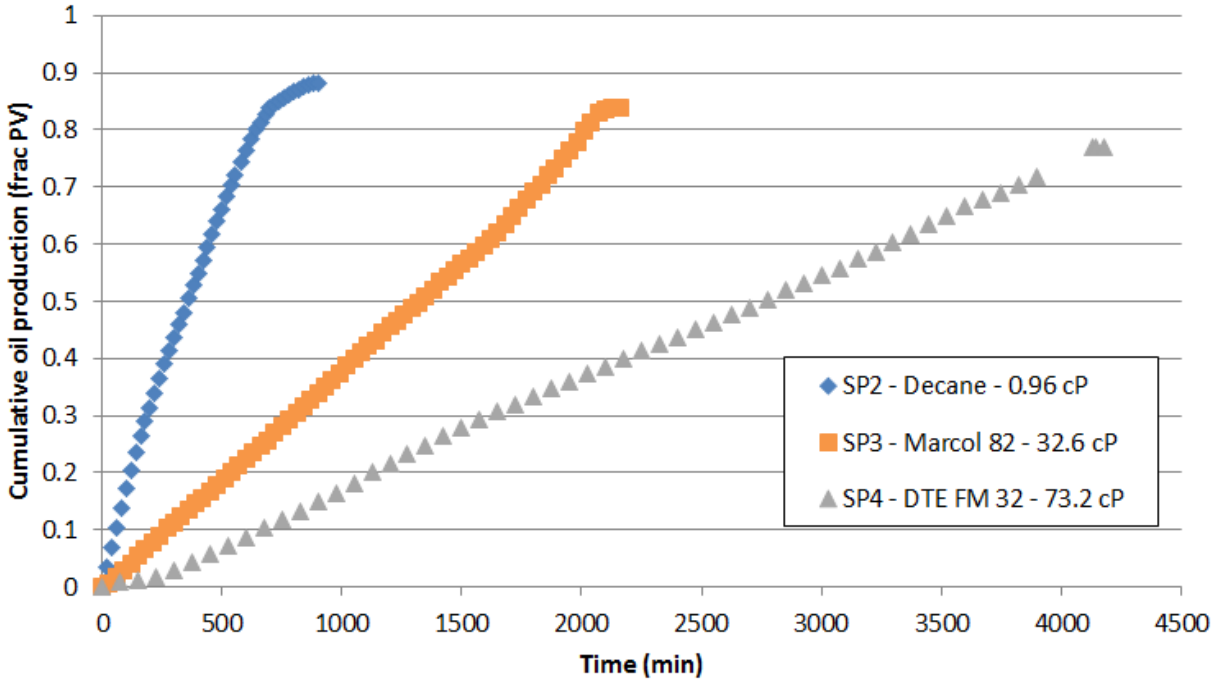

Figure 39: Spontaneous co-current imbibition in sandpacks where brine as the wetting phase and oils with varying viscosity were used as the non-wetting phase. This plot show the cumulative production as a fraction of total pore volume plotted versus time in minutes.

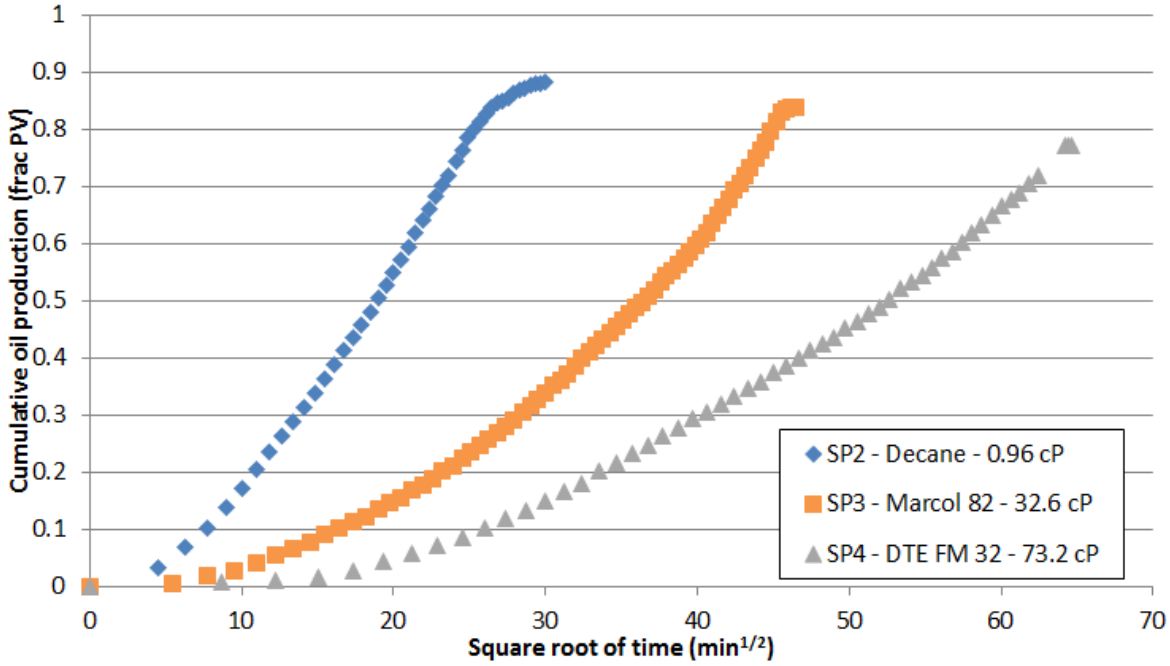

Figure 40: Spontaneous co-current imbibition in sandpacks where brine was used as the wetting phase and oils with varying viscosity were used as the non-wetting phase. This plot shows the cumulative production as a fraction of total pore volume plotted versus square root of time.

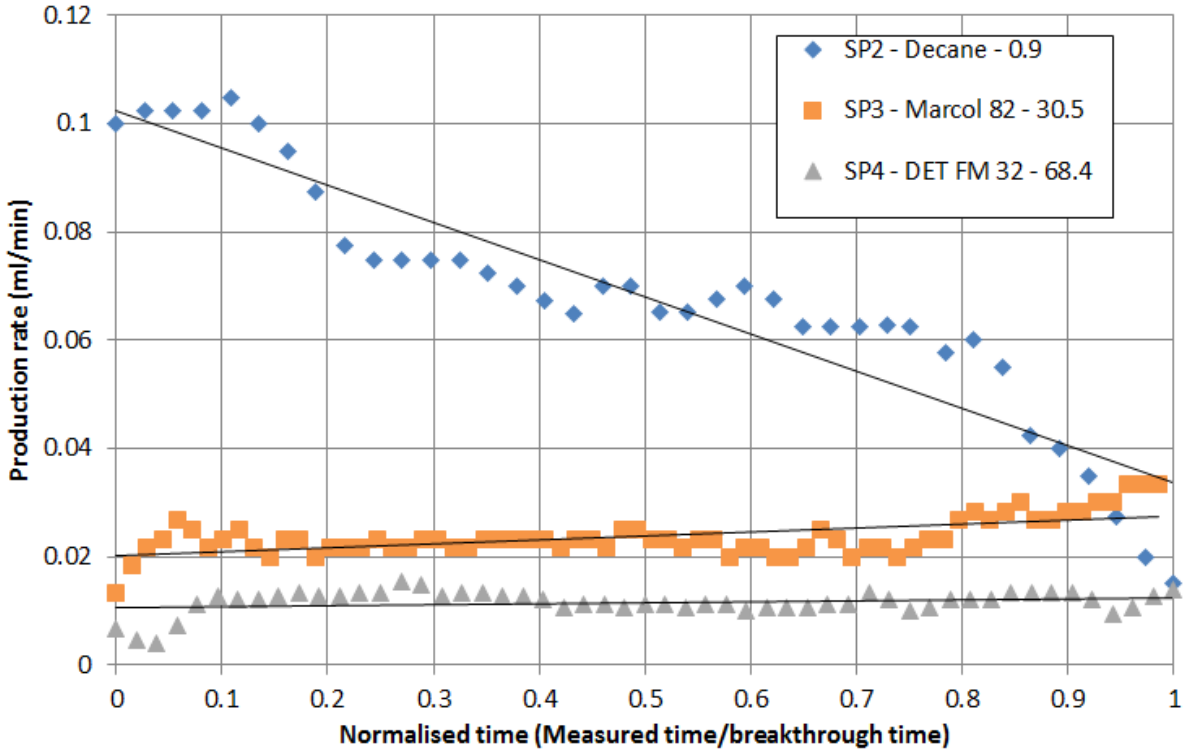

Figure 41: Rate development during spontaneous co-current imbibition where brine was used as the wetting phase and oil with varying viscosity was used as the non-wetting phase. The plot shows oil production rate (ml/min) versus normalised time. The time has been normalised to the breakthrough time to give an easier comparison between the experiments. Viscosity ratio is shown in legend.

For the experiments that had counter-current production, an average of 6.7 % of the oil recovery was produced counter-currently. This is close to what Haugen et al. (2014) found during spontaneous imbibition with the TOEFSI boundary condition. In their work, counter-current production stopped within a relative short time, and 93% of the oil was produced co-currently. Similarly, in this thesis, a combination of counter- and co-current production was observed at the start of the some of the experiments, but within a relative short time, counter-current production stopped, and the rest of the oil was produced co-currently. For SP2, the initial 360 minutes (0.4 of the total time) after immersing the sample in brine was a combination of counter- and co-current production. For SP4, the initial 1125 minutes (0.26 of the total time) after immersing the imbibition tube in brine consisted of both counter- and co-current production.

As there is no external force being applied to the systems in this thesis, spontaneous imbibition is driven entirely by the capillary pressure at the front. At the start of the experiments, due to the short distance from the inlet to the front, a smaller portion of the pressure drop dissipates in the wetting phase. That leads to a bigger portion of the pressure being able to overcome the capillary back pressure at the inlet, required for oil to produce, and counter-current production of oil occurs. However, as the front progresses, more pressure is required to draw the wetting phase from the inlet to the front. This leads to a smaller portion of the pressure being available to push oil back through the wetting phase and produce at the inlet end (Haugen et al., 2014). Counter-current production of oil at the inlet end is essentially a drainage process, and the capillary back pressure that the oil must overcome to be produced is proportional to the interfacial tension and depends inversely on the size of the large pores which the oil is exiting from (Li et al., 2006).

For SP3, no counter-current production was observed. There is no clear reason for this behaviour. In fact, since spontaneous imbibition is resisted by viscous forces, the resistance at the inlet end is initially smaller than at the outlet end, and hence counter-current production should increase as non-wetting phase viscosity is increased. Asymmetrical production during spontaneous imbibition with two ends open can be attributed to small differences in the capillary back pressure at each end of the imbibition tube. This can be as a result of a gradient of pore size along the tube, or a difference in pore size at each end face (Mason and Morrow, 2013). Since the sand used in this thesis is sifted to have a narrow size distribution, the pore size along the tube is assumed to be homogeneous. Lastly, the paper filter at the inlet end may have caused an increase in the capillary back pressure, and therefore resisted counter-current production of oil at the inlet.

3.3.2 Front behaviour during spontaneous imbibition

Pictures of the front were taken using a web camera, similar to the experiment described in chapter 3.2.2. Pictures were taken every 5 minutes for SP2, every 10 minutes for SP3, and every 15 minutes for SP4. Figure 42 shows the front behaviour during spontaneous imbibition for SP2. During the start of the experiment, brine started to imbibe at the bottom of the imbibition tube. Further, the front spread out evenly across the imbibition tube at a slight angle. A small pocket of oil was bypassed by the imbibing brine. However, some of the oil in this pocket was produced counter-currently. As the front progressed the lower part of front remained 2-4 centimetres ahead of the top part. This started at the beginning of the experiment and continued until about 440 minutes of production. After this, the front sharpened, and the top part of the front as close to parallel with the bottom part of the front.

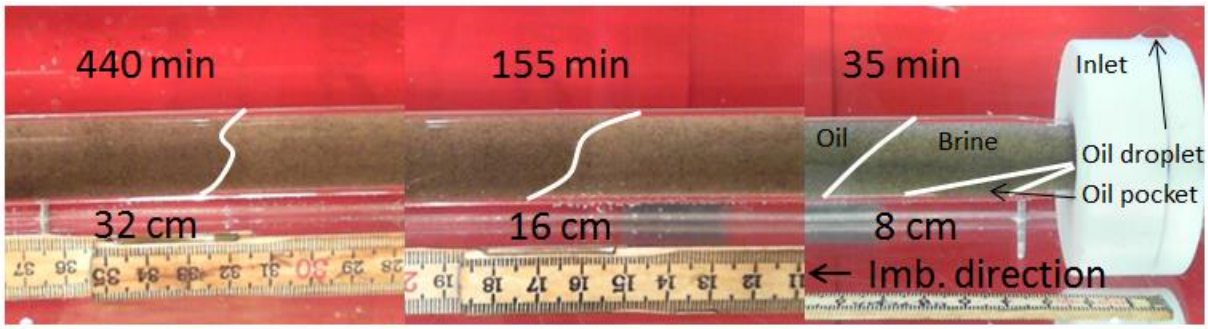

Figure 42: Front behaviour during spontaneous imbibition. Brine with a viscosity of 1.15 cP was used as the wetting phase, whereas decane with a viscosity of 0.96 cP was used as the non-wetting phase. The front moves from right to left. Note the small pocket of oil, as well as the oil droplet producing from the inlet, shown in the picture to the right.

Figure 43 shows the front behaviour during spontaneous imbibition for SP3. Brine started to imbibe in the bottom part of the imbibition tube. After about 180 minutes a stable front was formed, and piston-like displacement was observed. A small pocket of oil was bypassed near the inlet. It did not seem to affect the flow of brine through the imbibition tube in the same way as it did in experimental setup C. In system GB1, the rate quickly started to drop, whereas for SP3 the rate remained stable through the experiment, increasing towards the end. This may lead to the conclusion that experimental setup C, due to the extra restriction to flow provided by the glass filter, is more sensitive to the cross-sectional area available for brine to imbibe.

The middle picture in Figure 43 shows the overall trend for system SP3. Mostly piston-like displacement was observed, but at random intervals, small pockets of oil would be left behind, and trapped. Towards the end of the experiment, after approximately 1500 minutes of production, the start of a long pocket of left behind oil started to form. The front seemed to flow faster at some points of the imbibition tube, leaving a long pocket of oil behind. The left picture in Figure 43 shows the long pocket about 300 minutes after formation. The oil pocket remained until the end of the experiment, although some of the oil left behind was produced after breakthrough of the front.

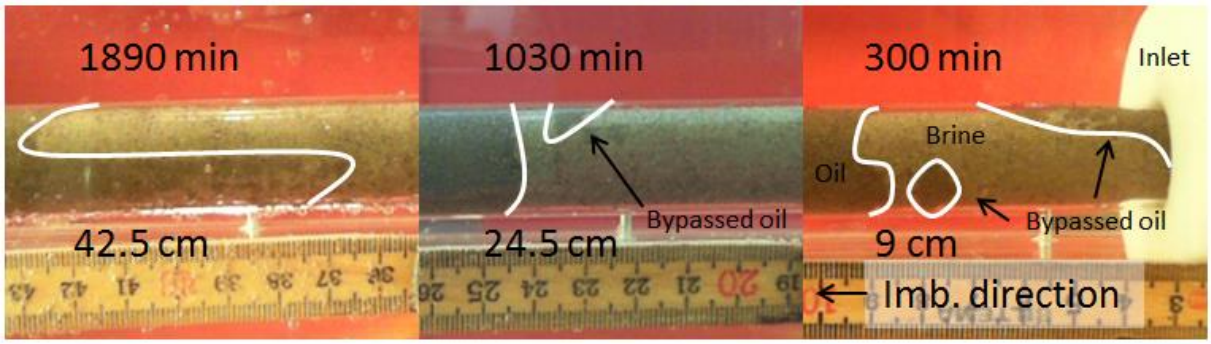

Figure 43: Front behaviour during spontaneous imbibition. Brine with a viscosity of 1.15 cP was used as the wetting phase, whereas Marcol 82 was with a viscosity of 32.6 cP was used as the non-wetting phase. The front moves from right to left.

Figure 44 shows the front behaviour during spontaneous imbibition for SP4. In this experiment brine started to imbibe at the bottom part of the imbibition tube, leaving some oil behind. A small part of the oil left behind was produced counter-currently, but most of the oil was trapped. After producing for 1425 minutes, the initial sign of a stable front was observed, shown in the middle picture in Figure 44. From that point, piston-like displacement was observed for approximately 1000 minutes. However, after 2415 minutes of production, the front returned to having an alternating, non-piston-like behaviour. About 20 centimetres from the outlet, the front started to progress simultaneously at the top and bottom of the imbibition tube, leaving a trail of oil in the middle. Shortly after (about 15 centimetres from the outlet), the front progressed through the middle of the imbibition tube, leaving a trail of oil at the top and bottom of the imbibition tube. However, these trails of oil were thinned out due to production of oil after breakthrough, leaving only a few, small pockets of oil behind. Most of the oil trapped during this experiment was trapped during the first 1500 minutes of production.

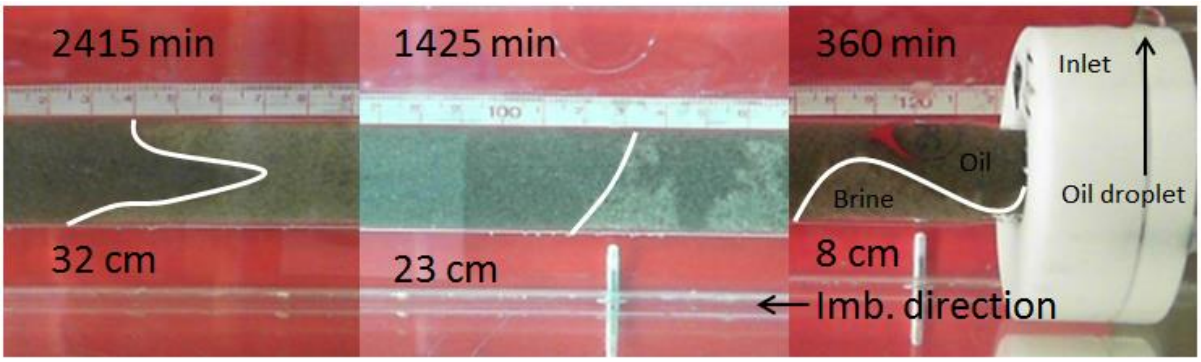

Figure 44: Front behaviour during spontaneous imbibition. Brine with a viscosity of 1.15 cP was used as the wetting phase, whereas DTE FM 32 with a viscosity of 73.8 cP was used as the non-wetting phase. Note the small oil droplet producing counter-currently from the inlet side.

An overall trend of the front behaviour during spontaneous co-current imbibition in sandpacks, described above, is that the brine seemed to invade the imbibition tube from bottom part first. For all experiments, the brine imbibed at the bottom part of imbibition tube, and started to form a stable front a few centimetres into the sandpack. The distance it took for the stable front to form, increased with increasing viscosity of the non-wetting phase. Fernø et al. (2013) had similar observation for experiments where OEO spontaneous imbibition was monitored using MRI. The MRI images showed that brine invaded the core plugs hemi-spherically from localised points, which merged into a front. However, the brine had advanced one third of the core length before merging.

In addition to an unstable front at the start of the imbibition, an increasing degree of entrapment was observed as the viscosity of the non-wetting phase was increased. As mentioned above, a non-uniform pore size distribution may lead to a lower recovery. In a system with non-uniform pore size distribution, the front will advance faster in the smaller pores faster than in the larger pores (Dong et al., 1998). This will in turn lead to snap-off of oil in the larger pores, and hence the oil is trapped. This effect is more apparent if the viscosity of the non-wetting phase is increased. As the viscosity of the non-wetting phase is increased, the difference in rate of advance between the larger and the smaller pores will increase, which in turn leads to more oil being trapped (Dong et al., 2006).

3.3.3 Viscosity effect on production profile

In order to compare the results with each other, the results for spontaneous co-current imbibition in sandpacks were plotted as normalised cumulative production versus normalised time. The production was normalised to total production at breakthrough, and the time was normalised to the breakthrough time, see Figure 45. For all the experiments brine was the wetting phase. System SP 2 (blue diamonds) used decane as the non-wetting phase, and had a viscosity ratio of 0.8. SP 3 (orange squares) used Marcol 82 as the non-wetting phase, and had a viscosity ratio of 28.3. Lastly, SP 4 (grey triangles) used DTE FM 32 as the non-wetting phase, and had viscosity ratio of 63.7.

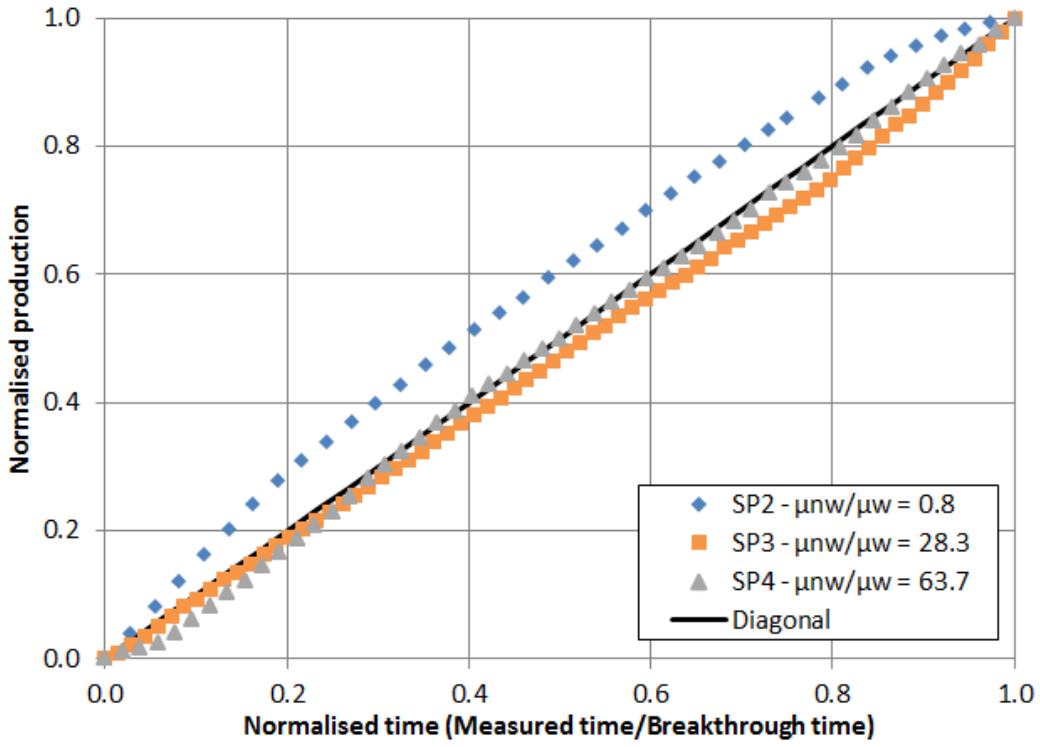

Figure 45: Co-current spontaneous imbibition in sand packs with a range of viscosities. The wetting phase was brine in all experiments, and the non-wetting phase was decane for SP 1, Marcol 82 for SP 2 and DTE FM 32 for SP4. The figure shows normalised cumulative production versus normalised time. Time and production were normalised to breakthrough time and total production at breakthrough. The viscosity ratio for the different experiments are shown in the legend. The diagonal line shows the theoretical production for a sample with viscosity ratio equal to 1.

According to the theory in chapter 1.3.1, the production profiles should vary with viscosity ratio during spontaneous co-current imbibition (see Figure 7). For low viscosity ratios the production rate should be high at the start of the experiment and decrease as the experiment progresses. When the viscosity of the non-wetting phase and the wetting phase is equal, the production profile should be a straight line, i.e. the rate should be constant. For higher viscosity ratios, the production rate should be low at the start of the experiment and increase as the experiment progresses. Note that this assumes a single capillary tube. As Figure 45 shows, the production profiles are close to theory for low viscosity ratios ($\mu_{nw}/\mu_w < 1$). However, as the viscosity of the non-wetting fluid increases, and thus the viscosity ratio increases, the production profiles deviate from theory. The production profile for both SP 3 and SP4 show minor increase in rate over time, but the effect was less than expected, according to theory for a single capillary tube.

3.3.4 Theoretical front position versus measured front position

After plotting the normalised production versus normalised time, the normalised production was used to calculate the theoretical position of the front. The front position was found by dividing the amount of brine imbibed at a given time (equal to oil produced) by the brine imbibed when the front had reached the outlet. It was then plotted against the front position measured by web camera. As Figure 46 shows, the front position calculated from the normalised production matches the measured front position quite well for low and medium viscosity ratio. However, as the viscosity ratio was increased, the match was worse. A reason for this behaviour may be the non-piston-like displacement observed at the start of the spontaneous imbibition test. As oil was trapped at the start of the experiment, the front position estimated later in was underestimated by the calculations.

By using equation 36, and the technique described by Haugen et al. (2014), the theoretical position of the front was calculated, and plotted versus the measured position of the front, see Figure 47. Only co-current displacement has been included in the plots. First, a value of D was found that made a straight line. Once D was found, a value for E that gave a gradient of unity was found. By assuming that the relative permeability to oil is 1 ahead of the front, and because the fluid viscosities are known, the relative permeability to brine behind the front was calculated by equation 31. Figure 48 shows the calculated relative permeability to brine for SP2, SP3 and SP4, compared with the relative permeability to brine for glass beads and quartz sand in the work of Meng et al. (2015), given in Figure 14. For SP2, the calculated relative permeability was 0.45, for SP3 it was 0.03, and for SP4 it was 0.01. This shows that the calculated relative permeability behind the front decreased as the viscosity of the non-wetting phase was increased. However, the estimated relative permeability for both SP3 and SP4 are quite low and may be considered unreliable, especially for SP4. As the non-wetting phase viscosity was increased, more non-piston-like displacement was observed, and thus the calculations may have been affected, as the theory assumes a sharp front and a piston-like displacement.

By using the fitted value for E and equation 37, the capillary pressure at the front, $P_{c,f}$, was calculated. For SP2, the calculated capillary pressure at the front was 0.026 kPa, for SP3 it was 0.238 kPa, and for SP4 it was 0.397 kPa. The estimated capillary pressure is similar to the capillary pressure calculated in the work of Haugen et al. (2014) for sandstone cores. In their work $P_{c,f}$ ranged from 0.312 kPa to 0.379 kPa for sandstone cores, whereas it ranged from 77.7 kPa to 166.1 kPa for Portland chalk cores. Again, the non-piston-like behaviour observed as the non-wetting phase viscosity was increased may cause unreliable calculations. For SP2, due to a faster imbibition, as well as significant counter-current production, fewer data points were included in the calculations. This is also a source of error, and may affect the calculated capillary pressure. In general, a lower capillary pressure is expected for unconsolidated media than for consolidated rock cores, as capillary pressure is inversely proportional to pore throat radius.

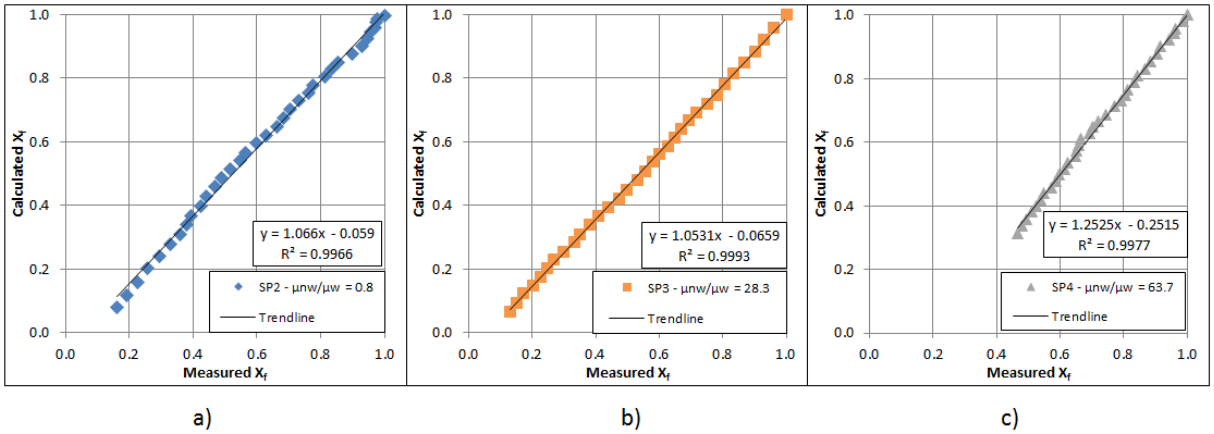

Figure 46: Plots of calculated front position (normalised production) versus measured front position for a) SP2, b) SP3, and c) SP4. The viscosity ratio is increasing from left to right.

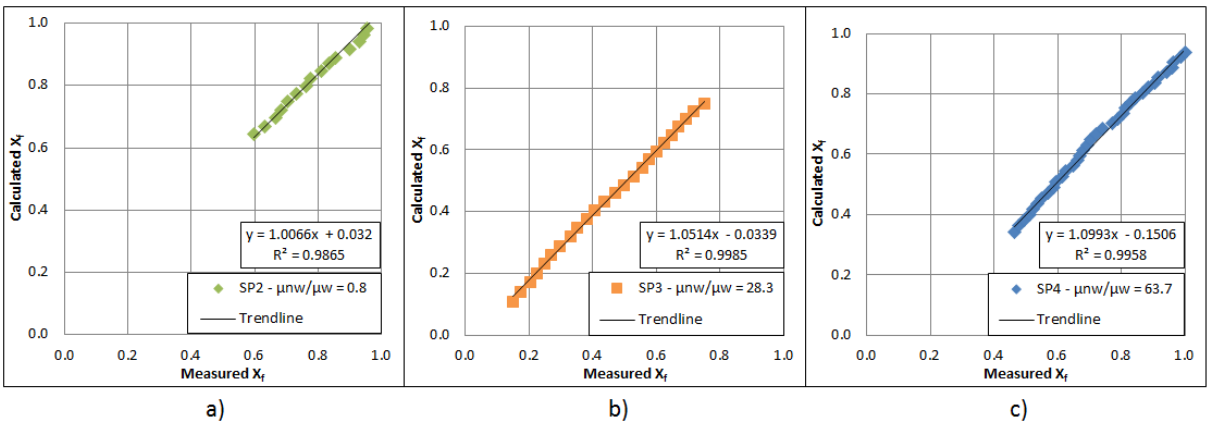

Figure 47: Plots of theoretically calculated position of the front using the method from Haugen et al. (2014) versus the measured position of the front for a) SP2, b) SP3, and c) SP4, during co-current displacement.

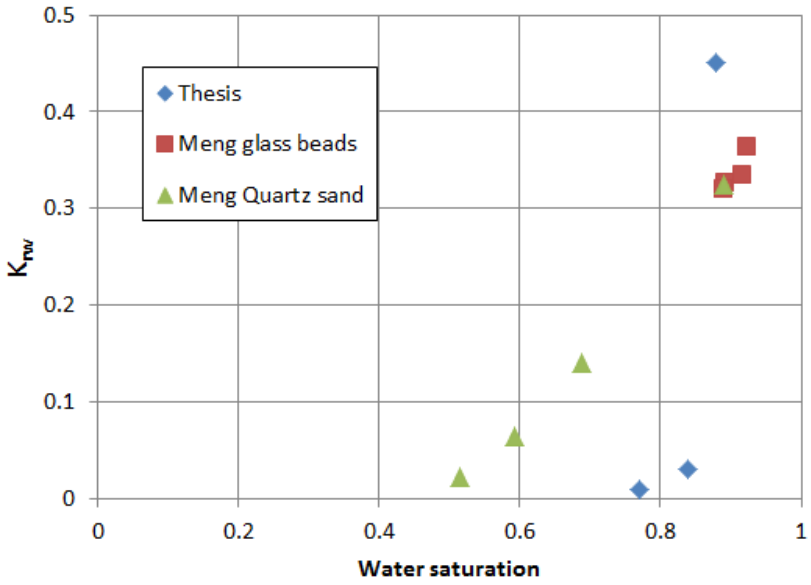

Figure 48: Relative permeability calculated using theory presented by Haugen et al. (2014). The blue diamonds show the relative permeability for the experiments in this thesis, whereas red squares and green triangles show the relative permeability calculated in the work of Meng et al. (2015).

3.4 Polymer and glycerol/brine displacing oil

3.4.1 Overview and production curves

Three experiments were conducted where the viscosity of the wetting phase was altered. All experiments in this chapter were conducted in cooperation with Tore Føyen. In the two first experiments, HPAM polymer was used to increase the viscosity of the wetting phase. In the last experiment, glycerol was added to the brine in order to increase the viscosity. Table 8 shows the properties of the imbibition tubes used during these experiments. Two additional imbibition tubes were prepared. However, when removing the end piece at the start of the experiments, air entered the system at the outlet end. As a result of this, these experiments where not continued.

Table 8: Properties of the imbibition tubes used during spontaneous imbibition. * The front in SP5 never reached breakthrough.

Name	Weight sand (g)	Weight before saturating with oil (g)	Weight after saturating with oil (g)	Length of the pack (cm)	Porosity (frac)	Pore volume (ml)	R_f at break-through (frac PV)	Total R_f (frac PV)
SP5	259.61	920.21	966.62	48.2	0.406	63.93	-	0.57
SP6	256.27	911.88	956.88	48.2	0.393	61.98	0.76	0.77
SP7	250.67	906.03	950.08	48.2	0.385	60.67	0.80	0.82

Figure 49 shows the production curve for experiments SP5, SP6 and SP7. In all experiments, decane was used as the non-wetting phase. In systems SP5 (blue diamonds) and SP6 (red dots), HPAM polymer was used as the wetting phase, and in system SP7 (purple crosses), a mixture of brine and glycerol was used as the wetting phase.

System SP5 had a total cumulative oil production of had a total cumulative oil production of 57% of the pore volume after 12059 minutes of production. System SP6 had a total cumulative oil production of 77% of the pore volume after 4530 minutes of production. System SP7 had a total cumulative oil production of 82% of the pore volume after 8248 minutes of production. No counter-current production was observed for any of the experiments.

Initially system SP5 was produced with the paper filter placed in the end piece. After producing for about 3000 minutes, the production levelled off and no more oil seemed to produce. The filter was then removed, in order to see whether more oil produced. Immediately after the filter was removed, oil started to produce again. The assumed reason for this behaviour was retention of polymers, either mechanical entrapment in the filter, or adsorption of polymers in the sandpack. Because of the fast decline in imbibition rate, it is believed that polymer molecules quickly started to clog the paper filter, effectively reducing the cross-sectional area available for polymer to imbibe. Eventually, the filter would be completely blocked, and imbibition of polymer stopped. Subsequently, another experiment (SP6) was conducted, using the same polymer solution, but without the paper filter placed in the end piece. In this experiment, imbibition progressed as normal. Although measurements of both

polymer molecule size and pore size of the filter have not been measured, the most likely reason for the abnormal production in system SP5 was mechanical entrapment in the filter.

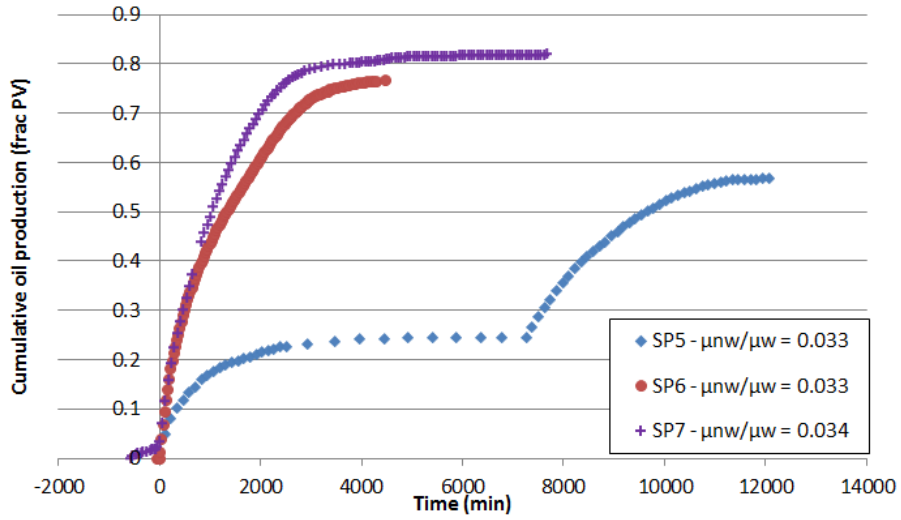

Figure 49: Spontaneous co-current imbibition in sand packs, where decane was used as the wetting phase, and either HPAM polymer or a brine/glycerol mixture was used as the wetting phase. This curve shows the production as a fraction of pore volume plotted versus time in minutes.

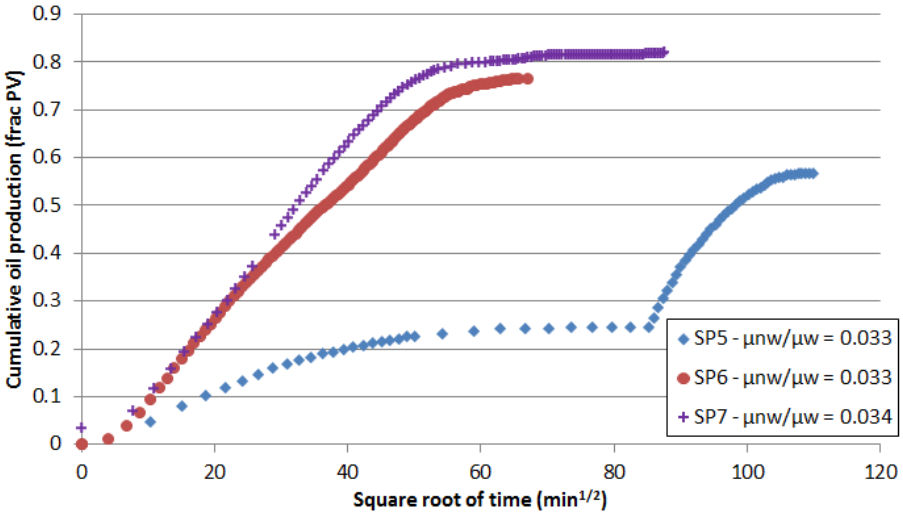

Figure 50: Spontaneous co-current imbibition in sand packs, where decane was used as the wetting phase, and either HPAM polymer or a brine/glycerol mixture was used as the wetting phase. This curve shows the production as a fraction of pore volume plotted versus square root of time ($min^{1/2}$).

Even though trapping of polymers occurred in the filter, system SP5 was expected to have a higher recovery than 57% PV. The main reason for the low recovery was attributed to an area close to the outlet in which small bubbles (air or vacuum) created an extra resistance to flow. During saturation of the sample, the flow direction into the tube is reversed, i.e. oil flows in through the outlet plug, and out through the end piece containing the paper filter. During this process oil saturates the sandpack, and no air should remain in the sample. However, if the oil rate through the outlet plug is too high, an area forms in which the imbibition tube is not fully saturated with oil. An area with a mixture of oil and air, or vacuum, was observed close to the outlet, see Figure 54. This area initially stretched 10 cm into the sample, but was displaced over time. When the production stopped, a 3 cm long pocket with a mixture of oil and air/vacuum, and a 6 cm long pocket of oil, remained in the imbibition tube. The area created

an extra resistance to flow which caused the imbibition rate to decline slowly. Eventually the capillary pressure at the front did not manage to overcome the capillary back pressure at the outlet, effectively stopping the imbibition.

During experiments SP6 and SP7, an induction time was observed. SP6 had an induction time of 47 minutes, and SP7 had an induction time of 570 minutes. For system SP7, sand started to flow out of the inlet after the imbibition tube was immersed in the brine/glycerol mixture, see Figure 51. The flow of sand continued for about 500-570 minutes. It is believed that some of the capillary pressure contributed to push sand out of the imbibition tube, instead of pushing oil. When the flow of sand stopped, the imbibition started, and the imbibition front started to move through the tube.

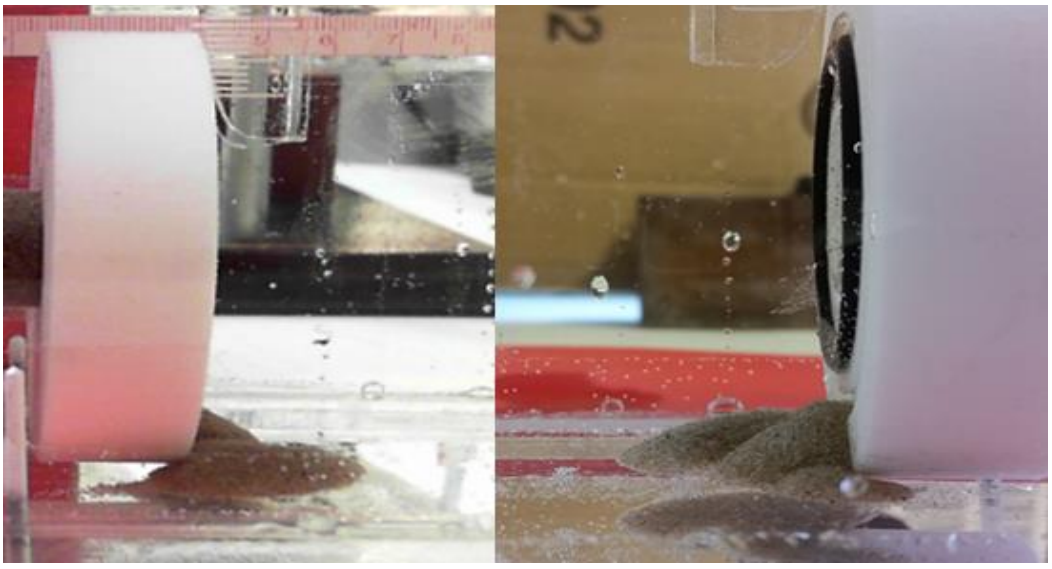

Figure 51: Sand from the imbibition tube at the inlet. During the first 500-570 minutes after the imbibition tube was immersed in brine, sand was flowing out through the inlet. After the flow of sand stopped, imbibition started, and the imbibition front started to move.

Although the viscosity was increased with different liquids, the viscosity ratio was almost the same for both polymer and glycerol. Yet, recovery was higher when glycerol was used as the wetting phase than when polymer was used as the wetting phase. The reason for this behaviour is not clear. Several reasons may cause the recovery to decrease when polymers are used as the wetting phase during spontaneous imbibition. Piston-like displacement was more evident for the experiment where glycerol was the wetting phase. When polymer was used as the wetting phase, the front was less sharp, as well as bypassing a small pocket of oil towards the end. As the difference between the two recoveries was only 5% of the pore volume, this may have been the cause.

Wettability alteration may also have caused a lower recovery. Wettability affects the spatial distribution of fluids in the sandpack, as well as the recovery during waterfloods (Anderson, 1987b). Romero-Zeron et al. (2010) showed that polymer flooding of sandpacks saturated with oil is much more efficient under strongly water-wet conditions, than under preferentially oil-wet conditions. Although the oils used in this thesis were filtered to remove polar components, remaining polar components in the oil could potentially have altered the wettability of the sandpack towards a less water-wet condition. This would in turn have lowered the expected recovery for that particular system.

Permeability reduction due to polymer adsorption and/or retention may also cause a reduction in recovery. Sorbie et al. (1982) modelled polymer flooding in the BRENT sands using a chemical simulator. The incremental oil recovery was 17.3 % after waterflooding when adsorption effects were excluded from the simulations. After adsorption effects were included in the simulations, incremental oil recovery from polymer flooding decreased to 6.6 %. Elmkies et al. (2001) showed that during polymer flooding of limestone cores, adsorption of polymers occurred regardless of the wetting conditions of the rock. In their work, polymer adsorption was measured by measuring effluent viscosity and observing a delay in the front during polymer flooding compared with a tracer flood.

3.4.2 Front behaviour during spontaneous imbibition

Similar to experiments described above, the front was observed using web cameras. For the first test using polymers as the wetting phase, pictures of the front were taken every 20 minutes. For the following tests, pictures of the front were taken every 30 minutes. Figure 52 shows the front behaviour during spontaneous imbibition for the first polymer experiment. At the start of the experiment, brine imbibed across the entire cross-section of the imbibition tube. The front had a small angle for the first 250 minutes before sharpening. After about 2500 minutes the production stopped, and the front slowed down at 17 cm. Between t = 2500 min and t = 7230 min the front moved 6 cm, bypassing a small pocket of oil, shown in Figure 53.

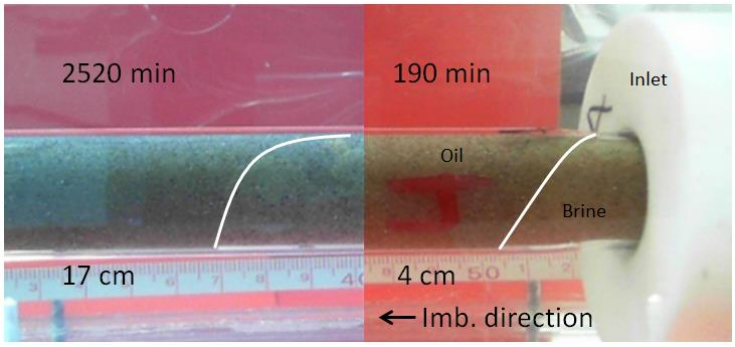

Figure 52: Front behaviour during co-current spontaneous imbibition where polymer was used as the wetting phase, whereas decane was used as the non-wetting phase. The right picture shows front behaviour at the start of the experiment. The left picture shows the position of the front after production had stopped, but before the paper filter was removed.

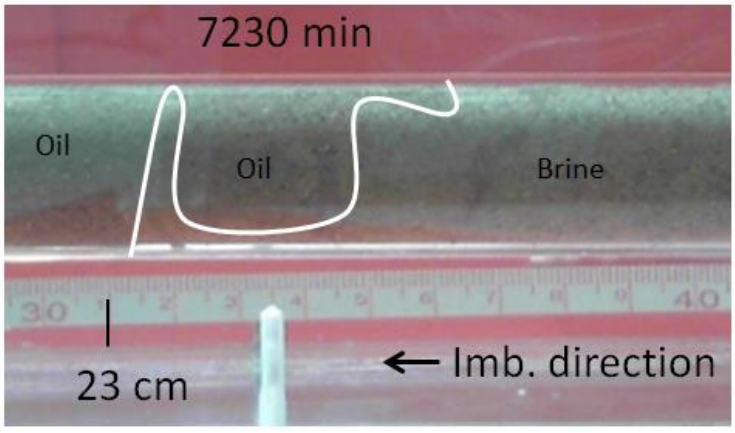

Figure 53: Front behaviour during co-current spontaneous imbibition. This picture shows the observed behaviour when production had slowed down, due to reduction of cross-sectional area available for flow in the filter.

After the filter was removed, the oil production rate increased, along with the progression of the front. Figure 54 shows the overall trend from t = 7230 min to t = 8380 min. Non-piston-like displacement, with the bottom part of the front advancing 2-5 cm ahead of the top part of the front. A pocket of oil mixed with vacuum or air provided an extra resistance to flow. As the front advanced, the pocket was displaced and the size decreased. After 12000 minutes, the front stopped moving, leaving a 6 cm long pocket of oil, as well as a 3 cm long pocket of oil mixed with vacuum or air.

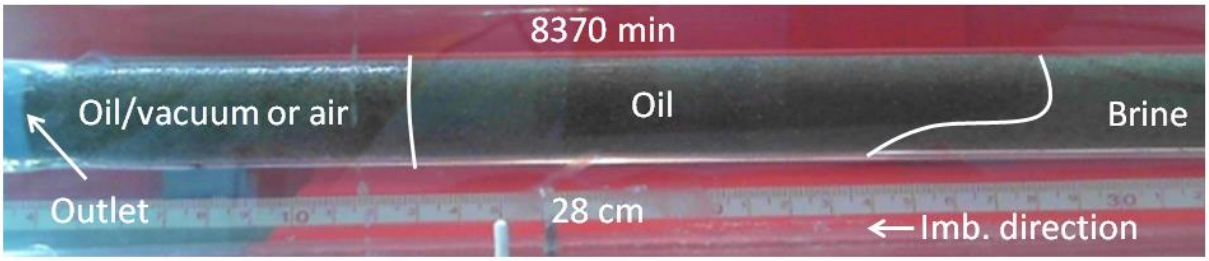

Figure 54: Front behaviour during spontaneous co-current imbibition where polymer was used as the wetting phase, whereas decane was used as the non-wetting phase. This picture shows the front behaviour after the filter was removed, during the later stages of the experiment.

Figure 55 shows the front behaviour for system SP6 during spontaneous imbibition. At the start of the experiment, brine imbibed evenly across the entire cross-section of the imbibition tube, and piston-like displacement was observed. However, after 600 minutes of production, brine started to finger through at the bottom part of the imbibition tube. After 900 minutes of production this finger was 8 centimetres long (Figure 55 middle picture). This trend continued for about 1100 minutes. Shortly after the left picture in Figure 55 was taken, a new piston-like front was formed. Some of the oil remaining behind the front was produced through the small channel at the top of the imbibition tube, but a small pocket was left behind. The piston-like displacement continued until breakthrough.

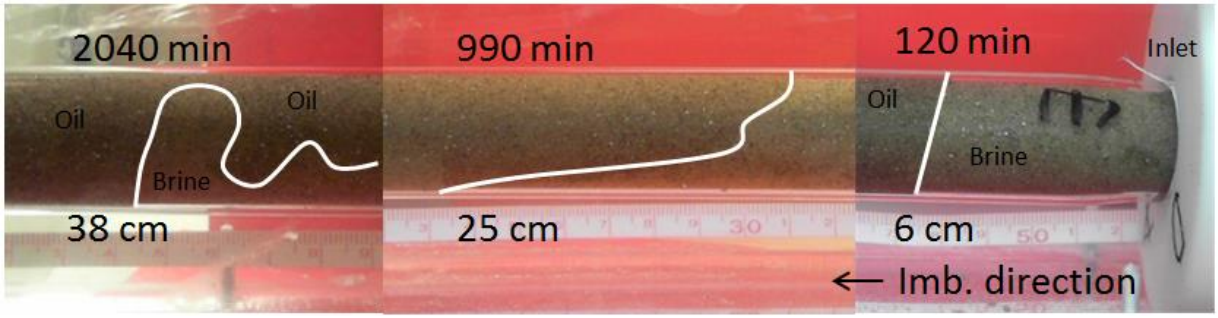

Figure 55: Front behaviour during spontaneous co-current imbibition where the viscosity of the wetting phase was increased by HPAM polymer, whereas decane was used as the non-wetting phase.

Figure 56 shows the front behaviour during spontaneous imbibition when glycerol was used as the wetting phase, and decane was used as the non-wetting phase. After an induction time of 570 minutes, brine started to imbibe across the entire cross-section of the imbibition tube, and displace the oil in a piston-like manner. This behaviour was evident throughout the entire experiment, although the angle of the front varied somewhat. After about 3800 minutes of production, the front stopped just before the outlet plug. 4000 minutes later the front had not displaced the remaining oil in the imbibition tube, visually. It is therefore believed that a small channel of brine had displaced through the sand in the centre of the imbibition tube, as some oil (0.9 ml) was produced after the front had reached 46 centimetres. However, some oil remained trapped in the imbibition tube.

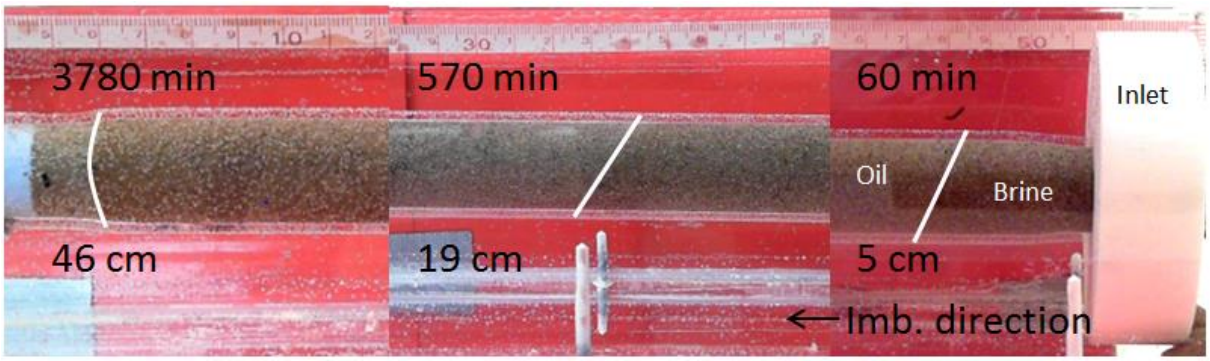

Figure 56: Front behaviour during spontaneous co-current imbibition where the viscosity of the wetting phase was increased by adding glycerol to the brine. Decane was used as the non-wetting phase. Note that the time in the pictures take the induction time into account. For example the picture to the right is 60 minutes after the imbibition started.

3.4.3 Viscosity effect on production profile

To compare the results with each other, the results for spontaneous co-current imbibition where the wetting phase viscosity was altered with either HPAM polymer or glycerol were plotted as normalised production versus normalised time. Production was normalised to total cumulative production at breakthrough, and time was normalised to the breakthrough time, see Figure 57. For SP5, the production was normalised to total production, and time was normalised to total time. A summary of important factors used during calculation of the normalised production plots are given in Table 9.

Table 9: This table shows a summary of viscosity ratio, breakthrough time, total time, breakthrough recovery and total recovery for the different spontaneous imbibition tests.

Name	Viscosity ratio	Breakthrough time (min)	Total time (min)	Breakthrough recovery (frac PV)	Total recovery (frac PV)
SP5	0.033	-	12059	-	0.57
SP6	0.033	3930	4530	0.76	0.77
SP7	0.034	4348	8248	0.80	0.82

According to the theory, given in chapter 1.3.1, the production profiles should vary with viscosity ratio during spontaneous co-current imbibition (see Figure 7). For very low viscosity ratios ($\mu_{nw}/\mu_w < 0.1$), it is expected that the imbibition rate is high initially, and decreasing towards the end of the experiment. As Figure 57 shows, both SP6 and SP7 are in line with theory. For both systems, the rate was initially high, before decreasing as the experiment progressed. This can be explained by the piston-like behaviour seen during the experiments. As the front behaves more like a piston than what was observed for higher viscosity ratios, the assumptions made in the theory holds, and thus the calculations are more valid.

In the special case of SP5, where production was reduced due to retention in the filter, normalised production curve had a peculiar shape. At the start of the experiment, before t = 0.1, the shape of the production curves follows the shape expected by theory. For the rest of the experiment however, the shape of the curve is far from what is expected by the theory.

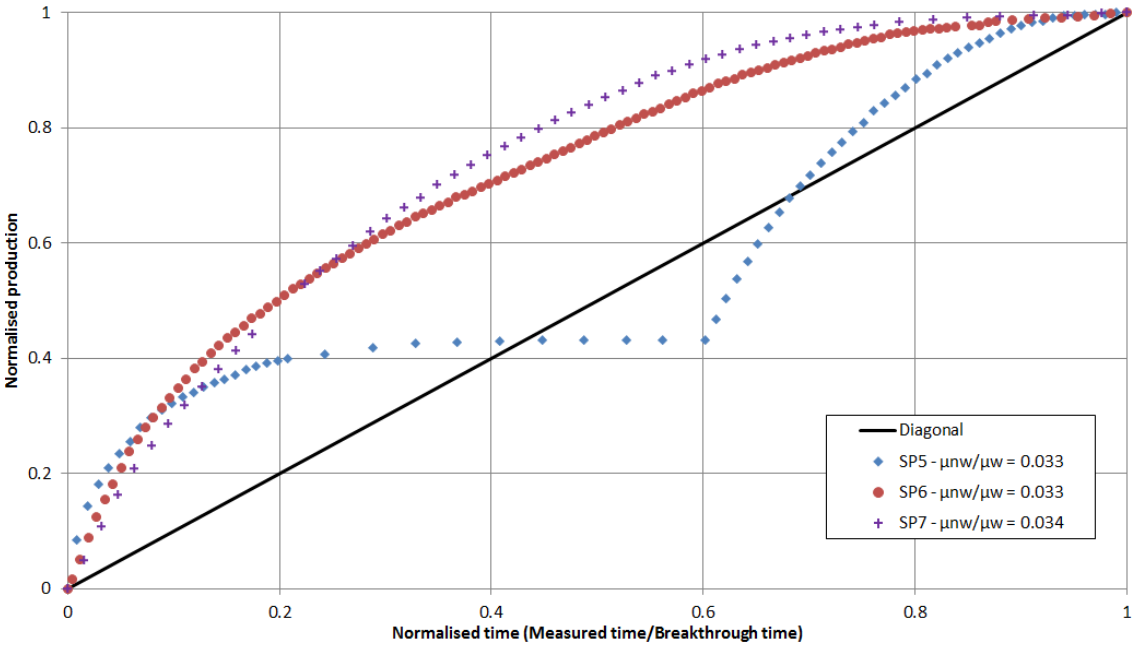

Figure 57: Spontaneous co-current imbibition in sandpacks, where HPAM polymer or a brine/glycerol mixture was used as the wetting phase, whereas decane was used as the wetting phase. This figure shows normalised production versus normalised time. Production was normalised to total cumulative production at breakthrough, and time was normalised to the breakthrough time. The diagonal represent theoretical imbibition where the viscosity ratio is equal to 1.

3.4.4 Theoretical front position versus measured front position

By plotting calculated front position (normalised production) versus measured front position, information regarding the nature of the front can be interpreted, see Figure 58. Calculated front position versus measured front position is expected to yield a straight line with a gradient of unity, if piston-like displacement is evident. In general, a good match was obtained for all experiments where the viscosity of the wetting phase was increased. However, for the first polymer experiment, the measured front position between t = 0.3 and t =0.5, was higher than the calculated front position. This coincides with a small pocket of oil being bypassed before the filter was removed. After the filter was removed, the pocket of oil was produced, and a match between measured front position and calculated front position was regained.

Similar to section 3.3.4, theoretical position of the front was calculated using equation 36, and the technique described by Haugen et al. (2014). Values for D and E were found in order to fit the calculated front position to the measured front position, see Figure 59. Plots were made for the second polymer experiment and the glycerol experiment. Due to the abnormal production for the first polymer experiment, a match was unattainable. Again, by assuming that the relative permeability to oil is 1 ahead of the front, and because the fluid viscosities are known, the relative permeability to brine behind the front was calculated by equation 31 and the fitted value for D. Figure 60 shows the calculated relative permeability to the wetting phase for experiments conducted in this thesis, compared with the relative permeability to brine for glass beads and quartz sand in the work of Meng et al. (2015), given in Figure 14. For the polymer experiment the calculated relative permeability to polymer behind the front was 0.51, and for the glycerol experiment the calculated relative permeability to glycerol behind the front was 0.38. These results indicate that relative permeability was higher when polymer was used as the wetting phase, compared with glycerol as the wetting phase.

The fitted value for E was used in equation 37 to calculate the capillary pressure at the front, $P_{c,f}$. For the polymer experiment, the calculated capillary pressure at the front was 0.139 kPa, and for the glycerol experiment it was 0.304 kPa. The estimated capillary pressure was in the same order of magnitude compared with the experiments where non-wetting phase viscosity was increased, as well as the calculated capillary pressure at the front for sandstone cores in the work of Haugen et al. (2014).

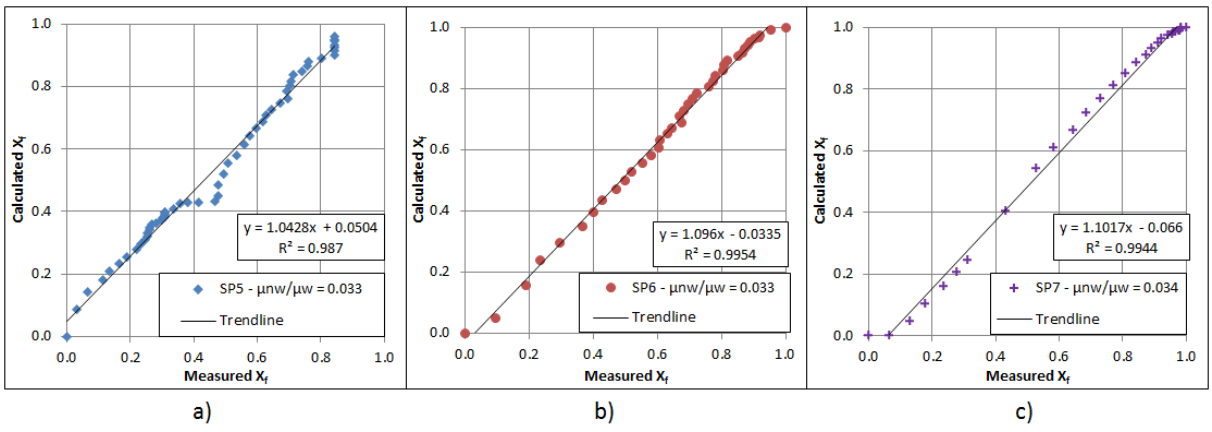

Figure 58: Plots of calculated front position (normalised production) versus measured front position for a) SP5, b) SP6, and c) SP7. The viscosity ratio is increasing from left to right.

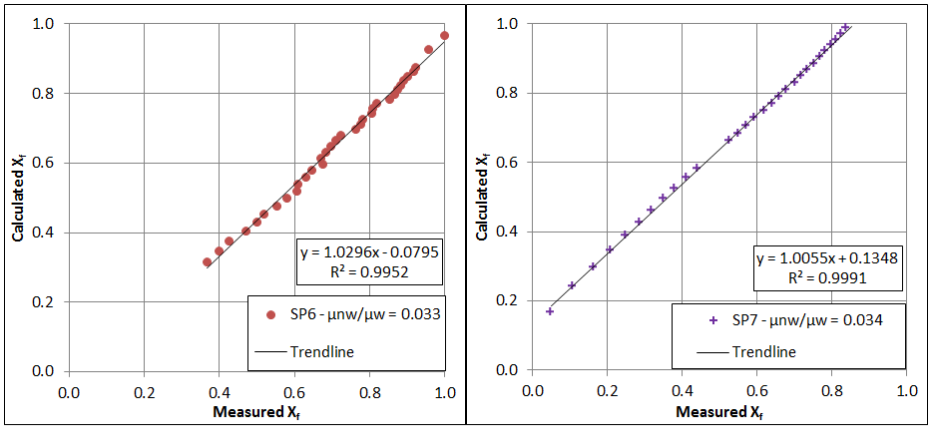

Figure 59: Plots of theoretically calculated position of the front using the method from Haugen et al. (2014) versus the measured position of the front for a) SP6 and b) SP7 during co-current displacement.

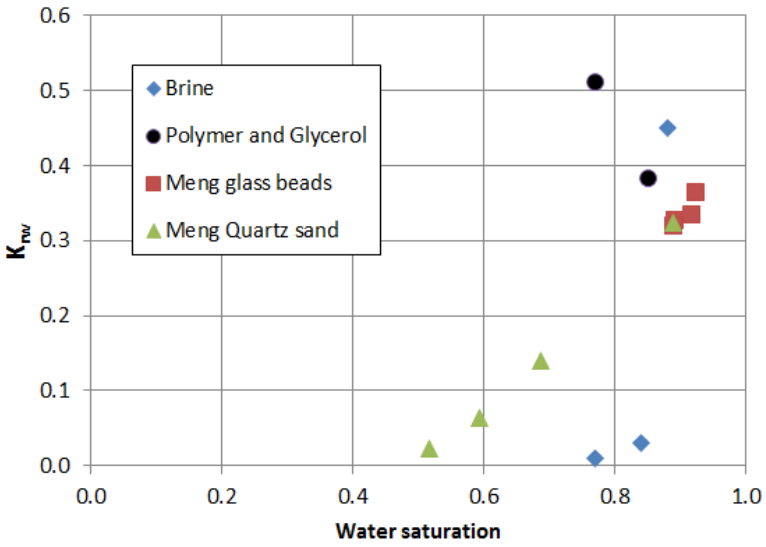

Figure 60: Relative permeability calculated using equation theory presented by Haugen et al. (2014). The blue diamonds show the relative permeability for experiments where brine was used as the wetting phase, black dots show the relative permeability for experiments where glycerol and polymer was used as the wetting phase, whereas red squares and green triangles show the relative permeability calculated in the work of Meng et al. (2015).

3.5 Normalised production curve overview

Figure 61 shows an overview of normalised production curves for all experiments conducted using experimental setup D, along with theoretical curves calculated with equation 20. This gives a good visual comparison, both between the experimental results themselves, and between the experimental results and the theory. An overview of fluids used as wetting- and non-wetting phase is given in Table 10, with associated viscosity ratio.

Table 10: An overview of which fluids were used as well as viscosity ratio for the different systems.

Name	Wetting phase	Non-wetting phase	Viscosity ratio (μ_{nw}/μ_w)
SP1	Brine	Air	0.016
SP5	HPAM polymer	Decane	0.033
SP6	HPAM polymer	Decane	0.033
SP7	Brine/glycerol mixture	Decane	0.034
SP2	Brine	Decane	0.8
SP3	Brine	Marcol 82	28.3
SP4	Brine	DTE FM 32	63.7

As expected by theory, the production curves for the different systems vary with viscosity ratio. For very low viscosity ratio (below 0.1), the production curves behaves similar to theory during the initial stages of the experiments. However, as the experiments progressed, the production curves were higher than expected, according to theory for single capillary tubes. For higher viscosity ratio (above 30), the production curve show minor increase in rate over time, but the effect was less than expected, according to theory for single capillary tubes. The experiments with a viscosity ratio between 0.1 and 1 had the best fit with theory. Spontaneous imbibition with air as the non-wetting phase had an almost exact match with the theoretical curves, whereas brine displacing oil with low viscosity ratio had a close match when comparing the shape of the curve with theory.

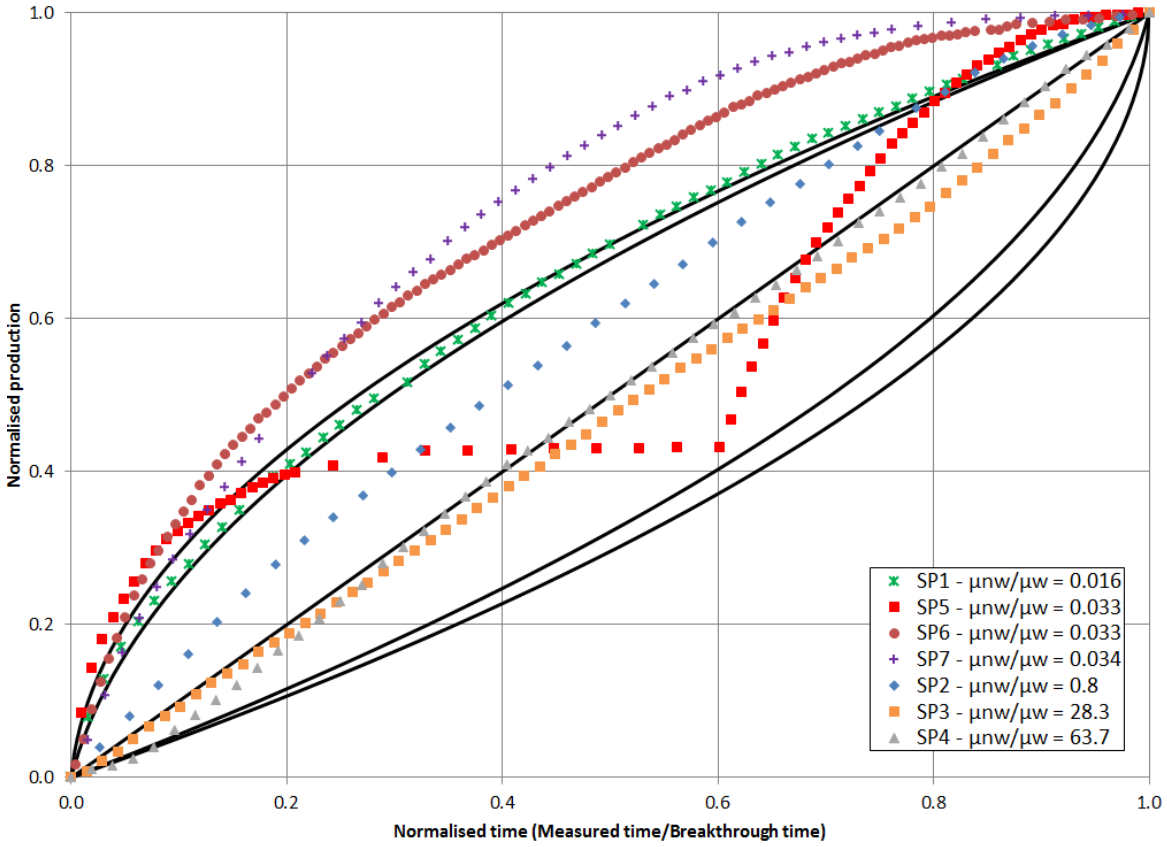

Figure 61: Spontaneous co-current imbibition in sand packs. An overview of the different fluids used as wetting and non-wetting phase ratio is given in Table 10. In addition, the viscosity ratio is given in the legend. The black lines represent the theoretical curves for viscosity ratios ranging from 0.01 (top) to 100 (bottom). A viscosity ratio of 1 yields a straight line with a gradient of unity.

4 Conclusions and future work

Conclusions

In this experimental thesis, spontaneous imbibition was conducted in columns of unconsolidated sand and glass beads, using the two ends open free spontaneous imbibition boundary condition. Viscosity of the wetting phase was varied using brine, HPAM polymer and glycerol, whereas the non-wetting phase was varied using different mineral oils. The main objective was to compare the use of polymer and glycerol to increase aqueous phase viscosity, as well as investigate the effect of viscosity ratio between the wetting and the non-wetting phase on recovery and front behaviour. Following conclusions were made:

- The effect of viscosity ratio on front behaviour and recovery during spontaneous imbibition was studied over 4 orders of magnitude, from μ_{nw}/μ_w =0.016 to μ_{nw}/μ_w = 63.7. Recovery decreased from 98% of the pore volume at μ_{nw}/μ_w = 0.016 to 77% of the pore volume at μ_{nw}/μ_w = 63.7. Visual observation of the front confirmed piston-like displacement for all viscosity ratios, except initially for higher viscosity ratios. When using a low viscosity ratio, piston-like displacement was observed from the onset of imbibition. As the viscosity ratio increased, fingering of the wetting phase and entrapment of the non-wetting phase was observed.
- HPAM polymer and glycerol were used to increase wetting phase viscosity during spontaneous imbibition. Results show that glycerol yielded a 5% higher recovery compared with polymer with matching viscosity. The lower recovery may be due to retention of polymers or wettability alteration. Further studies are required to quantify and understand the mechanisms behind the experimentally assumed difference, but it is likely to be influenced by polymer retention during spontaneous imbibition with polymer as the wetting phase.
- The impact of inlet- and outlet conditions was investigated using an experimental setup that promoted co-current imbibition. The adverse effects observed in previous work discussed by Vabø (2016) has been eliminated by improvements in the experimental setup, confirmed by piston-like displacement for all experiments.
- Front position was calculated using theory based on the assumption of piston-like displacement during co-current imbibition, presented by Haugen et al. (2014). A successful match was obtained for 5 out of 7 experiments, allowing the calculation of capillary pressure at the front and relative permeability to the wetting phase behind the front.
    - The calculated $P_{c,f}$ show a clear dependency on variation in wetting and non-wetting phase viscosity. With non-wetting phase viscosity ranging from 0.96 to 73.2 cP and a constant wetting phase viscosity of 1.15 cP, $P_{c,f}$ increased from 26 Pa to 397 Pa. When wetting phase viscosity was increased using polymer (29.1 cP) and glycerol (28.3cP), and non-wetting phase was kept constant at 0.96 cP, $P_{c,f}$ increased from 139 Pa for polymer to 304 Pa for glycerol.
    - The calculated k_{rw} also show a clear dependency on variation in non-wetting phase viscosity. As the viscosity of the non-wetting phase was increased from 0.96 cP to 73.2 cP, while wetting phase viscosity was kept constant at 1.15 cP, k_{rw} decreased from 0.45 to 0.01. When wetting phase viscosity was increased with polymer (29.1 cP) and glycerol (28.3), and non-wetting phase remained constant (0.96 cP), k_{rw} decreased from 0.51 for polymer to 0.38 for glycerol.

Future work

Building on the experience gained in collaboration with Vabø (2016), the experimental setup was altered to eliminate adverse inlet effects restricting flow. Performing spontaneous imbibition using the current experimental setup provides consistent piston-like front behaviour during experiments. However, constant development and adjustments should be considered, in order to find new and better technology.

- As spontaneous imbibition using experimental setup D was performed in sand, extending the study by using an alternative porous media, such as glass beads, may be considered. Using glass beads with a narrow pore size distribution will enlighten the effects of pore size distribution on front behaviour and recovery.

- I suggest using fluids with other viscosities to further investigate the effect of viscosity ratio on front behaviour and recovery, especially for higher viscosity ratios, where results in this thesis showed lack of a sharp front in the initial stages of imbibition.

- Incorporating pumps into the setup will enable forced imbibition. Performing flow experiments and measuring permeability, before performing spontaneous imbibition with initial water saturation, will provide useful information under conditions closer to actual reservoir conditions. In the current experimental setup, however, the outlet plug is vulnerable to increased pressure. A new outlet configuration must be developed if increased pressures are to be used.

- Further studies using polymer as the wetting phase during spontaneous imbibition are required to understand and quantify mechanisms such as retention and wettability alteration.

- Reservoir simulations are a major part of field development. Matching experimental results with simulations should be considered, as spontaneous imbibition is an important mechanism in reservoir flow.

- Wettability effects on spontaneous imbibition may be introduced by mixing water-wet sand with preferentially oil-wet sand. Another option is to mix water-wet glass beads with preferentially oil-wet basalt beads.

Appendix I – Uncertainty

This appendix contains principles and equations regarding experimental uncertainty. Equations are taken from Erdal (1997).

Uncertainty related to experimental work is generally derived from two sources; the uncertainty of the instruments used and the uncertainties related to the observer and the experiment itself. The first source is generally a quantified uncertainty, measured by the manufacturers of the instruments. Table 11 lists uncertainties associated with instruments used in this thesis. The second source is harder to quantify as it comprises fluctuations in temperature, evaporation of liquids, leakage and so forth. These uncertainties are often assumed to be larger than the uncertainties related to the instruments.

Following equation were used to calculate uncertainty in experiments were the instrumental uncertainty was known:

When R is a function of multiple uncorrelated variables x, y, z…, the uncertainty $s_{\bar{R}}$ is given by:

$$s_{\bar{R}} = \sqrt{\left(\frac{\partial R}{\partial x} s_{\bar{x}}\right)^2 + \left(\frac{\partial R}{\partial y} s_{\bar{y}}\right)^2 + \left(\frac{\partial R}{\partial z} s_{\bar{z}}\right)^2 + \cdots} \qquad \text{(A1)}$$

Standard deviation is given by:

$$s = \sqrt{\frac{1}{N-1}\sum_{i=1}^{N}(x_i - \bar{x})^2} \qquad \text{(A2)}$$

Where N is the number of measurements, x_i is the measurements and $\bar{x}$ is the mean value.

Table 11: Instrumental uncertainties.

Instrument	Parameter	Uncertainty
Weight (gram)	Mass	±0.01
Caliper (cm)	Length	±0.05
Ruler (cm)	Length	±0.5
Volumetric flask 500 ml	Volume	±0.25
Graded cylinder 5 ml	Volume	±0.05
Graded cylinder 10 ml	Volume	±0.1
Graded cylinder 25 ml	Volume	±0.25
Graded cylinder 50 ml	Volume	±0.5
Beaker 50 ml	Volume	±0.5
Beaker 100 ml	Volume	±5%
Beaker 250 ml	Volume	±5%
Beaker 500 ml	Volume	±5%
Beaker 1000 ml	Volume	±5%

Bibliography

AMOTT, E. 1959. Observations relating to the wettability of porous rock. *Petroleum Transactions, AIME,* 216**,** 156-162.

ANDERSON, W. G. 1986a. Wettability Literature Survey-Part 1: Rock/Oil/Brine Interactions and the Effects of Core Handling on Wettability. *Journal of Petroleum Technology,* 38**,** 1,125-1,144.

ANDERSON, W. G. 1986b. Wettability Literature Survey-Part 2: Wettability Measurement. *Journal of Petroleum Technology,* 38**,** 1,246-1,262.

ANDERSON, W. G. 1987a. Wettability Literature Survey-Part 4: Effects of wettability on capillary pressure. *Journal of Petroleum Technology,* 39**,** 1,283-1,300.

ANDERSON, W. G. 1987b. Wettability Literature Survey-Part 6: The effects of wettability on waterflooding. *Journal of Petroleum Technology,* 39**,** 1,605-1,622.

ARONOFSKY, J. 1952. Mobility ratio-Its influence on flood patterns during water encroachment. *Journal of Petroleum Technology,* 4**,** 15-24.

BAVIERE, M. 1991. Basic Concepts in Enhanced Oil Recovery Processes. *Elsevier Applied Science.*

BEAL, C. 1946. The viscosity of air, water, natural gas, crude oil and its associated gases at oil field temperatures and pressures. *Transactions of the AIME,* 165**,** 94-115.

BELL, J. M. & CAMERON, F. 1906. The flow of liquids through capillary spaces. *The Journal of Physical Chemistry,* 10**,** 658-674.

BROSETA, D., MEDJAHED, F., LECOURTIER, J. & ROBIN, M. 1995. Polymer Adsorption/Retention in porous media: Effects of core wettability on residual oil. *SPE Advanced Technology Series,* 3**,** 103-112.

BROWN, R. J. & FATT, I. Measurements of fractional wettability of oil fields' rocks by the nuclear magnetic relaxation method. Fall Meeting of the Petroleum Branch of AIME, 1956. Society of Petroleum Engineers.

CHANG, H. L. 1978. Polymer flooding technology yesterday, today, and tomorrow. *Journal of Petroleum Technology,* 30**,** 1,113-1,128.

CHAUVETEAU, G. & KOHLER, N. Polymer flooding: The essential elements for laboratory evaluation. SPE Improved Oil Recovery Symposium, 1974. Society of Petroleum Engineers.

CRAIG, F. F. 1971. *The Reservoir Engineering Aspects of Waterflooding,* New York, Henry L. Doherty Memorial Fund of AIME.

DESREMAUX, L., CHAUVETEAU, G. & MARTIN, M. Communication No. 28. Colloque de L. association de Recherches, Sur les Techniques d. exploitation due Petrole, Paris, 1971.

DONALDSON, E. C., CHILINGARIAN, G. V. & YEN, T. F. 1989. *Enhanced oil recovery, II: Processes and operations,* Elsevier.

DONG, M., DULLIEN, F. A. L., DAI, L. & LI, D. 2006. Immiscible Displacement in the Interacting Capillary Bundle Model Part II. Applications of Model and Comparison of Interacting and Non-Interacting Capillary Bundle Models. *Transport in Porous Media,* 63**,** 289-304.

DONG, M., DULLIEN, F. A. L. & ZHOU, J. 1998. Characterization of Waterflood Saturation Profile Histories by the 'Complete' Capillary Number. *Transport in Porous Media,* 31**,** 213-237.

DULLIEN, F. A. 2012. *Porous media: fluid transport and pore structure,* Academic press.

ELMKIES, P., BERTIN, H., LASSEUX, D., MURRAY, M. & ZAITOUN, A. Further investigations on two-phase flow property modification by polymers: Wettability effects. SPE International Symposium on Oilfield Chemistry, 2001. Society of Petroleum Engineers.

ERDAL, A. 1997. *Elementær innføring i sannsynlighetsregning og problemløsninger ved analyse av måleresultater,* Bergen, Alma mater.

FERNØ, M., HAUGEN, A., BRATTEKAS, B., MORROW, N. & MASON, G. Spontaneous Imbibition Revisited-A New Method to Determine Kr and Pc by Inclusion of the Capillary Backpressure. IOR 2015-18th European Symposium on Improved Oil Recovery, 2015.

FERNØ, M., HAUGEN, Å., WICKRAMATHILAKA, S., HOWARD, J., GRAUE, A., MASON, G. & MORROW, N. 2013. Magnetic resonance imaging of the development of fronts during spontaneous imbibition. *Journal of Petroleum Science and Engineering,* 101**,** 1-11.

FISCHER, H. & MORROW, N. R. 2006. Scaling of oil recovery by spontaneous imbibition for wide variation in aqueous phase viscosity with glycerol as the viscosifying agent. *Journal of Petroleum Science and Engineering,* 52**,** 35-53.

GOGARTY, W. 1967. Mobility control with polymer solutions. *Society of Petroleum Engineers Journal,* 7**,** 161-173.

GRATON, L. C. & FRASER, H. 1935. Systematic packing of spheres: with particular relation to porosity and permeability. *The Journal of Geology***,** 785-909.

HAMON, G. & VIDAL, J. Scaling-up the capillary imbibition process from laboratory experiments on homogeneous and heterogeneous samples. European Petroleum Conference, 1986. Society of Petroleum Engineers.

HAUGEN, Å., FERNØ, M., MASON, G. & MORROW, N. 2014. Capillary pressure and relative permeability estimated from a single spontaneous imbibition test. *Journal of Petroleum Science and Engineering,* 115**,** 66-77.

JEANES, A., PITTSLEY, J. & SENTI, F. 1961. Polysaccharide B-1459: a new hydrocolloid polyelectrolyte produced from glucose by bacterial fermentation. *Journal of Applied Polymer Science,* 5**,** 519-526.

JENKINS, R. J. 1966. Accuracy of porosity determinations. *The Log Analyst,* 7.

KIRBY, B. J. 2010. *Micro-and nanoscale fluid mechanics: transport in microfluidic devices*, Cambridge University Press.

KYTE, J. & RAPOPORT, L. 1958. Linear waterflood behavior and end effects in water-wet porous media. *Journal of Petroleum Technology,* 10**,** 47-50.

LAKE, L. W. 1989. *Enhanced oil recovery*.

LATIL, M. 1980. *Enhanced oil recovery*, Éditions Technip.

LI, Y., MORROW, N. R. & RUTH, D. 2003. Similarity solution for linear counter-current spontaneous imbibition. *Journal of Petroleum Science and Engineering,* 39**,** 309-326.

LI, Y., RUTH, D., MASON, G. & MORROW, N. R. 2006. Pressures acting in counter-current spontaneous imbibition. *Journal of Petroleum Science and Engineering,* 52**,** 87-99.

MA, S., MORROW, N. R. & ZHANG, X. 1997. Generalized scaling of spontaneous imbibition data for strongly water-wet systems. *Journal of Petroleum Science and Engineering,* 18**,** 165-178.

MAERKER, J. M. 1973. Dependence of polymer retention on flow rate. *Journal of Petroleum Technology,* 25**,** 1,307-1,308.

MARSHAK, S. 2011. *Earth: Portrait of a planet*, W. W. Norton & Company, Inc.

MASON, G., FISCHER, H., MORROW, N. R., JOHANNESEN, E., HAUGEN, Å., GRAUE, A. & FERNØ, M. A. 2010. Oil production by spontaneous imbibition from sandstone and chalk cylindrical cores with two ends open. *Energy & Fuels,* 24**,** 1164-1169.

MASON, G., FISCHER, H., MORROW, N. R. & RUTH, D. W. 2009. Spontaneous counter-current imbibition into core samples with all faces open. *Transport in porous media,* 78**,** 199-216.

MASON, G. & MORROW, N. R. 2013. Developments in spontaneous imbibition and possibilities for future work. *Journal of Petroleum Science and Engineering,* 110**,** 268-293.

MATTAX, C. C. & KYTE, J. 1962. Imbibition oil recovery from fractured, water-drive reservoir. *Society of Petroleum Engineers Journal,* 2**,** 177-184.

MENG, Q., LIU, H. & WANG, J. 2015. Entrapment of the Non-wetting Phase during Co-current Spontaneous Imbibition. *Energy & Fuels,* 29**,** 686-694.

MORROW, N. R. & MASON, G. 2001. Recovery of oil by spontaneous imbibition. *Current Opinion in Colloid & Interface Science,* 6**,** 321-337.

NEEDHAM, R. B. & DOE, P. H. 1987. Polymer flooding review. *Journal of Petroleum Technology,* 39**,** 1,503-1,507.

RAPOPORT, L. & LEAS, W. 1953. Properties of linear waterfloods. *Journal of Petroleum Technology,* 5**,** 139-148.

ROGERS, J. J. & HEAD, W. B. 1961. Relationships between porosity, median size, and sorting coefficients of synthetic sands. *Journal of Sedimentary Research,* 31.

ROMERO-ZERON, L., ONGSURAKUL, S., LI, L. & BALCOM, B. 2010. Visualization of the effect of porous media wettability on polymer flooding performance through unconsolidated porous media using magnetic resonance imaging. *Petroleum Science and Technology,* 28**,** 52-67.

SATTER, A., IQBAL, G. M. & BUCHWALTER, J. L. 2008. *Practical enhanced reservoir engineering: assisted with simulation software,* Pennwell Books.

SORBIE, K., ROBERTS, L. & FOULSER, R. 1982. Polymer Flooding Calculations For Highly Stratified BRENT Sands In The North Sea. *Enhanced Oil Recovery***,** 175.

SORBIE, K. S. 2013. *Polymer-improved oil recovery,* Springer Science & Business Media.

STANDNES, D. C. 2004. Experimental study of the impact of boundary conditions on oil recovery by co-current and counter-current spontaneous imbibition. *Energy & fuels,* 18**,** 271-282.

SYDANSK, R. 2006. Polymer, gels, foams, and resins. *SPE petroleum engineering handbook.* Richardson, Texas: SPE.

SYDANSK, R. D. & ROMERO-ZERON, L. 2010. *Reservoir Conformance Improvement*, Richardson, US, Society of Petroleum Engineers.

UNSAL, E., MASON, G., RUTH, D. W. & MORROW, N. R. 2007. Co- and counter-current spontaneous imbibition into groups of capillary tubes with lateral connections permitting cross-flow. *Journal of Colloid and Interface Science,* 315**,** 200-209.

VABØ, T. 2016. *Viscosity Effects on Imbibition Rate and Front Behavior during Co-Current Spontaneous Imbibition in Unconsolidated Porous Media.* University of Bergen.

WASHBURN, E. W. 1921. The dynamics of capillary flow. *Physical review,* 17**,** 273.

WICKRAMATHILAKA, S., HOWARD, J., STEVENS, J., MORROW, N., MASON, G., HAUGEN, Å., GRAUE, A. & FERNØ, M. Magnetic resonance imaging of oil recovery during spontaneous imbibition from cores with two-ends open boundary condition. Proceeding of the International Society of Core Analysts Annual Meeting. September, 2011. 18-21.

ZHANG, X., MORROW, N. R. & MA, S. 1996. Experimental verification of a modified scaling group for spontaneous imbibition. *SPE Reservoir Engineering,* 11**,** 280-285.

ZOLOTUKHIN, A. B. & URSIN, J.-R. 2000. *Introduction to petroleum reservoir engineering*, Norwegien Academic Press (HóyskoleForlaget).